2022

# A New Car-Following Model with Incorporation of Markkula's Framework of Sensorimotor Control in Sustained Motion Tasks

Umair Durrani
*University of Windsor*

**A New Car-Following Model with Incorporation of Markkula's Framework of Sensorimotor Control in Sustained Motion Tasks**

by

**Umair Durrani**

A Dissertation

Submitted to the Faculty of Graduate Studies

through the Department of Civil and Environmental Engineering

in Partial Fulfillment of the Requirements for

the Degree of Doctor of Philosophy

at the University of Windsor

Windsor, Ontario, Canada

2022

© 2022 Umair Durrani

A New Car-Following Model with Incorporation of Markkula's Framework of

Sensorimotor Control in Sustained Motion Tasks


by


Umair Durrani


APPROVED BY:


_____
L. Kattan, External Examiner
University of Calgary


_____
J. Tofflemire, Special Member
Department of Civil and Environmental Engineering

_____
J. Johrendt
Department of Mechanical, Automotive & Materials Engineering


_____
W. Anderson
Department of Political Science


_____
H. Maoh
Department of Civil and Environmental Engineering



_____
C. Lee, Advisor
Department of Civil and Environmental Engineering


April 06, 2022

# Declaration of Co-Authorship / Previous Publication

I.    Co-Authorship

I hereby declare that this thesis incorporates material that is result of joint research, as follows:

Chapter 4 and Chapter 6 of the thesis utilized the material from a published article in the journal of *Accident Analysis and Prevention* that was co-authored by Dr. Chris Lee and Dhwani Shah. Moreover, Chapter 5 and Chapter 6 of the thesis are based on a paper that was co-authored by Dr. Chris Lee. This paper is submitted to the journal of *Accident Analysis and Prevention*, but there has been no decision yet.

In the above cases, the primary data analysis and writing were performed by the author. The co-authors, namely Dr. Chris Lee, provided frequent supervisory input on the overall direction of the papers and provided editing support for the text and revisions before final acceptance for publication. In addition, Dhwani Shah participated in the discussion of the ideas and the overall direction of the research questions.

I am aware of the University of Windsor Senate Policy on Authorship and I certify that I have properly acknowledged the contribution of other researchers to my thesis, and have obtained written permission from each of the co-author(s) to include the above material(s) in my thesis.

I certify that, with the above qualification, this thesis, and the research to which it refers, is the product of my own work.

II.  Previous Publication

This thesis includes 2 original papers that have been previously published/submitted to journals for publication, as follows:

| Thesis Chapter | Publication title/full citation | Publication status* |
|---|---|---|
| Chapter 4 | Durrani, U., Lee, C. and Shah, D., 2021. Predicting driver reaction time and deceleration: Comparison of perception-reaction thresholds and evidence accumulation framework. *Accident Analysis & Prevention*, *149*, p.105889. | Published |
| Chapter 5 | Applying the Accumulator Model to Prediction of Driver's Reaction Time based on Looming in Approaching and Braking Conditions | Submitted |
| Chapter 6 | Durrani, U., Lee, C. and Shah, D., 2021. Predicting driver reaction time and deceleration: Comparison of perception-reaction thresholds and evidence accumulation framework. *Accident Analysis & Prevention*, *149*, p.105889. | Published |
| Chapter 6 | Applying the Accumulator Model to Prediction of Driver's Reaction Time based on Looming in Approaching and Braking Conditions | Submitted |

I certify that I have obtained a written permission from the copyright owner(s) to include the above published material(s) in my thesis. I certify that the above material describes work completed during my registration as a graduate student at the University of Windsor.

III.    General


I declare that, to the best of my knowledge, my thesis does not infringe upon anyone's copyright nor violate any proprietary rights and that any ideas, techniques, quotations, or any other material from the work of other people included in my thesis, published or otherwise, are fully acknowledged in accordance with the standard referencing practices. Furthermore, to the extent that I have included copyrighted material that surpasses the bounds of fair dealing within the meaning of the Canada Copyright Act, I certify that I have obtained a written permission from the copyright owner(s) to include such material(s) in my thesis.

I declare that this is a true copy of my thesis, including any final revisions, as approved by my thesis committee and the Graduate Studies office, and that this thesis has not been submitted for a higher degree to any other University or Institution.

# Abstract

The main aim of this research is to develop a new car-following model that realistically predicts the trajectories of speed, acceleration, jerk and spacing in congested and uncongested freeway conditions. The research has three objectives. First, the start time of driver reaction was investigated in various car-following conditions. Specifically, the assumption of a constant reaction time of the existing car-following models was investigated using the observed driver behaviour data collected from a driving simulator. Moreover, the perception limits and the process that drivers use to start reaction were also studied. Second, a new car-following model was developed to reproduce the observed driver's intermittent start time of acceleration/deceleration and realistic ranges of magnitudes of speed, spacing, acceleration and jerk. For this task, the model adapted the Markkula's Framework of Sensorimotor Control in Sustained Motion Tasks. Third, the effect of lead vehicle type (car and truck) and the effect of the lead vehicle brake lights on the start time of driver reaction in car-following conditions were studied.

For this purpose, a total of 50 drivers' car-following behaviour was observed in 4 different scenarios using a driving simulator – reaction to a decelerating lead vehicle, reaction to a stopped lead vehicle, perception of a lead vehicle's speed change, and perception of a slow-moving lead vehicle. It was found that the drivers neither reacted after a specific reaction time from the start of perception nor reacted at a specific value of a perceptual variable. Rather, the drivers generally reacted when the accumulation of evidence (e.g., perceptual variable) over time reached a threshold. This demonstrates that the evidence accumulation framework was a promising method of predicting the start time of driver reaction in car-following conditions.

Therefore, a new car-following model called "Intermittent Intelligent Driver Model (IIDM)" was developed based on evidence accumulation to start driver reaction unlike the existing car-following models that use a constant reaction time parameter. Moreover, the IIDM uses the shape and duration of acceleration adjustments that accurately represents the actual shape and duration of acceleration maneuvers in the data. The prediction of accuracy of the new car-following model was evaluated using both the driving simulator data and real-world trajectory data.

Compared to the three existing car-following models – the Gipps' Model, the Wiedemann Model and the Intelligent Driver Model (IDM), the IIDM realistically reproduced trajectories of speed, acceleration, jerk and spacing for both types of data. Moreover, the estimated surrogate measures of safety from trajectories predicted using the IIDM were similar to the surrogate measures of safety estimated from the observed data. Furthermore, the IIDM can incorporate the effects of lead vehicle brake lights and lead vehicle type (car and truck) for more accurate estimation of the driver reaction time. This demonstrates that the IIDM can generate more realistic vehicle trajectories (start time of reaction and magnitude of reaction) in various car-following conditions, which can be used to predict vehicle speeds and assess safety.

# Dedication

Dedicated to my parents, Jameel Asghar Durrani and Tahira Durrani.

# Acknowledgements

I am deeply grateful to my advisor, Dr. Chris Lee. His unconditional support and encouragement made this work possible. I was able to improve my research ability under his guidance, which I consider a lifetime treasure for my professional development. I am also indebted to Dr. Hanna Maoh's support in my research and his constant encouragement whenever I sought guidance from him.

I am also grateful to the extreme generosity and support of Dr. Gustav Markkula, Chair in Applied Behaviour Modeling at University of Leeds, UK. I am thankful to him for answering all my questions about his work with patience and encouraging fruitful discussions about my modeling efforts.

I would like to acknowledge the committee members, Dr. Lina Kattan, Dr. William Anderson, Dr. Jennifer Johrendt, and Prof. John Tofflemire, for their valuable comments and suggestions to improve the quality of this work.

I would like to thank all my past and present colleagues – Peibo Zhao, Dhwani Shah, HaeSung Ahn, and Anas Abdulghani. I have received tremendous help from their ideas and support.

I would like to thank the research sponsors: Natural Sciences and Engineering Research Council of Canada, Canada Foundation for Innovation, and the University of Windsor.

I would like to thank my wife, Saba Ikhlaq, for the unconditional support and love she provided in all these years. I also want to acknowledge the support of my siblings and my parents in my graduate studies.

# Table of Contents

# List of Tables

# List of Figures

# List of Appendices

# List of Symbols

$x_i$      Position (m) of subject vehicle $i$

$x_{i-1}$      Position (m) of lead vehicle $i$-1

$v_i, a_i$      Speed (m/s) and acceleration (m/s$^2$) of vehicle $i$, respectively

$v_{i-1}, a_{i-1}$      Speed (m/s) and acceleration (m/s$^2$) of vehicle $i$-1, respectively

$l_i, l_{i-1}$      Length (m) of vehicle $i$ and $i$-1, respectively

$g_i^x$      Spacing (m) between rear bumper of vehicle $i$-1 and front bumper of vehicle $i$

$g_i^t$      Time headway (s) between rear bumper of vehicle $i$-1 and front bumper of vehicle $i$

$s_i$      Spacing (m) between vehicle $i$ and vehicle $i$-1

$h_i$      Time headway (s) between vehicle $i$ and vehicle $i$-1

$\tau_i$      Reaction time (s)

$v_{opt}$      Optimal velocity (m/s)

$v_0$      Desired speed (m/s)

$g_0^x$      Standstill spacing (m)

$A_i$      Maximum acceleration when starting from zero speed (m/s$^2$)

$\theta_W, \theta_H$      Visual angles due to width and height of lead vehicle (radians)

$\dot{\theta}_W, \dot{\theta}_H$      Angular velocity due to width and height of lead vehicle (radians/s)

$\dot{\theta}_{W(TH)}$      Threshold of angular velocity due to width of lead vehicle (radians/s)

$\tau, \tau^{-1}$      Visual time-to-collision (s) and its inverse (1/s)

$\dot{\tau}$      Rate of change in time-to-collision

$s^*$      Desired spacing (m)

$AX$      Standstill spacing (m)

$ABX$      Desired distance in following condition (m)

$SDX$      Maximum distance in following condition (m)

| | |
|---|---|
| $SDV$ | Threshold of positive speed difference at large spacing (m/s) |
| $CLDV$ | Threshold of positive speed difference at small spacing (m/s) |
| $OPDV$ | Threshold of negative speed difference at small spacing (m/s) |
| $BMAX$ | Acceleration in free-driving (m/s$^2$) |
| $V_{MAX}$ | Maximum speed of a vehicle (m/s) |
| $BNULL$ | Acceleration at desired speed in free-driving and following conditions |
| $B(i)_{App}$ | Deceleration while approaching a slow vehicle (m/s$^2$) |
| $B(i)_{Emg}$ | Deceleration in emergency braking (m/s$^2$) |
| $BMIN$ | Maximum possible deceleration of a vehicle (m/s$^2$) |
| $P(t)$ | Control error |
| $\epsilon(t)$ | Control error prediction error |
| $A(t)$ | Accumulated value of $\epsilon(t)$ at time $t$ |
| $\varepsilon(t)$ | Noise |
| $\lambda$ | Leakage in the evidence |
| $a_{BL}, p_{BL}$ | Effect of lead vehicle brake lights |
| $\tilde{g}_i$ | Magnitude of acceleration (m/s$^2$) |
| $\Delta T$ | Duration of the acceleration control |
| $\Delta T_p$ | Duration of predicted control error |
| $G(t)$ | Shape of acceleration control |
| $H(t)$ | Shape of predicted control error |

# Chapter 1:  Introduction

## 1.1    Motivation

Car-following behaviour refers to the evolution of position, speed, and acceleration of a subject vehicle over time as it follows a lead vehicle in the same lane (Treiber and Kesting, 2013). In the context of car-following, a subject vehicle interacts with a lead vehicle in various conditions. These conditions include free-driving, approaching a slow moving or stopped lead vehicle, and accelerating behind a faster lead vehicle. Understanding and modeling car-following behaviour is essential for proposing solutions to many traffic engineering problems. These include developing effective forward collision warning systems, estimating rear-end collision risk and vehicle emissions, improving adaptive cruise control technology, motion planning for self-driving cars by predicting motion of human-driven vehicles, etc. Most importantly, car-following models serve as one of the core algorithms of microscopic traffic simulation models. The traffic simulation models can be used to test various traffic scenarios in a virtual road network before actual implementation of the proposed solutions.

Although several car-following models have been proposed since early 1950s, they have been of limited use in many practical applications described above due to various reasons (Saifuzzaman and Zheng, 2014; Aghabayk et al., 2015). Most existing car-following models can reasonably predict the driver behaviour only in close-following conditions, i.e., when the subject and lead vehicles are moving at near-identical speeds and keep a safe following distance. Only a few existing car-following models are considered to be *complete* - i.e., they can predict the speed or acceleration of a subject vehicle in all car-following

conditions. The limited practical application of the existing car-following models is mainly due to the model parsimony and the use of assumptions that are often too simple to represent actual driver behaviour (Treiber and Kesting, 2013).

There are three key challenges in developing a car-following model for an accurate representation of actual driver behaviour – 1) start time of driver reaction, 2) magnitude and duration of acceleration adjustments and 3) effects of lead vehicle type and brake lights. These challenges and the corresponding modeling efforts and the research gaps are discussed as follows.

### 1.1.1 Start time of driver reaction

In general, car-following behaviour changes as the driver starts reaction to the lead vehicle - i.e., an acceleration/deceleration adjustment. Most car-following models assume that the driver instantly starts reaction (i.e., zero reaction time) or the driver starts reaction only after constant reaction time. These models assume that drivers continuously apply acceleration (no reaction time) or apply acceleration after regular intervals (constant reaction time) based on the speed difference and distance to lead vehicle (Khodayari et al., 2012). However, constant or no reaction time generally results in a smooth speed trajectory which is more similar to the adaptive cruise control rather than human driver behaviour (Treiber and Kesting, 2013).

Since driver characteristics and vehicle and environmental conditions significantly influence the reaction time (Shinar, 2017), the reaction time is assumed to follow a pre-specified distribution - e.g., log-normal distribution (Triggs and Harris, 1982). This

distribution of reaction time is generally assumed to be independent of urgency and expectancy in different car-following conditions (Green, 2000).

However, several studies have demonstrated that the reaction time is strongly correlated with urgency which is determined based on spacing, time-to-collision (TTC), and lead vehicle deceleration in close-following conditions (Wang et al., 2016; Elhenawy, El-Shawarby and Rakha, 2017; Wu and Lin, 2019). Yet, there is a lack of studies that investigated the reaction time in low urgency or rapid transition from low to high urgency (Green, 2017b). These conditions are typical in high-speed driving on freeways when drivers approach a slow-moving or an unexpectedly stopped lead vehicle from a large spacing. In these conditions, it is hard to define the start time of driver reaction since the lead vehicle brake lights are not visible.

Instead of using a constant reaction time or the distribution of reaction time without considering urgency of reaction, many past studies investigated the driver's start of reaction based on perceptual variables (Green, 2017a, 2017b; Markkula et al., 2020, 2021). As Gibson (1986) suggested, human visual perception depends on gradients of variation in environments (e.g., position, size, headlights luminance and distance of oncoming vehicle). Since perceptual variables capture these gradients of variation instead of absolute values, they reflect the driver's capability of detecting the lead vehicle motion. However, no study has extensively estimated the reaction time for various car-following conditions based on perceptual variables. Particularly, the condition of approaching a slow moving or stopped lead vehicle from a large spacing has not been investigated in the past studies.

Furthermore, past studies reported that drivers adjust to the lead vehicle speed changes intermittently, not continuously (Wiedemann and Reiter, 1992; Markkula, 2014). For

instance, Markkula (2014) found from naturalistic driving data that the rates of change of accelerator and brake pedal mostly stayed at zero and driver's reactions occurred irregularly. These intermittent start times of driver reaction are assumed to occur either when the instantaneous value or the accumulated value of a perceptual variable exceeds a fixed threshold (Wiedemann and Reiter, 1992; Markkula, 2014).

However, there is a lack of studies that experimentally tested if drivers react after a constant reaction time or at intermittent times after the instantaneous value or the accumulated value of perceptual variable exceeds a threshold. Thus, there is a need to investigate how to predict the start time of driver reaction in all car-following conditions more realistically.

### 1.1.2 Magnitude and duration of acceleration adjustments

Accurate representation of the magnitude and duration of acceleration/deceleration adjustment is an important component of car-following models. However, most car-following models ignored the perception limits of drivers and acceleration limits of vehicles (Treiber and Kesting, 2013). Thus, these models assume that in close-following conditions, the drivers' goal is to keep a safe spacing to the lead vehicle and zero speed difference. These models also assume that drivers have the perfect information on speed difference and spacing, and always apply the acceleration/deceleration such that the spacing becomes equal to the safe spacing and speed difference becomes zero (Treiber and Kesting, 2013). As the models predict the driver reaction in this manner at regular intervals (constant reaction time), the magnitude of acceleration is either too small or too large compared to the actual magnitude of acceleration.

Other car-following models assume that drivers always decelerate to safely stop behind a lead vehicle (Lee, 1976; Wiedemann and Reiter, 1992; Treiber and Kesting, 2013). This assumption leads to a hard deceleration followed by a gradual decrease in deceleration in all cases. However, this assumption is not valid when a driver approaches a slow lead vehicle from a large spacing. Unlike the assumption of an initial hard deceleration, the magnitude of deceleration is initially small while approaching a slow lead vehicle from a large spacing.

Recent literature suggests that the magnitude of deceleration is strongly correlated with a perceptual variable at the start of deceleration adjustment in urgent braking conditions (Markkula et al., 2016). However, no study has investigated the correlation between the magnitude of deceleration and a perceptual variable in other car-following conditions.

### 1.1.3   Effects of lead vehicle type and brake lights

Driver's reaction time in car-following varies among different drivers. This heterogeneity is due to various perceptual and symbolic cues that are only used by a proportion of driver population. For instance, since perceptual variables are correlated with the width and height of the lead vehicle, drivers can detect a large truck more easily than a car at a large spacing. Consequently, the reaction time is also likely to vary with the size of the lead vehicle even if the speed difference and spacing are the same. However, no study has analyzed the effect of the lead vehicle size on the driver's perception and reaction in a car-following context.

Also, lead vehicle brake lights provide a symbolic cue to the subject vehicle's driver about the need to start deceleration. Recent studies suggested that driver's reaction depends on the lead vehicle brake lights and the perceptual cues (Xue et al., 2018). Therefore, it is

important to include the effect of lead vehicle brake lights in car-following models. However, the existing car-following models have not considered the effect of the lead vehicle brake lights.

## 1.2    Research Objectives

The objectives of this research are 1) to investigate the start time of driver reaction in various car-following conditions, 2) to develop a car-following model that reproduces the observed car-following behaviour – i.e., intermittent start time of acceleration/deceleration and realistic ranges of variables such as speed, spacing, acceleration and jerk, and 3) to investigate the effects of lead vehicle type (car and truck) and the lead vehicle brake lights on driver reaction.

## 1.3    Contributions

This thesis has the following contributions:

- This study demonstrates that drivers accumulate the evidence for acceleration and deceleration over time in various car-following conditions and react when the accumulated evidence reaches a threshold. This new finding is in contrast with the assumptions of a fixed reaction time or threshold in the conventional car-following models.

- This study also develops a new-car-following model that adapts intermittent nature of the driver's reaction to accurately reproduce the start and the magnitude of the driver reaction in different car-following conditions.

- The new car-following model can generate more realistic vehicle trajectories of speed, acceleration, jerk, and spacing, which are fundamental input data for the estimation of traffic delay, crash risk, and vehicle fuel consumption and emission.

- The new car-following model can include various pieces of evidence available to a driver from a road scene. That includes the type of lead vehicle, leakage of evidence due to driver distraction, the effect of lead vehicle brake lights, the effect of the presence of a connected and autonomous vehicle, etc.

## 1.4    Outline of Thesis

This thesis includes 7 chapters. This chapter (Chapter 1) introduced the background and the research objectives of this study.

Chapter 2 reviews the previous research on the car-following behaviour and the assumptions and limitations of various existing car-following models. This chapter also discusses the key requirements for developing a model for predicting more realistic car-following behaviour.

Chapter 3 explains the existing theoretical frameworks of developing driver behaviour models including car-following models. This chapter also explains the concepts and variables used in the development of models based on the driver perception system.

Chapter 4 presents hypotheses on the start time of driver reaction in car-following condition. Three hypotheses were tested based on the assumptions of the reaction time in the existing car-following models and the current literature on driver perception abilities. The chapter describes the method of data collection using a driving simulator for testing

the described hypotheses and modeling the car-following behaviour. The chapter also explains real-world vehicle trajectory data for validating a new car-following model developed in this thesis.

Chapter 5 develops a new car-following model and describes the functional specification and the characteristics of the model. The chapter also discusses the measures used to compare the performance among the existing and new car-following models. The chapter explains the methods of calibrating and validating the car-following models.

Chapter 6 presents the results of hypothesis testing and the evaluation of the new car-following model developed in Chapter 5. The chapter also extensively discusses the features and the applications (such as safety evaluation) of the new car-following model.

Lastly, Chapter 7 draws conclusions based on the findings. The chapter also recommends future studies.

# Chapter 2:  Literature review

The purpose of traffic flow theory is to present models that can reliably predict the state of road traffic in refined time scales. Knowing the future state of traffic helps engineers devise the traffic control strategies for optimal and safe traffic flow. Macroscopic traffic flow models describe the behaviour of a traffic stream as fluid flow where all particles (vehicles) are assumed to be identical. With an increase in number of vehicles with different types and variation in driving styles over the last 70 years, macroscopic models are inadequate to characterize and understand the patterns in traffic flow and road incidents.

In this regard, microscopic traffic flow models describe the combined behaviour of a driver-vehicle unit during longitudinal movement in a lane and lateral movement while changing lanes. The former is termed as 'Car-following behaviour' that predicts the speed or acceleration of a subject vehicle in a lane in different conditions. These conditions are driving in free-flow ("Free-driving"), approaching a slow or stopped lead vehicle ("Approaching"), following a lead vehicle at small distance but similar speed ("Following"), braking in urgent/non-urgent conditions ("Braking") and accelerating behind an accelerating lead vehicle (Treiber and Kesting, 2013). A car-following model is considered to be a *complete* model only when it can predict the speed or acceleration of a subject vehicle in all of the conditions described above (Treiber and Kesting, 2013).

Car-following models are used in microscopic traffic simulation software to simulate vehicle trajectories. These vehicle trajectories can be used for various applications such as the estimation of vehicle emissions and surrogate measures of safety. Furthermore, car-following models can be used to simulate mixed traffic flow of large trucks and cars, as well as the mixed traffic flow of human-driven vehicles and self-driving vehicles.

Therefore, it is essential for a car-following model to realistically predict speed, acceleration, and distance (spacing) to the lead vehicle. If the physical properties of the subject vehicle and its lead vehicle are known, a descriptive equation can capture the car-following behaviour. However, this modeling process becomes non-trivial when the complex human decision making process of a driver is taken into account (Hancock, 1999). Therefore, understanding a normative driver behaviour is important for the development of vehicle control and safety systems (Kim and Lovell, 2005). Hence, since early 1950s, many studies on understanding and modeling of car-following behaviour have been performed. This chapter describes these studies, models, and their limitations. The purpose of this chapter is to ascertain the main requirements for a car-following model to realistically reproduce the actual car-following behaviour of drivers.

This chapter is structured as follows. Section 2.1 describes the studies on observed car-following behaviour. Section 2.2 describes the existing car-following models developed on the basis of equations of motion. Section 2.3 explains the perception abilities of human drivers and how some studies incorporated them in car-following models. Finally, Section 2.4 describes the car-following models developed based on drivers' cognitive abilities. Each section lists the assumptions and limitations of these existing car-following models.

## 2.1    Observed Car-following Behaviour

This section describes various past studies on the car-following behaviour observed in the field and the laboratory. Section 2.1.1 discusses the stimuli that drivers use to perceive car-following conditions. Sections 2.1.2 and 2.1.3 review the studies on the start time of driver

reaction and its magnitude, respectively. Finally, Section 2.1.4 discusses the studies on the effects of the subject and lead vehicle type on car-following behaviour.

### 2.1.1 Stimuli in Car-following

There is an unsettled debate in human visual system literature about what exactly a driver sees in a road scene to make car-following decisions (Green, 2017a). A driver encounters various stimuli while following a vehicle. These stimuli are classified into physical and perceptual categories (Green, 2017a).

The *physical* stimuli include speed difference between the lead and subject vehicles, i.e., 'relative speed' (subject vehicle speed minus lead vehicle speed), spacing (bumper to bumper distance to the lead vehicle), and the size of the lead vehicle. However, the information in the physical stimuli is often unknown or partially known to the driver. For example, drivers do not know the speed of the lead vehicle, the speed difference with the lead vehicle, and the spacing.

However, drivers can indirectly perceive relative motion using the angle subtended by the rear of the lead vehicle's width or height on a driver's eye which is a *perceptual* stimulus called visual angle. An increase in visual angle over time indicates a decrease in spacing (Green, 2017a). Moreover, the speed of increase in visual angle, called angular velocity, indicates how fast the image of the lead vehicle grows on the driver's retina – i.e., how fast a driver is approaching a slower lead vehicle. Similarly, the time-to-collision to a slower lead vehicle is also measured by a perceptual stimulus called tau ($\tau$) (Lee, 1976). These perceptual stimuli are available subconsciously at a driver's eye and serve as indirect sources of car-following information. Tau is coincidentally equivalent to the time-to-

collision (TTC) which can also be calculated using physical stimuli (i.e., spacing and relative speed). Therefore, using the perceptual stimuli in car-following modeling process, instead of physical stimuli, seem to be a better approach.

Perception threshold of a stimulus is defined as the minimum detectable value of that stimulus by a driver. Thus, it is assumed that the driver's control of gas/brake pedal is intermittent, i.e., a driver starts a reaction (acceleration/deceleration) only after a stimulus (e.g., angular velocity) exceeds the driver's perception threshold of the stimulus.

### 2.1.2 Start time of Driver Reaction

Markkula (2014) argued that a driver does not always start a reaction at a fixed perception threshold in all car-following conditions. For instance, it has been found that in urgent conditions, drivers start deceleration at empirically measured perception thresholds, but in routine following, drivers reacted at much larger values of stimuli than the perception thresholds. For instance, past studies have reported a wide range of angular velocity thresholds - 0.0001 to 0.04 radians/s at which the drivers started their reaction in the field or the laboratory (Michales, 1963; Todosiev, 1963; Hoffman, 1994; Hoffman and Mortimer, 1996; Summala et al., 1998; Lamble et al., 1999; Brown et al., 2002; Maddox and Kiefer, 2012; Markkula et al., 2016).

This difference in start times of driver reaction implies that the driver's decision-making processes are different between following and urgent braking conditions. However, near-accident conditions that require urgent braking are generally rare. Therefore, Markkula (2014) raised the question "from where does the, albeit limited, near-accident ability of handling pedals and steering wheel come, if not from routine driving experience?"

Therefore, Markkula (2014) proposed the evidence (stimulus) accumulation framework which assumes that driver's brake reaction starts only after the accumulated stimulus exceeds the threshold, instead of an instantaneous stimulus that exceeds a fixed perception threshold. Markkula et al. (2021) concluded that the evidence accumulation framework can explain the start time of driver's reaction more realistically than a fixed perception threshold. However, the evidence accumulation framework has not been evaluated to predict the start time of reaction in other car-following conditions such as approaching a slow or stopped lead vehicle.

### 2.1.3 Magnitude of Acceleration

In addition to determining the start time of driver reaction, it is critical to accurately estimate the magnitude of acceleration (positive or negative) in different conditions for a realistic modeling of the car-following behaviour. Lee (1976) proposed that a driver modulates the deceleration rate using 'tau-dot' ($\dot{\tau}$), i.e., the rate of change of time-to-collision (= spacing divided by speed difference between lead and following vehicles) called tau ($\tau$).

According to Lee (1976), a driver needs to maintain a constant tau-dot of -0.5 to stop just behind the lead vehicle or a constant tau-dot of greater than -0.5 to follow the lead vehicle at a safe spacing. Past studies validated the assumption of constant tau-dot (Yilmaz and Warren, 1995). If tau-dot is constant, the deceleration rate is not constant (i.e., the brake force continuously varies). In this regard, Green (2017b) suggested that the driver "would brake hardest at first and then gradually ease off as he slows and nears the lead vehicle". However, some studies found that drivers did not apply harder brake followed by

gradual ease-off unlike the assumption of constant tau-dot. For instance, Wang et al. (2016) found that drivers initially applied the brake moderately and then held the brake pedal. If the drivers perceived that they would not be able to avoid the hazard by moderate braking, they changed to full brake application (Wang et al., 2016).

Another recent naturalistic driving study showed that in urgent braking conditions, the jerk (i.e., the rate of change in deceleration) was directly proportional to the magnitude of perceptual stimuli, i.e., angular velocity or tau, at the start of braking (Markkula et al., 2016). Thus, there is a need to investigate whether drivers modulate deceleration rate at a constant tau-dot or apply deceleration proportional to the magnitude of stimulus.

### 2.1.4 Types of Subject and Lead Vehicles

Ossen and Hoogendoorn (2011) found that the variation in speeds during car-following was smaller for trucks than cars. Truck drivers drove mostly at a constant speed and were less likely to restore their desired spacing. However, passenger car drivers were more likely to keep their desired spacing by adjusting their speeds frequently. Furthermore, Sarvi and Ejtemai (2011) observed that truck drivers kept longer time headway (bumper-to-bumper time difference) and spacing than passenger car drivers on freeways.

Similarly, the type of lead vehicle also influences car-following behaviour. Aghabayk et al. (2012) observed that a heavy-vehicle following the lead heavy-vehicle (H-H) had longer spacing and time headway than a car following the lead car (C-C). They also observed that for speeds lower than 30 km/h, both headway and spacing were higher for the car following heavy-vehicle (C-H) than the heavy-vehicle following car (H-C). However, the opposite was observed for speeds greater than 30 km/h. They also found that

the driver's reaction time (time taken by the subject vehicle's driver to react to the lead vehicle's acceleration or deceleration) was longer for the H-H case (2.0 s) than the C-C case (1.8 s). The reaction times were the same between the C-H and H-C cases (1.9 s).

## 2.2 Modelling Car-following Behaviour

A car-following model is a microscopic traffic flow model that describes the dynamics of traffic in a lane from the perspective of individual driver-vehicle units (Treiber and Kesting, 2013). The term "driver-vehicle" unit emphasizes that car-following behaviour depends on both driver characteristics (estimation abilities, perception-reaction time, etc.) and vehicle dynamics such as acceleration and braking capabilities. The goal of the car-following model is to accurately compute the speed/acceleration of a vehicle in any car-following condition at a given time instance. Therefore, a model is *complete* only if it can describe the behaviour in all car-following conditions.

Car-following model assumes that the following vehicle (subject vehicle) only responds to the movement of the lead vehicle in the current lane. Fig. 2-1 illustrates a car-following scenario in a single lane where the subject vehicle $i$ follows the lead vehicle $i$-1.
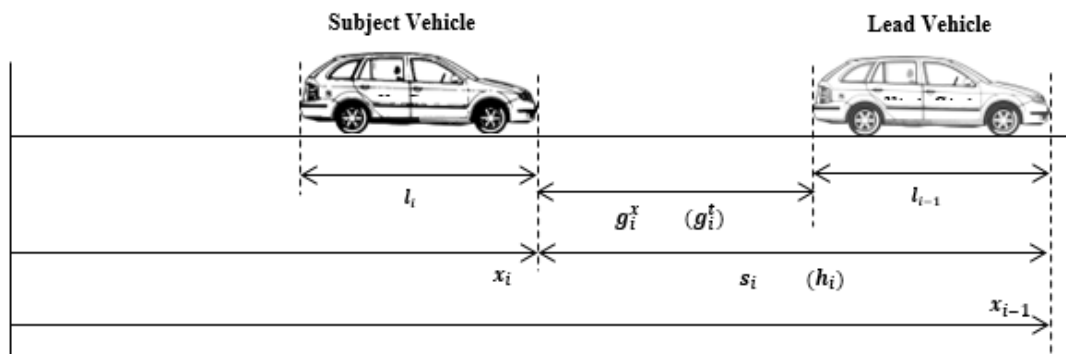


**Fig. 2-1. A car-following scenario (adapted from Ni (2015))**

The variables in the figure at time $t$ are defined as follows:

$x_i$ = position (m) of subject vehicle $i$;

$x_{i-1}$ = position (m) of lead vehicle $i$-1;

$v_i, a_i$ = speed (m/s) and acceleration (m/s$^2$) of vehicle $i$, respectively;

$v_{i-1}, a_{i-1}$ = speed (m/s) and acceleration (m/s$^2$) of vehicle $i$-1, respectively;

$l_i, l_{i-1}$ = lengths (m) of vehicle $i$ and $i$-1, respectively;

$g_i^x$ = spacing (m) between rear bumper of vehicle $i$-1 and front bumper of vehicle $i$ (front-to-rear spacing);

$g_i^t$ = time headway (s) between rear bumper of vehicle $i$-1 and front bumper of vehicle $i$;

$s_i$ = spacing (m) between front bumper of vehicle $i$ -1 and front bumper of vehicle $i$;

$h_i$ = time headway (s) between front bumper of vehicle $i$ -1 and front bumper of vehicle $i$.

There are several types of car-following models such as engineering models, psychophysical models, driver behaviour model in cognitive architecture, and artificial intelligence (AI) models. Some artificial intelligence models, based on fuzzy-logic and/or neural-nets, can mimic drivers' perception abilities along with traffic dynamics. Although the AI models can predict driver behaviour well, they cannot identify the effects of driver characteristics or vehicle types on car-following behaviour because they are predictive rather than explanatory in nature (Aghabayk et al., 2015). Additionally, the models have a tendency to overfit the observed data and they are unable to predict car-following

behaviour for previously unobserved traffic conditions. Furthermore, they require a huge amount of data for training and prediction. Moreover, defining fuzzy sets is not a trivial task in context of car-following behaviour due to variance in human behaviour. Therefore, only first three types of car-following models will be discussed in this chapter.

### 2.2.1 Engineering car-following models

The engineering car-following models include stimulus-reaction, optimal velocity, collision-avoidance and desired-headway models (Saifuzzaman and Zheng, 2014). These models do not account for drivers' perception abilities. However, these models are fundamental to understand the critical factors in car-following behaviour and provide basis for more advanced models. In general, these models use the equations of motion with suitable assumptions in car-following context. Different engineering car-following models are summarized in Table 2-1. The assumptions and limitations of these models are discussed as follows.

*Stimulus-reaction Models*

The stimulus-reaction models assume that the reaction (positive, negative or no acceleration) of a subject vehicle's driver depends on input signals called "stimuli" – e.g., relative speed and spacing - and driver's sensitivity to the stimuli. The model also assumes that driver's reaction occurs after a perception-reaction time.

For instance, the General Motors (GM) models (Chandler et al., 1958; Gazis et al., 1961) are the most commonly used stimulus-reaction models. The models have been developed after extensive field experiments and improvements. The non-linear GM model (Gazis et al. 1961) considered both relative speed and spacing as stimuli, and the driver's response

to the stimuli depends on current speed of subject vehicle. The mathematical expression of

GM model is shown in Table 2-1.

**Table 2-1. Engineering Car-following Models**

| Model | Equations |
|---|---|
| General Motors Model (Gazis et al., 1961) | $$a_i(t + \tau_i) = \alpha \frac{v_i(t + \tau_i)^m \cdot [v_{i-1}(t) - v_i(t)]}{[x_{i-1}(t) - x_i(t)]^l}$$ $\tau_i$ = reaction time, $\alpha$, $m$ and $l$ = the calibration parameters |
| Optimal Velocity Model (Bando et al., 1998) | $$a_i(t + \tau_i) = \frac{v_{opt}(t) - v_i(t)}{\tau_{adapt}}$$ $v_{opt}(t)$ = optimal velocity, $\tau_{adapt}$ = the time to adapt the current speed to optimal speed |
| Full Velocity Difference Model (Jiang et. al., 2001) | $$a_i(t + \tau_i) = \frac{v_{opt}(t) - v_i(t)}{\tau_{adapt}} - \gamma \Delta v$$ $$v_{opt}(t) = \max\left[0, \min\left(v_0, \frac{g^x(t) - g_0^x}{\tau_i}\right)\right]$$ $\Delta v$ = relative velocity, $\gamma$ = a calibration parameter, $v_0$ = the free-flow speed, $g^x$ = the current front-to-rear spacing, and $g_0^x$ = the minimum standstill spacing |
| Gipps Model (Gipps, 1981) | $$v_i(t + \tau_i) = \min \begin{cases} v_i(t) + 2.5 A_i \tau_i \left(1 - \frac{v_i(t)}{v_0}\right)\sqrt{0.025 + \frac{v_i(t)}{v_0}} \\ \qquad \text{if free driving} \\ -b_i \tau_i + \sqrt{b_i^2 \tau_i^2 - b_i \left[-v_i(t)\tau_i - \frac{v_{i-1}^2(t)}{B_{i-1}} - 2l_{i-1} + 2s_i(t)\right]} \\ \qquad \text{if following} \end{cases}$$ $\tau_i$ = reaction time including safe buffer time $A_i$ = the maximum desired acceleration starting from standstill $b_i$ = the comfortable maximum deceleration of subject vehicle $B_{i-1}$ = most severe lead vehicle deceleration that the following vehicle estimates, $l_{i-1}$ = the length of lead vehicle, $s_i(t)$ = the current front-to-front spacing |
| Intelligent Driver Model (IDM) (Treiber and Kesting, 2013) | $$a_i(t) = A_i \left[1 - \left(\frac{v_i(t)}{v_0}\right)^\delta - \left(\frac{g_i^*(t)}{g_i^x(t)}\right)^2\right]$$ $$g_i^*(t) = g_0^x + \max\left(0, v_i(t)g_i^t(t) + \frac{v_i(t)\Delta v(t)}{2\sqrt{A_i b_i}}\right)$$ $\delta$ = a calibration parameter, $g_i^*(t)$ = the current desired front-to-rear spacing, $g_i^t(t)$ = the current front-to-rear time headway |

However, the GM models have several limitations as follows. First, the values of the calibration parameters ($m$, $l$ and $\alpha$) which produce the best model performance are different in different conditions. For example, $m = 0$ and $l = 1$ performed well when the traffic flow was uncongested, but they did not perform well in congested conditions (Brackstone and McDonald, 1999). These results indicate that separate car-following models can be developed for congested and uncongested conditions.

Second, the GM model does not consider driver's desired spacing during the following condition (Aghabayk et al., 2015). This means that driver will not respond if the relative speed is zero regardless of the current spacing. However, this assumption is not realistic. Third, the GM model does not consider vehicle capabilities, i.e., maximum acceleration or deceleration. Therefore, the model cannot accurately predict the car-following behaviour of larger vehicles, particularly trucks. Fourth, the GM model assumes that the reaction time is the same for all drivers and drivers will respond to a small change in relative speed even at a very large spacing (Saifuzzaman and Zheng, 2014). These assumptions are also unrealistic because drivers have a limited capability of perceiving relative speed and spacing (Michaels, 1963). Finally, the GM model can only predict acceleration in the Following condition, but not in the other car-following conditions.

*Optimal Behaviour Models*

The optimal behaviour models assume that a subject vehicle's driver always tries to adapt its current speed to an optimal velocity in a given traffic situation during some adaptation time. For instance, the Optimal Velocity Model (OVM) (Bando et al., 1998) assumes that drivers choose the optimal velocity based on their desired speed in free flow and minimum

front-to-rear spacing when the lead and following vehicles stop. The equation of the OVM is shown in Table 2-1.

Treiber and Kesting (2013) tested the OVM for the traffic on highway and city streets, and concluded that predicted accelerations were unrealistic because the model does not consider relative speed. However, the model is unrealistically sensitive to driver's reaction time (Saifuzzaman and Zheng, 2014). Moreover, the assumption of an 'optimal velocity' that a driver strives to achieve is questionable as driving is a satisficing task rather than an optimizing task.

Jiang et al. (2001) extended the OVM to develop the Full Velocity Difference Model (FVDM) which considers both negative and positive relative speeds as shown in Table 2-1. They found that the FVDM realistically predicted the subject vehicle's accelerations based on relative speed. However, the model ignores the association of relative speed with spacing. For instance, the model assumes that a subject vehicle will decelerate even if a slow lead vehicle is very far ahead. So, even on a long road with no other vehicles, the subject vehicle does not reach free-flow speed. Moreover, the FVDM uses the same function for both acceleration and deceleration although driver behaviour is different in these circumstances (Saifuzzaman and Zheng, 2014). Moreover, similar to the stimulus-reaction models, the OVM and FVDM do not incorporate the driver's perception abilities and vehicle capabilities (e.g., maximum deceleration).

*Car-following Models based on Driving Strategies*

Some car-following models account for vehicle capabilities and drivers' control strategies to overcome the limitations of the stimulus-reaction models and the optimal behaviour models. Gipps (1981) proposed two separate car-following models, one for free-driving

20

and other for the following condition as shown in Table 2-1. The Gipps' model for the free-driving condition assumes that the driver applies maximum acceleration to reach the desired free-flow speed. The Gipps' model for the following condition assumes a safety rule - "The subject vehicle's driver selects the speed to bring the vehicle to a safe stop when the lead vehicle comes to a sudden stop" (Gipps, 1981). For safe stopping, the Gipps' model incorporates a safe buffer time equal to half of reaction time in addition to the braking time and perception-reaction time. For each time step, the minimum of the two speeds is selected as the subject vehicle's speed.

The Gipps' model is the simplest car-following model that realistically predicts accelerations and assumes that vehicle collisions do not occur (Treiber and Kesting, 2013). However, the Gipps' model underestimates the observed capacity and traffic volumes (Treiber and Kesting, 2013) because drivers do not always keep the safe distance (= current speed × a half of reaction time) as calculated in the model (Brackstone and McDonald, 1999; Aghabayk et al., 2015). Moreover, the Gipps' model does not consider the driver's perception abilities similar to the other engineering car-following models discussed above. Therefore, the model assumes that the driver reacts to even very small changes in speed and spacing (Aghabayk et al., 2015).

Similar to the Gipps' model, the Intelligent Driver Model (IDM) also considers driving strategies (Treiber and Kesting, 2013). The IDM predicts the subject vehicle's acceleration based on the desired front-to-rear spacing as shown in Table 2-1. The IDM compares the current speed to the desired speed and current spacing to the desired spacing to determine the acceleration. Similar to the Gipps' model, the IDM produces realistic acceleration/deceleration rates based on maximum acceleration and comfortable

21

deceleration (Saifuzzaman and Zheng, 2014). However, unlike the Gipp's model, the safe

distance varies with not only current speed, but also the driver's desired speed in the IDM.

This assumption of the IDM is more realistic because the safe distance cannot be the same

for all drivers.

The term 'intelligent' in the IDM refers to the intelligent acceleration and braking

strategy as expected by human drivers. The maximum acceleration that can be applied in

free-flow is the term, $A_i \left[ 1 - \left( \frac{v_i}{v_0} \right)^\delta \right]$, where the current speed is compared with the free-

flow speed and the acceleration decreases as the current speed increases. Higher value of

the parameter $\delta$ implies higher maximum acceleration for the current speed. When the

subject vehicle approaches a slow lead vehicle, the term, $\frac{v_i \Delta v}{2\sqrt{A_i b_i}}$, is the deceleration required

to reach the desired spacing $(g_0^x + v_i g_i^t)$ in the following condition.

The IDM has been modified several times to reflect the real-world traffic conditions and

driver behaviour (Treiber and Kesting, 2013). An example of a modified IDM is the 2D-

IDM that considers the difference between the driving behaviors at high speeds and low

speeds in the framework of three-phase traffic theory (Tian et al., 2016). The time headway

parameter $g_i^t$ in 2D-IDM is not a constant but a variable based on the range of time

headway variation in the congested steady-state traffic. However, similar to the IDM, 2D-

IDM does not consider the driver reaction time.

Although the IDM considers drivers' control strategies, it does not incorporate their

perception abilities. This results in smooth transition from one car-following state to

another (e.g. free flow to approaching). However, this behaviour is not realistic since the

driver's acceleration behaviour drastically changes from one car-following state to another

(Treiber and Kesting, 2013). In fact, both IDM and Gipps' model better represent the semi-automated driving by Adaptive Cruise Control than human driving (Treiber and Kesting, 2013) .

In summary, the main limitation of the engineering car-following models is that the models do not consider the driver's perception abilities. Moreover, the use of a fixed or no reaction time in these car-following models does not reproduce the intermittent start time of reaction as discussed in section 2.1.2. As a result, even when the predicted magnitudes of acceleration and jerk are within the range of actual magnitudes, the predicted trajectories of acceleration and jerk are drastically different from the actual trajectories. Specifically, the start time and duration of speed adjustments predicted by these models are significantly different from the observed start time and duration. Furthermore, the current model framework cannot explicitly consider the influence of type of lead vehicle (car/truck) on the subject vehicle.

### 2.2.2  Psychophysical Car-following Models

A common limitation of the engineering car-following models is that they assume drivers adjust their speed only based on physical stimuli such as relative speed and spacing. However, according to Boer (1999), this assumption is unrealistic as drivers cannot accurately perceive relative speed and spacing. Instead, drivers adjust their speed based on perceptual stimuli. These perceptual stimuli include visual angles subtended by objects (e.g., lead vehicle), tau (visual angle divided by rate of change in visual angle), etc. Fig. 2-2 illustrates the horizontal visual angle subtended by the lead vehicle on the subject driver's eyes during a car-following condition. This angle changes as both lead and

following vehicles move in the same lane. The perceptual stimuli are described in detail in Chapter 3.
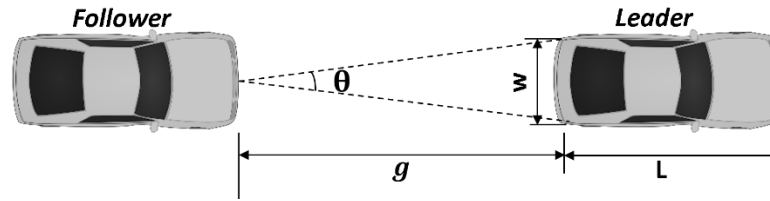


**Fig. 2-2. Horizontal visual angle subtended by the lead vehicle**

Unlike the engineering car-following models, the psychophysical car-following models consider drivers' perception abilities. Two different psychophysical car-following models, the Wiedemann model (Wiedemann and Reiter, 1992) and the Fritzche model (Fritzsche and Ag, 1994) have been used. These two models are different in terms of perception thresholds – the Wiedemann model uses the thresholds of relative speed and spacing whereas the Fritzsche model uses the thresholds of relative speed and time headway (instead of spacing). However, the acceleration equations of the Fritzsche model are not publicly available.

Few past studies investigated the speed and acceleration patterns in multiple car-following conditions such as free-driving, approaching a slow vehicle and following at the speed similar to the lead vehicle's speed (Todosiev, 1963; Michaels, 1963; Hoefs, 1972). Wiedemann (1974) combined the observations in these studies to propose a theoretical framework for a psychophysical car-following model that captured driver's perception limits and explained the corresponding reactions (accelerations) in a given car-following condition. The Wiedemann model incorporates the heterogeneity in driver estimation

abilities, safety needs and vehicle control using normally distributed random parameters. All random parameters range from 0 to 1 with a mean value of 0.5 and standard deviation of 0.1. Furthermore, the model assumes that drivers will always accelerate or decelerate whenever relative speed or spacing exceeds a threshold of relative speed or spacing (perception threshold). The thresholds and car-following states as defined in the Wiedemann model are described in detail in Chapter 3.

*Limitations in psychophysical car-following models*

Psychophysical car-following models account for driver's perception, skills and needs using normally distributed random parameters in functions of perception thresholds and accelerations in different car-following conditions. However, these random parameters do not explicitly describe why the perception thresholds vary between drivers in the same conditions. There is a need for studies that test the hypothesis of a fixed perception threshold of a stimulus (e.g., angular velocity) and the hypothesis of the accumulation of a stimulus to a threshold based on the evidence accumulation framework proposed by Markkula (2014) (refer to section 2.1.2)).

Similar to engineering car-following models, psychophysical car-following models do not distinguish the driver behaviour behind different types of lead vehicles. Peeta et al. (2005) found that passenger car drivers feel discomfort around a truck and they want to keep longer spacing behind the lead trucks. Moreover, a lead truck's height is significantly larger than a lead car. However, there is a lack of research on how different stimuli could affect driver behaviour between a car driver following a lead car and a car driver following a lead truck.

### 2.2.3   Driver behaviour models in a cognitive architecture

A few studies have modeled the actions (steering, accelerate, decelerate, etc.), rather than predicting the speed or acceleration, in a framework of a cognitive architecture (Salvucci, Boer and Liu, 2001; Salvucci, 2006). According to Salvucci et al. (2001), a "cognitive architecture is a theory of human cognition and perceptual-motor actions that provides a rigorous framework for building, running, and testing computational models of human behaviour". The model is called the "driver behaviour model" because it mimics driver's decision-making process and control actions. For instance, Salvucci et al. (2001) developed the models for steering and acceleration based on visual angle and headway in a cognitive architecture.

The cognitive architecture can realistically capture driver behaviour - e.g., forgetfulness, error, attention-allocation, and eye and foot movements. A cognitive architecture, such as Adaptive Control of Thought-Rational (ACT-R), contains three main components: 1) knowledge representation, 2) performance and 3) learning (Salvucci, Boer and Liu, 2001; Carnegie Mellon University, 2002). These components are modelled as several independent modules that work together to perceive, decide and act to achieve a certain task (e.g., steer right, push accelerator pedal, etc.).

Knowledge is represented in two aspects: factual knowledge and skill knowledge. Factual knowledge contains information about perception (e.g., location of lane markings), situation (e.g., a vehicle in blind spot), and navigation (e.g., destination is at exit 5). The perceptual module updates this knowledge for the current situation. Skill knowledge is specified by the analyst as condition-action rules (i.e., an action is taken when a condition is satisfied). For instance, "IF the current goal is to steer and all perceptual variables for

26

steering have been noted, THEN control steering according to these variables" (Salvucci et al. 2001).

There are several advantages of the driver behaviour model in ACT-R. First, the perception limits and memory aspects of drivers are directly incorporated in the modules which are regularly updated in accordance with the latest research (Carnegie Mellon University 2002). Second, as the model is estimated for each driver separately, the model can be used to study heterogenity in driving control strategies due to drivers' different driving needs.

In the model, a condition-action rule is specified for all drivers and the coefficients of independent parameters are estimated. The driver behaviour model helps comprehensively understand the driver's needs, strategies and behaviour. However, due to complexity of the model, it is computationally expensive to calibrate a number of condition-action rules for many individual drivers. Also, the calibration method is not currently available. Thus, researchers have assigned the values of parameters using their subjective judgments (Salvucci et al., 2001; Salvucci, 2006). Moreover, this driver behaviour model has not been applied to the prediction of car-following behaviour.

### 2.2.4 Markkula framework of sensorimotor control in sustained motion tasks

Markkula et al. (2018) proposed a general framework for sustained motion tasks that uses the human perception ("sensori-") and movement ("motor"). Examples of sustained motion include using a mouse to track an object on a screen, steering, urgent braking, etc.

The outputs of this framework are the prediction of the start time of reaction and the magnitude of the reaction. The required inputs are the evidence for the need of control. For

example, the evidence for the emergency braking condition is the perceptual stimulus in the form of angular velocity or tau-inverse (discussed in Chapter 3). However, unlike the psychophysical car-following models, Markkula framework does not compare only a single value of the evidence (angular velocity) with a threshold. Instead, Markkula framework assumes that driver accumulates the evidence over time and reacts only when that accumulated evidence reaches a pre-defined threshold (Markkula et al., 2018). Moreover, the magnitude of reaction - e.g., the brake pedal force - is assumed to be correlated with the evidence at the start of the reaction.

Markkula framework has been successful in modeling of driver steering as well as urgent braking conditions (Markkula, 2014; Markkula et al., 2018). However, Markkula framework is not a complete car-following model as it does not currently predict the acceleration in all car-following conditions. The details of this framework are discussed in Chapter 3.

## 2.3    Chapter Summary

This chapter reviewed the empirically observed car-following behaviour and the existing car-following models which predict the subject vehicle behaviour based on the lead vehicle motion. The main findings from the literature review are summarized as follows:

- Conventional car-following models use physical stimuli such as speed difference and distance to lead vehicle (spacing) to predict speed and acceleration of the subject vehicle. These models predict driver reaction even when the stimulus is

28

negligible. Thus, these models do not account for the limits in human perception abilities.

- Some car-following models use perceptual stimuli to predict the subject vehicle behaviour. These models assume that drivers instantaneously react whenever the stimuli exceed a threshold. However, recent studies suggested that drivers react only when the accumulated perceptual stimuli over time reach a threshold.

- In the existing car-following models, driver reaction in terms of acceleration and deceleration is assumed to be a function of physical stimuli or a heuristic such that a fixed value of rate of change in tau (perceptual stimulus which is mathematically equivalent to time-to-collision) is maintained while decelerating. However, recent studies suggests that deceleration rate in urgent braking condition is described as a function of perceptual stimuli at the start of braking.

- Most car-following models are incomplete as they only predict speed and acceleration in the close following condition with a short spacing but not in the conditions when a driver approaches a slow or stopped vehicle with a large spacing. Moreover, car-following models do not differentiate the type of lead vehicle.

- There is a lack of studies that predicted car-following behaviour based on the start time of reaction, the magnitude of reaction, and the effect of lead vehicle type in various car-following states.

# Chapter 3:  Theoretical Frameworks

This chapter comprehensively explains the theoretical frameworks used in this study to analyze and model the observed car-following behaviour. Specifically, the following discussion describes the sensory evidence that a driver is assumed to use to perceive and respond to a slow or decelerating lead vehicle. Subsequently, the theory behind the drivers' use of the sensory evidence in the Wiedemann car-following model is described. Furthermore, the derivation of the acceleration equations in the Wiedemann model, that explain the driver response, is also presented. Lastly, an alternative theory of the use of sensory evidence that affects both start time and magnitude of the driver response is discussed. The next two chapters build on the theories presented in this chapter to explain the data collection procedures and the methods of analyses used in this study.

## 3.1 Sensory Evidence in Car-following

Chapter 2 provided a review of the engineering car-following models. These models assume that drivers use physical stimuli such as speed difference and spacing to continuously respond to a lead vehicle. However, in order to determine the speed difference and spacing, drivers need access to other physical stimuli such as the size and speed of the lead vehicle. Furthermore, drivers are unable to perceive the depth-in-motion (i.e., the spacing) because the design of the human eye could only form a two-dimensional image of a three-dimensional road scene. Thus, drivers must rely on their visual system for the perception of motion relative to a lead vehicle. Green (2017d) explained that this perception happens using the "sensory evidence" available at the eye of the driver, without any cognitive effort to mentally reconstruct the three-dimensional road scene and infer the

spacing and speed difference. The various available pieces of sensory evidence are explained below.

### 3.1.1 Sensory evidence for the direction of motion

When a driver in the subject vehicle looks at the rear of a lead vehicle, the image is projected on his/her eye. This is illustrated in Fig. 3-1. Visual angle subtended by a lead truck on a driver's eye (a). In this example, the subject vehicle (car) is moving faster than a lead truck which is moving at a uniform speed. Therefore, the front-to-rear spacing ($S$) between them is decreasing with time. Note that there are three measurements of spacing in the car-following literature. The spacing between the front bumper of the subject vehicle and the rear bumper of the lead vehicle ($S$), the front bumper-to-front bumper spacing ($DX$), and the spacing between the eye of the driver and the rear of the lead vehicle. Throughout this thesis, the term 'spacing' means the front-to-rear spacing ($S$) unless otherwise noted.

The rear of a lead truck with width $W$ and height $H$ subtends two visual angles, $\theta_W$ and $\theta_H$, respectively. These visual angles are mathematically expressed as:

$$\theta_W = \frac{W}{S} \tag{3-1}$$

$$\theta_H = \frac{H}{S} \tag{3-2}$$

Fig. 3-1. Visual angle subtended by a lead truck on a driver's eye (a) shows that these subtended visual angles make a two-dimensional image on the driver's retina, with $\theta_W$ and $\theta_H$ dimensions. As Eqs. (3-1) and (3-2) show, at any given time, a visual angle is computed

31

based on width (or height) of a lead vehicle and spacing with a lead vehicle. For instance, the same $\theta_W$ of 0.04 radians is subtended when a lead car with a width of 2.3 m is at a spacing of 57.5 m or a lead truck with a width of 2.6 m is at a spacing of 65.0 m from the subject vehicle.
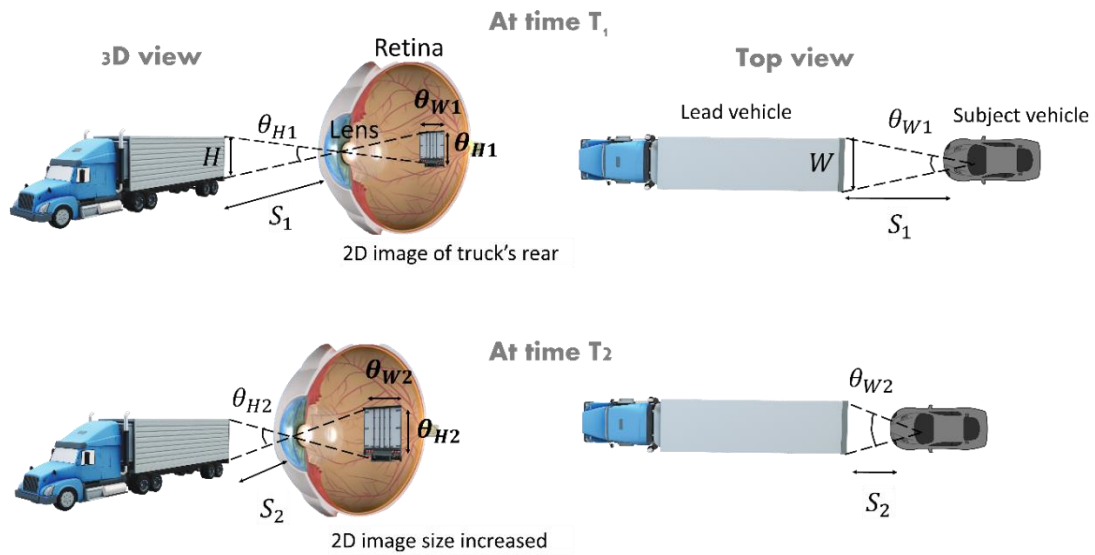


(a) Increase in the visual angles on retina during approaching a slow lead truck (not to scale)

(Sources: Eye - https://youtu.be/Sqr6LKIR2b8,
Car- https://openclipart.org/image/2400px/svg_to_png/190175/SimpleOrangeCarTopView.png,
Truck - https://www.remix3d.com/details/G009SXJ54BV3?section=other-models)
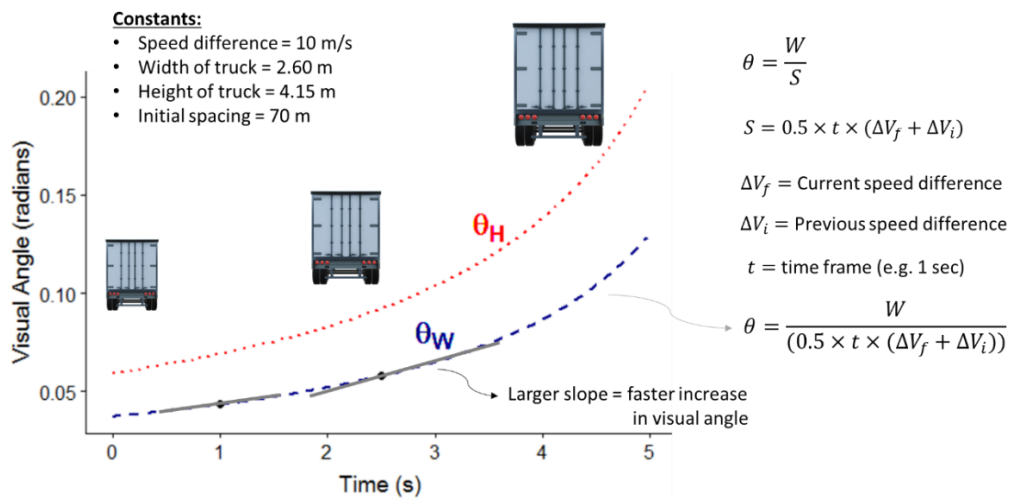


(b) The increase in visual angle with time

**Fig. 3-1. Visual angle subtended by a lead truck on a driver's eye**

32
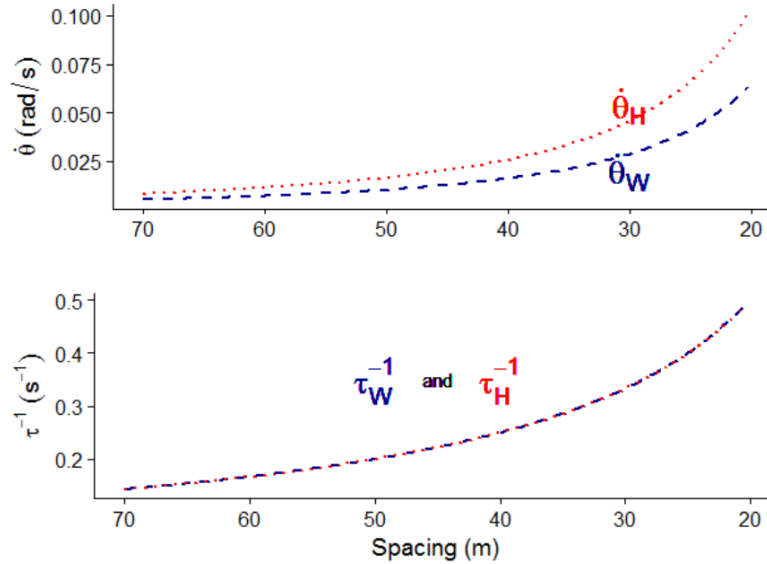
(c) Relationship between looming (angular velocity and inverse tau) and spacing

**Fig. 3-1. Visual angle subtended by a lead truck on a driver's eye (Continued)**

Eqs. (3-1) and (3-2) further show that these visual angles increase as the spacing decreases with time. As illustrated in Fig. 3-1. Visual angle subtended by a lead truck on a driver's eye (a), at time instant $T_1$, the spacing is $S_1$ and the subtended visual angles are $\theta_{W1}$ and $\theta_{H1}$. At the next time instant $T_2$, the spacing decreases to $S_2$ and the visual angles increase to $\theta_{W2}$ and $\theta_{H2}$ (larger projected image). Fig. 3-1. Visual angle subtended by a lead truck on a driver's eye (b) shows the increase in the visual angle as the subject vehicle approaches the slow lead vehicle as the time progresses. The equation for spacing in Fig. 3-1. Visual angle subtended by a lead truck on a driver's eye (b) is one of the equations of motion in Newtonian Physics.

Psychology literature suggests that there is some minimum change in the visual angle ($\Delta\theta$) that can be perceived by drivers which is called as *Just Noticeable Difference (JND)*

33

(Green, 2017d). According to the Weber's Law, the ratio of JND to the original visual angle is a constant (Weber, 1905). This can be expressed as follows:

$$\frac{\Delta\theta}{\theta} = K \tag{3-3}$$

where $\Delta\theta$ is the JND in the visual angle, $\theta$ is the visual angle before the change, and $K$ is a constant. An increase in the visual angle indicates that the subject vehicle is moving towards the lead vehicle whereas a decrease in the visual angle indicates that the subject vehicle is moving away from the lead vehicle. However, the visual angle does not contain the information about the rate of motion. Furthermore, the JND in visual angle is correlated to the JND in spacing. For example, the change in visual angle due to the lead truck width is calculated as follows:

$$\begin{aligned}\frac{\Delta\theta_W}{\theta_{W1}} &= \frac{\theta_{W2} - \theta_{W1}}{\theta_{W1}} \\[2mm]
&= \frac{\left[W/S_2\right] - \left[W/S_1\right]}{\left[W/S_1\right]} = \frac{[W \times (S_1 - S_2)]}{\left[W/S_1\right] \times S_2 \times S_1} \\[2mm]
&= \frac{(S_1 - S_2)}{S_2} = -\frac{\Delta S}{S_2}\end{aligned}$$

$$\tag{3-4}$$

Eq. (3-4) suggests that a driver notices a decrease in spacing because of the increase in the visual angle on his/her eye.

### 3.1.2  Sensory evidence for the rate of motion

Besides the absolute changes in visual angle (or spacing), there is also the rate of change in visual angle over time. This rate of change is illustrated as the slope of the line tangent

to a visual angle curve at a given time as shown in Fig. 3-1. Visual angle subtended by a lead truck on a driver's eye (b). This indicates that the rate of increase in visual angle (also the rate of increase in the projected image size) is smaller at a larger spacing (time = 1 s in Fig. 3-1. Visual angle subtended by a lead truck on a driver's eye (b)) and larger at a smaller spacing (time = 2.5 s). The rate of motion or *angular velocity* is calculated as follows:

$$\frac{d}{dt}(\theta_W) = \frac{d}{dt}\left(\frac{W}{S}\right)$$

Using the quotient rule of differentiation, the angular velocity for the lead vehicle's width ($\dot{\theta}_W$) is derived as follows:

$$\dot{\theta}_W = \frac{S \times \frac{d}{dt}(W) - W \times \frac{d}{dt}(S)}{S^2}$$

$$\dot{\theta}_W = \frac{S \times 0 - W \times \frac{d}{dt}(S)}{S^2}$$

$$\dot{\theta}_W = \frac{-W}{S^2} \cdot \frac{d}{dt}(S)$$

During approaching, the rate of change in spacing is negative as the spacing decreases. Also, the rate of change in spacing is the speed difference: $\Delta V = -\frac{dS}{dt}$. It is negative because the spacing is decreasing. Therefore, the angular velocity for the lead vehicle's width is expressed as follows:

$$\dot{\theta}_W = \frac{W \Delta V}{S^2} \tag{3-5}$$

Similarly, the angular velocity for the lead vehicle's height ($\dot{\theta}_H$) is expressed as follows:

$$\dot{\theta}_H = \frac{H \Delta V}{S^2} \tag{3-6}$$

where $\Delta V$ is the speed difference between the two vehicles (= the subject vehicle speed minus the lead vehicle speed). Fig. 3-1. Visual angle subtended by a lead truck on a driver's eye (c) and Eqs. (3-5) and (3-6) suggest that a driver is less likely to respond to a slow lead vehicle at a large spacing (say > 200 m) because the size of the lead vehicle's image (visual angle) is small and grows very slowly (angular velocity). As the driver gets closer to the lead vehicle (say 40 m), the visual angle is large and it also grows rapidly, which prompts the driver to apply brake. Thus, when the spacing is very short (or the speed difference is very high due to the lead vehicle deceleration), the projected image of the lead vehicle's rear looms over (fills) the retina, which indicates the urgency of the situation. For this reason, the angular velocity is also called as *looming*.

On the other hand, when the angular velocity is very small (e.g., at a spacing > 200 m and speed difference < 1 m/s), the size of the projected image of the lead vehicle's rear increases very slowly. Thus, the driver cannot perceive this change in the image. According to several past studies, the smallest angular velocity which the driver can perceive is called the *perception limit* or the *threshold* of angular velocity (Michaels, 1963; Wiedemann and Reiter, 1992). Thus, the driver can perceive the angular velocity only if the angular velocity exceeds the threshold of angular velocity. However, the threshold of angular velocity varies

among the drivers. Therefore, the threshold is described as a distribution rather than a constant value.

Similar to visual angle and angular velocity, the inverse of Time-To-Collision (*TTC*) is a sensory evidence, which is also called as *looming* in the literature (Markkula, 2014). *TTC* is defined as the time remaining until a collision between two vehicles occurs, given that both vehicles maintain their current speeds. In engineering studies, *TTC* is expressed as follows:

$$TTC = \frac{S}{\Delta V} \tag{3-7}$$

where $S$ is the front-to-rear spacing and $\Delta V$ is the speed difference. As the visual angle is the visual correlate of spacing and the angular velocity is the visual correlate of speed difference, TTC can also be expressed as the ratio of visual angle to angular velocity as follows:

$$TTC = \tau = \frac{\theta}{\dot{\theta}} \tag{3-8}$$

where $\tau$ (tau) is the visual correlate of *TTC*. The inverse of $\tau$ ($\tau^{-1}$) is expressed as follows:

$$\tau^{-1} = \frac{\dot{\theta}}{\theta} \tag{3-9}$$

As the subject vehicle gets closer to the lead vehicle, $\tau$ decreases and $\tau^{-1}$ increases. Fig. 3-1. Visual angle subtended by a lead truck on a driver's eye (c) shows that $\tau^{-1}$ increases

as the spacing decreases similar to $\dot{\theta}$. Therefore, both angular velocity ($\dot{\theta}$) and tau inverse

($\tau^{-1}$) can be used as looming variables.

### 3.1.3   Sensory evidence for control of braking

Angular velocity or tau inverse are the pieces of sensory evidence that a driver uses to perceive a slow or a decelerating lead vehicle. Thus, sufficiently large value of angular velocity or tau inverse prompts a driver to *start* braking. After drivers subconsciously determine the time of braking, they must also determine the *magnitude* of deceleration for safe car-following. Lee (1976) proposed that drivers use the rate of change of tau ($\tau$) to modulate the pressure on the brake pedal to avoid a collision. The rate of change of tau, tau-dot ($\dot{\tau}$), is expressed as:

$$\frac{d}{dt}(\tau) = \frac{d}{dt}\left(\frac{\theta}{\dot{\theta}}\right)$$

$$\dot{\tau} = \frac{d}{dt}\left(\frac{\theta}{\dot{\theta}}\right)$$

$$\dot{\tau} = \frac{d}{dt}\left(\frac{W/S}{\frac{W\Delta V}{S^2}}\right)$$

$$\dot{\tau} = \frac{d}{dt}\left(\frac{S}{\Delta V}\right)$$

$$\dot{\tau} = \frac{\Delta V \times \frac{d}{dt}(S) - S \times \frac{d}{dt}(\Delta V)}{\Delta V^2}$$

$$\dot{\tau} = \frac{\Delta V \times (-\Delta V) - S \times \Delta A}{\Delta V^2}$$

$$\dot{\tau} = \frac{-\Delta V^2 - S \times \Delta A}{\Delta V^2}$$

$$\dot{\tau} = -1 - \frac{S \times \Delta A}{\Delta V^2}$$

$$= -1 + \frac{S \times \Delta D}{\Delta V^2} \tag{3-10}$$

where $\Delta A$ is the acceleration difference (= the subject vehicle acceleration minus the lead vehicle acceleration) and $\Delta D = -\Delta A$. According to Green (2017a), maintaining a constant $\dot{\tau}$ while braking would create the following possible outcomes:

- $\dot{\tau} < -0.5$ $\rightarrow$ hit the lead vehicle

- $\dot{\tau} = -0.5$ $\rightarrow$ stop right behind the lead vehicles

- $\dot{\tau} > -0.5$ and $\dot{\tau} \leq 0$ $\rightarrow$ stop before the lead vehicle

- $\dot{\tau} > 0$ $\rightarrow$ move away from the lead vehicle (appropriate for following at steady-state speed)

Maintaining a constant $\dot{\tau} \geq -0.5$ means that *TTC* (or its visual correlate $\tau$) would decrease at a rate of 0.5 s/s or less. A constant $\dot{\tau}$ also means that the deceleration rate would not be constant - i.e., the brake pedal pressure must be continuously varied. Moreover, it means that the driver "would brake hardest at first and then gradually ease off as he slows and nears the lead vehicle" (Green, 2017a).

The discussion above explained a set of sensory evidence available at the driver's eye that helps him/her decide the start and control of braking. The next section describes two existing, but alternative modeling frameworks that use a few pieces of sensory evidence to model driver perception and reaction.

## 3.2 Theoretical Frameworks for Modeling Car-following Behaviour

As discussed in Chapter 3.1, physical stimuli such as spacing and TTC are not directly accessible to a driver, rather a driver indirectly accesses them via the sensory evidence available at his/her eye. This section explains two different modeling approaches that use the available sensory evidence to predict driver reaction time and magnitude of acceleration in car-following. These two approaches are the Wiedemann's model and the Markkula's model.

### 3.2.1 Wiedemann Model

The Wiedemann (1974) car-following model is a psychophysical model that accounts for perception thresholds of angular velocity (psychology), capabilities of vehicle performance, and equations of motion (physics). The model provides equations for driver reaction (acceleration/deceleration) in different car-following conditions, once a driver perceives a certain car-following condition (Wiedemann and Reiter, 1992; Aghabayk et al., 2013). The model also provides the equations for estimating when drivers perceive different car-following conditions. Thus, unlike other car-following models, the Wiedemann model does not use a perception reaction time but rather uses perception thresholds to control the start time of driver reaction. The discussion in this section is a synthesis of the studies by Todosiev (1963), Hoefs (1972), Wiedemann and Reiter (1992), Aghabayk et al. (2013) and Pariota and Bifulco (2015).

There are four car-following conditions as defined in the Wiedemann model. Fig. 3-2 illustrates the model in a graph of the speed difference (= the subject vehicle speed – the lead vehicle speed) on x-axis and spacing on y-axis. The solid lines and curves represent

the boundaries of car-following conditions, and the dashed line segments (with colours) indicate the trajectory of a subject vehicle with respect to a slower moving lead vehicle (i.e., a positive speed difference).

All four car-following conditions can be understood using the angular velocity formula (Eq. (3-5)) (Pariota and Bifulco, 2015). Note that the Wiedemann model only uses the angular velocity based on the width of lead vehicle (Eq. (3-5)) for defining driver perception thresholds – i.e., the angular velocity at which the driver first perceives a slow lead vehicle, as explained below. The model does not consider the effect of the lead vehicle's height (Eq. (3-6)). This is because drivers are found to be more sensitive to the lead vehicle's width rather than its height (Green, 2017a).

The boundaries of various car-following conditions as shown in Fig. 3-2 are the perception thresholds. The Wiedemann model assumes that the driver reacts as soon as the speed difference exceeds the perception thresholds of speed difference (*SDV*, *OPDV* or *CLDV*) and the spacing exceeds the perception thresholds of spacing (*ABX* and *SDX*). Note that the Wiedemann model expresses the perception thresholds in terms of speed difference and spacing instead of angular velocity.
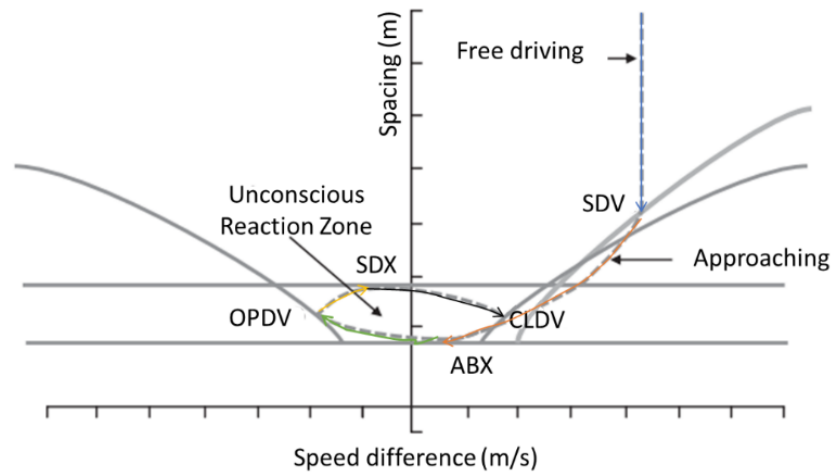
**Fig. 3-2. Graphical representation of Wiedemann Car-following Model**

(Source: Pariota & Bifulco, 2015)

*Free driving*

*Free driving* occurs when the spacing to the lead vehicle is very large (e.g., > 200 m). It is clear from Eq. ((3-5) that at large spacing (*S*), the subject vehicle's driver cannot perceive the speed difference from the slow-moving lead vehicle. This is because the instantaneous angular velocity at such a large spacing is much below the perception threshold of angular velocity. Even if the speed difference was known, the driver does not need to adjust the speed because the spacing is very large. Therefore, the driver accelerates until his/her speed reaches a desired speed or tries to maintain his/her desired speed. This was also observed from the data collected using a driving simulator as shown in Fig. 3-3. In this example, the driver started from a zero speed and accelerated to reach his desired speed. During the driver's acceleration, a lead vehicle appeared at 600 m spacing in front of the subject vehicle. When the driver reached the desired speed of about 30 m/s, he tried to maintain the speed by keeping the accelerator at same position.

If the driver is starting from a zero speed, the maximum possible vehicle acceleration is available at the beginning. As the speed increases, the available acceleration decreases. Therefore, the Wiedemann model considers the maximum speed of the subject vehicle and the driver's desired speed to express the functional relationship between the instantaneous speed and available acceleration as follows:

$$BMAX = BMAXmult \times (V_{MAX} - V \times FaktorV) \tag{3-11}$$

$$FaktorV = \frac{V_{MAX}}{V_{DESIRED} + FAKTORVmult.(V_{MAX} - V_{DESIRED})}$$

where $V_{MAX}$, $V_{DESIRED}$, and $V$ are the maximum speed of the vehicle, the driver's desired speed, and the instantaneous speed, respectively. $BMAXmult$ and $FAKTORVmult$ are the calibration parameters. Note that when $V = 0$, $BMAXmult \times V_{MAX}$ is the maximum acceleration available to the driver when starting from the zero speed.

When the driver's speed reaches $V_{DESIRED}$, he/she tries to maintain the desired speed. However, due to the driver's imperfect accelerator control, the speed oscillates. This speed oscillation is expressed in the model using the acceleration $BNULL$ as follows:

$$BNULL = BNULLmult \times (RND4(i) + NRND) \tag{3-12}$$

where $BNULLmult$ is the mean absolute constant acceleration that creates the oscillation in the desired speed and $(RND4(i) + NRND)$ is the combined variation due to the driver $i$'s ability to control acceleration $(RND4(i))$ and the variation within the same driver $(NRND)$. These last two parameters are normally distributed with a mean of 0.5 and a standard deviation of 0.1. The value is in a range of 0-1.

Fig. 3-3 shows that when the driver maintains the desired speed behind a slow-moving lead vehicle, the speed difference is positive and the spacing decreases in the Free driving condition. As a result of the decrease in spacing, the driver starts to approach a slow lead vehicle.
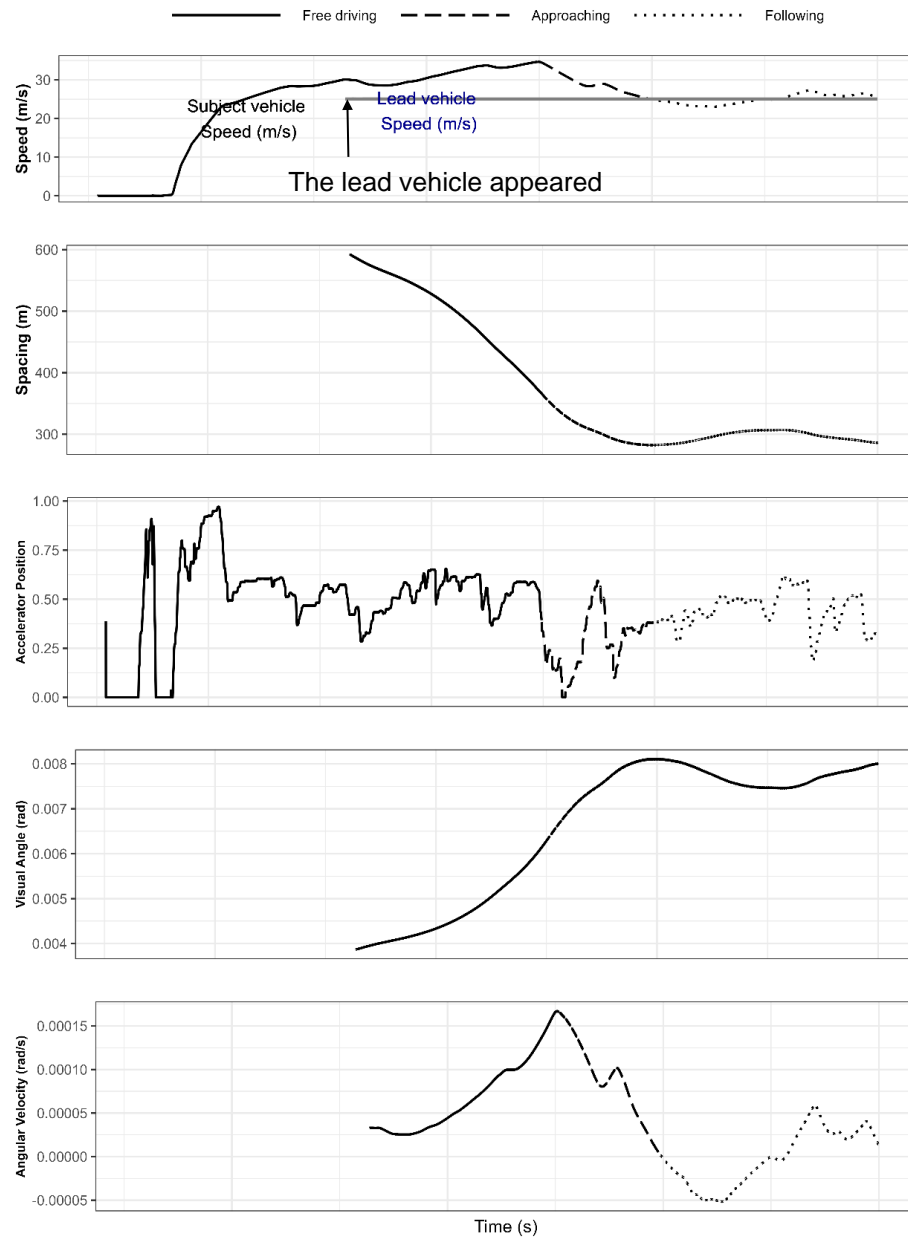


**Fig. 3-3. Trajectories of the observed driver behaviour for one pair of vehicles**

(Source of data: Data from a driving simulator study by the author)

*Approaching*

When the driver of a subject vehicle approaches a slow lead vehicle from a large spacing, the angular velocity increases as shown in Eq. (3-5). The equation is re-written below to calculate the speed difference as follows:

$$\Delta V = \frac{S^2 \times \dot{\theta}_W}{W}$$

The Wiedemann model uses the term '$DV$' instead of $\Delta V$. The speed difference *perceived* by the driver at large spacing is called *SDV*, which is expressed as follows:

$$SDV = \frac{S_{TH}{}^2 \times \dot{\theta}_{W(TH)}}{W} \tag{3-13}$$

where $\dot{\theta}_{W(TH)}$ is the perception threshold of angular velocity and *SDV* and $S_{TH}$ are the speed difference and the spacing, respectively, when $\dot{\theta}_W \geq \dot{\theta}_{W(TH)}$. Thus, a driver perceives the speed difference from the lead vehicle when the instantaneous angular velocity exceeds the perception threshold of angular velocity. This is illustrated in Fig. 3-2(b) where the driver instantaneously relaxes the accelerator as the angular velocity is sufficiently large enough for the driver to perceive.

Instead of considering the front-to-rear spacing to the lead vehicle ($S$), the Wiedemann model assumes the front-to-front spacing (*DX*) minus the distance that the subject vehicle keeps with lead vehicle when both subject and lead vehicles stop (*AX*). Then Eq. (3-13) is re-written as follows:

$$SDV = (DX - AX)^2 \times \frac{\dot{\theta}_{W(TH)}}{W} \tag{3-14}$$

where $DX$ is the front-to-front spacing and $AX$ is the front-to-front standstill spacing. $AX$ includes the length of the lead vehicle and the standstill front-to-rear spacing that a driver wants to keep as follows:

$$AX = L + AXadd + RND1(\text{i}) \cdot AXmult \tag{3-15}$$

where $L$ is the length of the lead vehicle, $AXadd$ and $AXmult$ are calibration parameters, and $RND1(i)$ is a random parameter for the driver $i$'s safety need. The suggested values for $AXadd$ and $AXmult$ are 1.25 and 2.5, respectively (Li, 2017). $RND1(i)$ is normally distributed with a mean of 0.5 and a standard deviation of 0.1. The value is in a range of 0-1.

In Eq. (3-14), the speed difference $SDV$ is perceived when the angular velocity, $\dot{\theta}_W$, exceeds the perception threshold of angular velocity, $\dot{\theta}_{W(TH)}$. Since this perception threshold varies among drivers, $\dot{\theta}_{W(TH)}$ is not a constant. It is rather a distribution which is derived from the field observations for a given width of the lead vehicle. In the Wiedemann model, the term $\frac{\dot{\theta}_{W(TH)}}{W}$ is replaced by a parameter $1/CX^2$, and Eq. (3-14) is re-written as follows:

$$SDV = \left(\frac{DX - AX}{CX}\right)^2 \tag{3-16}$$

The parameter $CX$ is expressed as follows:

$$CX = CXconst \cdot (CXadd + CXmult \cdot (RND1(i) + RND2(i))) \tag{3-17}$$

where *CXconst*, *CXadd* and *CXmult* are calibration parameters; *RND1*(*i*) is the driver *i*'s safety need (higher value indicates higher safety need), and *RND2*(*i*) is the driver *i*'s estimation abilities (higher value indicates better estimation abilities). Similar to *RND1*(*i*), *RND2*(*i*) is also normally distributed with a mean of 0.5 and a standard deviation of 0.1 and its range is 0-1.

The field observations show that the range of *CX* is 25-75 (Wiedemann and Reiter, 1992). A higher value of *CX* indicates that drivers can perceive lower angular velocity for a given width of the lead vehicle, which implies that drivers are more cautious. Similarly, a lower value of CX indicates that drivers are less cautious. From Eqs. (3-14) and (3-16), it is clear that $1/CX^2$ is expressed as follows:

$$\frac{1}{CX^2} = \frac{\dot{\theta}_{W(TH)}}{W} \tag{3-18}$$

For instance, if the width of a lead vehicle is 1.8 m, the perception threshold of angular velocity $\dot{\theta}_{W(TH)}$ could be calculated as follows:

For *CX* = 25      ;    For *CX* = 75

$$\dot{\theta}_{W(TH)} = \frac{1.8}{25^2} = 0.00290\,\frac{rad}{s} \quad ; \quad \dot{\theta}_{W(TH)} = \frac{1.8}{75^2} = 0.00032\,\frac{rad}{s}$$

Thus, Eq. (3-16) in the Wiedemann model suggests an observed angular velocity threshold range of 0.0003 – 0.003 rad/s, for an assumed lead vehicle width of 1.8 m. This variation in the threshold was attributed to drivers' safety need and estimation ability.

Fig. 3-2 shows that when the speed difference is equal to *SDV*, the vertical trajectory changes to a curve, indicating a deceleration. This deceleration is a result of the driver's relaxation of the accelerator after consciously perceiving that the lead vehicle is slow. This continuously reduces the speed of the subject vehicle until it becomes equal to the speed of the lead vehicle. The equation for deceleration during the Approaching condition in the Wiedemann model can be derived from Eq. (3-10), with the assumption that $\dot{\tau} = -0.5$, as shown below.

$$\dot{\tau} \quad = -1 - \frac{S \times \Delta A}{\Delta V^2}$$

$$-0.5 \quad = -1 - \frac{S \times \Delta A}{\Delta V^2}$$

$$\Delta A \quad = -\frac{0.5 \times \Delta V^2}{S}$$

$$B(i) - B(i-1) = -\frac{0.5 \times \Delta V^2}{S} \tag{3-19}$$

where $B(i)$ and $B(i-1)$ are the acceleration rates of the subject and lead vehicles, respectively.

The purpose of the deceleration during Approaching is to make the speed difference zero. Moreover, the driver wants to keep a safe distance from the lead vehicle when the speed difference becomes zero, to safely stop in case of an unexpected lead vehicle braking. This safe distance is a front-to-front spacing, called *ABX* in the Wiedemann model. Therefore, instead of using the complete front-to-rear spacing *S*, the difference between the front-to-front spacing *DX* and safe distance *ABX* is used in the denominator in the above

equation. Thus, the equation for deceleration after perceiving a slow lead vehicle (Eq. (3-19)) is re-written as follows:

$$B(i) - B(i-1) = -\frac{0.5 \times DV^2}{DX - ABX}$$

$$B(i) = \frac{1}{2} \times \frac{DV^2}{ABX - DX} + B(i-1)$$

(3-20)

To capture the variation between drivers, additional parameters are included in Eq. (3-20) as follows:

$$B(i)_{App} = \frac{1}{2} \times \frac{DV^2}{ABX - DX} + B(i-1) + \frac{(1 - RND2(i)).(1 - 2 . NRND)}{R(i)}$$

(3-21)

where $B(i)_{App}$ is the subject vehicle acceleration during Approaching, the first term on the right-hand side of Eq. (3-21) is the value of the minimum deceleration required to slow down behind a moving lead vehicle. The second term $B(i-1)$ is the lead vehicle $i$-1's acceleration (or deceleration). The third term represents the variation in the subject vehicle $i$'s deceleration and $R(i)$ represents the driver $i$'s ability of estimating the angular velocity. $ABX$ has its own equation as follows:

$$ABX = AX + (BXadd + BXmult \cdot RND1(i)) \times \sqrt{V}$$

(3-22)

where $BXadd$ and $BXmult$ are calibration parameters, $RND1(i)$ is a random parameter for the driver $i$'s safety need, and $V$ is the minimum of the speeds of the subject vehicle and the lead vehicle.

*Following*

As the driver consciously approaches the slow-moving lead vehicle with constant deceleration, the speed difference decreases (i.e., both vehicles move at similar speeds). But as the spacing decreases, the driver is prompted to further slow down for safe vehicle control. The spacing at which the driver perceives the need of further slowing down is called *ABX*. At this point, the driver further releases the accelerator and slightly pushes the brake pedal. Fig. 3-2 shows that when the trajectory touches the *ABX* line, a new curve that moves left-upwards is generated.

Due to the further decrease in subject vehicle speed, the speed difference becomes negative (i.e., the subject vehicle is slower than the lead vehicle) and the spacing between the vehicles starts increasing. At some point, the driver can perceive large speed difference because *DV* in Eq. (3-5) is sufficiently large (i.e., when the angular velocity exceeds the threshold of angular velocity). This speed difference in the "opening" process at a small spacing that a driver can perceive is called *OPDV*. Thus, the driver pushes the accelerator to increase the speed to follow the lead vehicle more closely and then the speed difference starts increasing.

As a result of this acceleration, the subject vehicle speed starts increasing. Initially, the spacing continues decreasing at a smaller rate. Fig. 3-2 shows this as the trajectory curve which moves upward. But as the subject vehicle speed increases, the spacing starts decreasing and the speed difference becomes positive. Then, this positive speed difference

50

becomes sufficiently large to stimulate the driver. This speed difference in the "closing" process at small spacing that a driver can perceive is called *CLDV*. Consequently, the driver relaxes the accelerator or pushes the brake pedal. The equations for *OPDV* and *CLDV* are as follows:

$$CLDV = SDV \cdot EX^2 \tag{3-23}$$

$$EX = EXadd + EXmult \cdot (NRND - RND2(i)) \tag{3-24}$$

$$OPDV = CLDV \cdot (-OPDVadd - OPDVmult \cdot NRND) \tag{3-25}$$

where *SDV*, *CLDV* and *OPDV* are perception thresholds of speed difference, *NRND* is the variation within the same driver, and *EX*, *EXadd*, *EXmult*, *OPDVadd* and *OPDVmult* are calibration parameters.

Again, the spacing decreases to *ABX*, which prompts the driver to further reduce the speed. Therefore, the trajectory continues moving back and forth between *OPDV* and *CLDV* - i.e., the driver continuously transitions between pushing the accelerator and relaxing the accelerator/pushing the brake pedal. This process of adjusting speed to maintain the speed difference to near zero at small spacing is called *Following*. Fig. 3-2 shows that after approaching the slow lead vehicle, the driver tries to maintain the speed but oscillates around a zero speed difference.

Empirical evidence shows that the speed differences *OPDV* and *CLDV* are not equal - i.e., a driver is stimulated differently by negative and positive speed differences (Michaels, 1963). This is because it is more critical to respond when the lead vehicle speed is slower (positive speed difference) than when the lead vehicle is faster (negative speed difference)

from a safety perspective. As a result of these differences in the perceived speed differences, the spacing between the vehicles significantly increases after several cycles of transitions between positive and negative speed differences. Then, the driver perceives this increase in spacing. The spacing at which the driver perceives the increase in the spacing from his/her desired safety distance (*ABX*) is called *SDX*. When the spacing is equal to *SDX*, the driver is prompted to push the accelerator pedal. This is shown in Fig. 3-2 as the trajectory curve which moves right-downwards after touching the *SDX* line due to the acceleration. *SDX* equation is shown as follows:

$$SDX = AX + EX(BXadd + BXmult \cdot RND1(i)).\sqrt{V} \tag{3-26}$$

*Emergency braking*

The emergency braking condition occurs if the lead vehicle suddenly applies hard brake. This decreases the spacing from *ABX* and the driver must apply a large deceleration as follows:

$$B(i)_{Emg} = \frac{DV^2}{2(AX-DX)} + B(i-1) + BMIN\frac{(ABX-DX)}{(ABX-AX)} + \frac{(1-RND2(i))\cdot(1-2.NRND)}{R(i)} \tag{3-27}$$

$$BMIN = \text{-}BMINadd - BMINmult \cdot RND3(i) + BMINVmult \cdot V$$

where $B(i)_{Emg}$ is the subject vehicle deceleration during Emergency braking, *BMIN* is the maximum possible deceleration when the spacing is equal to *AX*, *RND3(i)* is driver *i*'s capability of deceleration, and *BMINadd* and *BMINmult* are calibration parameters.The first term in Eq. (3-27) is similar to Eq. (3-21) with the difference that the minimum acceptable spacing to avoid collision is *AX* instead of *ABX* because the spacing is already

shorter than *ABX*. The third term represents the reduction in spacing from the safe distance which is estimated based on the difference between the current spacing *DX* and the safe distance *ABX*. If the current spacing at the sudden deceleration of the lead vehicle equals *ABX* (i.e., *ABX = DX*), then the third term is zero. This is because the maximum deceleration *BMIN* is not required when the current spacing is at the driver's safe distance. This third term linearly increases up to the maximum value, *BMIN*, as the spacing decreases to *AX*. The collision occurs if the spacing is shorter than *AX*.

*Summary and Limitations of Wiedemann Car-following Model*

The main assumption in the Wiedemann model is that a driver reacts as soon as the instantaneous angular velocity exceeds the driver's perception threshold of angular velocity. Thus, the model uses speed difference and spacing thresholds based on the perception threshold of angular velocity and does not consider a perception reaction time.

However, according to the signal detection theory, perception thresholds may not exist since driver perception is shaped by past experiences and payoffs (Green, 2017a). For instance, drivers do not always decelerate as soon as they notice that a lead vehicle is slow (perception threshold in Approaching condition) as the situation does not warrant an urgent reaction. Although the Wiedemann model accounts for heterogeneity between and within drivers' perception thresholds (and consequently the reaction time) by using the RND and NRND parameters, but it does not explain what controls this heterogeneity. The understanding of this variation in perception thresholds is important for understanding the relationship between reaction time and collision causation. Recent literature suggests that the accumulation of sensory evidence (angular velocity/tau-inverse), instead of the

perception thresholds, is the underlying neurobiological mechanism that controls driver reaction time (Markkula et al., 2020).

Furthermore, the Wiedemann model assumes an identical braking pattern for all drivers. As shown in Eq. (3-19), these braking equations were derived based on the assumption that $\dot{\tau} = -0.5$. Markkula et al. (2016) observed from the naturalistic driving data that drivers' start of braking depends on the situation urgency characterized by the spacing, speed difference and the deceleration rate of the lead vehicle. This implies that instead of using a fixed $\dot{\tau}$ as in the Wiedemann model, the use of $\dot{\tau}$ as the model parameter might predict braking response more accurately.

In this regard, Markkula and his colleagues proposed an alternative theory to explain how the sensory evidence is used to predict the start time and magnitude of driver reaction (Markkula, 2014; Markkula et al., 2016; Svärd et al., 2017; Xue et al., 2018). Thus, the theory of Markkula model is explained in the next section.

### 3.2.2  Markkula Model

Markkula model is a general framework of sensorimotor control in sustained motion tasks such as steering, longitudinal acceleration, etc. (Markkula et al., 2018). Since these tasks involve control by using perception and motor action (brake/accelerator control), they are considered as "sensorimotor" control. The model can predict the start time as well as the magnitude of reaction in a given task. Theoretically, the Markkula model can predict both acceleration and deceleration in all car-following conditions but the model has only been evaluated in emergency braking conditions (Svärd et al., 2017).

*Conceptual Framework*

Perceptual cues such as angular velocity and tau-inverse indicate a need for control called control error, $P(t)$. The Wiedemann model assumes that a driver starts a control adjustment (e.g., acceleration and deceleration) when the instantaneous value of the control error is equal to or larger than a threshold (e.g., $\dot{\theta}_{TH}$). However, the Markkula model assumes that a driver starts a control adjustment when the *accumulated* control error with noise reaches the threshold $A_{TH}$.

At this threshold, a control adjustment is initiated in the form of a motor primitive. A motor primitive is defined as "patterns of motion without regard to force or mass, e.g. strokes […] or cycles […]" (p. 156, Giszter, 2015). Motor primitives are the building blocks of human body movement that characterize the magnitude of control adjustment $i$, $g_i$ and its shape $G(t)$ (Markkula et al., 2018). For instance, brake pedal rate and brake pedal position represent the magnitude and the shape of brake control, respectively.

Any new motor primitive is superpositioned to the ongoing motor primitives, e.g., a new braking maneuver is superpositioned onto the previously applied brake control. Importantly, the magnitude $g_i$ is correlated and scaled by the control error $P(t)$.

As a motor primitive is initiated, a driver predicts how the control error (e.g., angular velocity) will be reduced due to the control adjustment (e.g., braking). This is called a predicted control error, $P_p(t)$. This prediction is superpositioned onto the previous predictions. The shape of the prediction $H(t)$ is based on the gradual decrease in control error after a control adjustment is made. The predicted control error $P_p(t)$ is subtracted from the actual control error $P(t)$, and this quantity is called *control error prediction error*,

$\epsilon(t_i)$. The time $t_i$ is the start time of control adjustment $i$. The Markkula model assumes that the accumulation and magnitude of control adjustment depend on the control error prediction error $\epsilon(t_i)$ instead of the control error $P(t)$.

As discussed in Chapter 2: , 3.1, and 3.2.1, engineering car-following models are either continuous with no reaction time, or discrete with a constant reaction time. Thus, these models do not consider the *intermittent* nature of human control behaviour. The Markkula model can convert continuous sensorimotor control models into intermittent sensorimotor control models. The rate of change of control adjustment to be applied, $\dot{C}(t)$, is specified in a continuous model as follows:

$$\dot{C}(t) = K \cdot P(t - \tau_d) \qquad\qquad (3\text{-}28)$$

where $K$ is the control gain, $P(t)$ is control error, and $\tau_d = \tau_p + \tau_c + \tau_m$ where $\tau_p, \tau_c, \tau_m$ are delays at perceptual, control decision, and motor stages, respectively (Markkula et al., 2018). The delay at motor stage occurs because it takes time for vehicle response (e.g., deceleration) after the human body movement (e.g., pressing brake pedal). Then the objective of control adjustment $C(t)$ is to make control error $P(t)$ to be zero by applying the rate of change $\dot{C}(t)$. For example, brake pedal rate can be considered as $\dot{C}(t)$ when the control error $P(t)$ is tau-inverse in braking conditions and $C(t)$ = brake pedal position (Markkula, 2014).

Fig. 3-4 shows the complete framework of the Markkula Model that converts Eq. (3-28) into an intermittent model. The following sections explain Fig. 3-4 and discuss the modifications in Eq. (3-28) to convert it into an intermittent model.
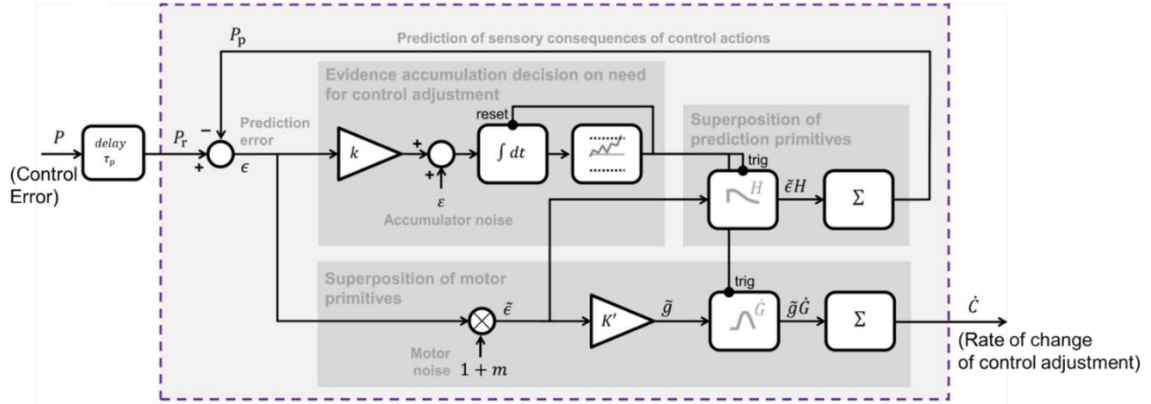
**Fig. 3-4. Markkula Model of Sustained Sensorimotor Intermittent Control**

(Source: Markkula et al., 2018)

*Control Error $P(t)$*

Consider tracking a moving object in one dimension on a computer screen as an example of sustained sensorimotor control. The control error $P(t)$ quantifies the *evidence* for the need of control. Therefore, $P(t)$ is estimated as the distance $D(t)$ between the instantaneous cursor position $C(t)$ and the moving target position $C_T(t)$ (Powers, 2008; Markkula *et al.*, 2018). This control error $D(t) = C_T(t) - C(t)$ can be reduced to zero by applying the rate of mouse cursor movement $\dot{C}(t)$ such that $C(t) = C_T(t)$. Consequently, Eq. (3-28) can be re-written as the following continuous model of tracking an on-screen moving target:

$$\dot{C}(t) = K \cdot D(t - \tau_d) \tag{3-29}$$

Thus, $P(t) = D(t)$ for the task of tracking the on-screen target. Note that $P(t)$ is input to the Markkula model before a perceptual delay $\tau_p$ as shown in Fig. 3-4. This delayed control

error is $P_r(t) = P(t - \tau_p)$. Similarly, the continuous model for the task of lane-keeping is as follows:

$$P(t) = k_{nI}\theta_n(t) + k_{nP}\dot{\theta}_n(t) + k_f\dot{\theta}_f(t) \tag{3-30}$$
$$\dot{C}(t) = P(t - \tau_d)$$

where $\theta_n(t)$ and $\theta_f(t)$ are the visual angles at 'near' and 'far' reference points as described in Salvucci and Gray (2004). Since $k_{nI}$, $k_{nP}$ and $k_f$ represent control gain, the control gain $K$ in Eq. (3-28) is not required. Therefore, $K$ is fixed to 1. Moreover, $\dot{C}(t)$ is the rate of change of steering wheel angle, and $C(t)$ is the steering wheel angle.

The continuous model of emergency braking can also be expressed as follows (Markkula, 2014):

$$P(t) = \tau^{-1} \tag{3-31}$$
$$\dot{C}(t) = K \cdot P(t - \tau_d)$$

where $\tau^{-1}$ is the inverse of time to collision, $\dot{C}(t)$ is the rate of change of brake pedal position, and $C(t)$ is the brake pedal position.

*Evidence Accumulation*

According to the Wiedemann's model, a driver initiates a brake adjustment as soon as the evidence for braking, i.e., $P(t) = \dot{\theta}_W(t)$ (instantaneous angular velocity), exceeds the threshold of angular velocity. This is illustrated as follows:

$$P(t) \geq \frac{1}{k} \tag{3-32}$$

where $1/k$ is the threshold of angular velocity, and $k$ is the accumulator gain. However, the signal detection theory of human behaviour suggests that the signal (i.e., $P(t)$) is always accompanied by noise (Green, 2017c). The most common source of noise is the "natural fluctuations in neural activity" which occurs even if there is no signal (Markkula et al., 2016). Thus, the driver must differentiate the signal from the noise to react. For instance, when the angular velocity is very small at a large spacing from the lead vehicle, it is hard for the driver to perceive that the lead vehicle speed is lower than his/her own speed. In this case, the signal of angular velocity is so weak that it is hard to detect the signal with the background noise. For example, in car-following, vehicles in other lanes could be the background noise in a road scene.

As the spacing decreases, the signal becomes stronger. Eventually when the signal becomes sufficiently strong, the driver can easily differentiate the signal from the background noise, which might prompt the driver to start braking. In this regard, Xue et al. (2018) expressed the control error as a stochastic measure by adding a noise term as follows:

$$P(t) + \varepsilon(t) \geq 1/k \tag{3-33}$$

where $\varepsilon(t)$ is noise; $\varepsilon(t) \sim N(0, \sigma_a)$. Eq. (3-33) is re-written as follows:

$$k \times (P(t) + \varepsilon(t)) \geq 1 \tag{3-34}$$

In contrast to Eq. (3-34), Markkula (2014) proposed that the driver starts braking based on the accumulation of the evidence rather than an instantaneous value of the evidence. This part of the Markkula model is highlighted as 'Evidence accumulation decision on need for control adjustment' in Fig. 3-4. It is also called the *accumulator model*. The

accumulator model can estimate the start time of any control adjustment. The model is described below in the context of the braking task.

Evidence from control error can be variable (e.g., angular velocity and tau-inverse) or static (e.g., lead vehicle brake light). The control error with noise is accumulated over time until it reaches a threshold of $A_{TH}$. Note that $A_{TH}$ is a combined threshold of accumulated sensory evidence for braking and noise. Moreover, as Fig. 3-4 shows, the prediction $P_p(t)$ is subtracted from control error $P(t)$ at each time $t$, which yields the control error prediction error $\epsilon(t)$ $(= P(t) - P_p(t))$. Therefore, before incorporating the accumulation process, Eq. (3-34) is re-written as follows:

$$k \times (\epsilon(t) + \varepsilon(t)) \geq 1 \tag{3-35}$$

The prediction $P_p(t)$ is the subconscious prediction of how a driver's control adjustment would change the control error over time. Typically, drivers expect that all vehicles ahead of them are driving at the same speed as their speed. Therefore, the control error must be close to or equal to zero and the prediction $P_p(t)$ is also zero as no control adjustment is required. However, $P_p(t)$ is non-zero after the accumulated value of control error and noise reaches the threshold $A_{TH}$. The prediction $P_p(t)$ is discussed in detail later in this section.

After incorporating the accumulation process in Eq. (3-35), the accumulator model is formulated as below (Markkula et al., 2018):

$$\frac{dA(t)}{dt} = \gamma\big[\eta\big(\epsilon(t)\big)\big] - \lambda A(t) + \varepsilon(t) \tag{3-36}$$

$$\epsilon(t) = P_r(t) - P_p(t)$$

$$P_r(t) = P(t - \tau_p)$$

where $A(t)$ is the activation, i.e., the accumulated evidence, $-\lambda A(t)$ represents the leakage in the evidence (e.g., leakage due to distraction), $\epsilon(t)$ is the control error prediction error, $\tau_p$ is the perceptual delay, and $\varepsilon(t)$ is the noise. Moreover, $\eta(\epsilon)$ is an activation function which can be sigmoidal or simply $\eta(\epsilon) = k\epsilon$ and $\gamma$ is a gating function defined as below:

$$\gamma(\eta) = sign(\eta) \times \max(0, |\eta| - M) \tag{3-37}$$

where $sign(\eta) = 1$ if $\eta(\epsilon) > 0$, $sign(\eta) = -1$ if $\eta(\epsilon) < 0$, and $sign(\eta) = 0$ if $\eta(\epsilon) = 0$. The accumulator model predicts the start time as the time when $A(t)$ exceeds the threshold $A_{TH}$.

An accumulator model with no leakage in the evidence ($\lambda = 0$) and $\eta(\epsilon) = k\epsilon$ is expressed as follows:

$$\frac{dA(t)}{dt} = k \times \epsilon(t) - M + \varepsilon(t) \tag{3-38}$$

where $M$ is the negative gating, i.e., the minimum evidence below which the accumulation does not start. Note that $\epsilon(t)$ could be positive (the lead vehicle is slower than the subject vehicle) or negative (the lead vehicle is faster than the subject vehicle) that would require a deceleration or acceleration, respectively. Therefore, the activation can be fixed as $A_{TH} = A_+ = +1$ which represents the accumulated evidence for a slower lead vehicle and $A_{TH} = A_- = -1$ for a faster lead vehicle.

The algorithm of the Accumulator model shown in Eq. (3-38) is described in Fig. 3-5. This algorithm is explained using an example scenario where a lead car decelerates at -8 m/s$^2$ from an initial speed of 25 m/s. At the onset of the lead car's deceleration, the speed difference was zero, i.e., the subject car speed was also 25 m/s. In this example, the tau-

inverse due to the width of the lead car ($\tau_W{}^{-1}$) is used as the control error. The prediction $P_p(t)$ is assumed to be zero in this simple example. Therefore, $\epsilon(t) = P(t)$.
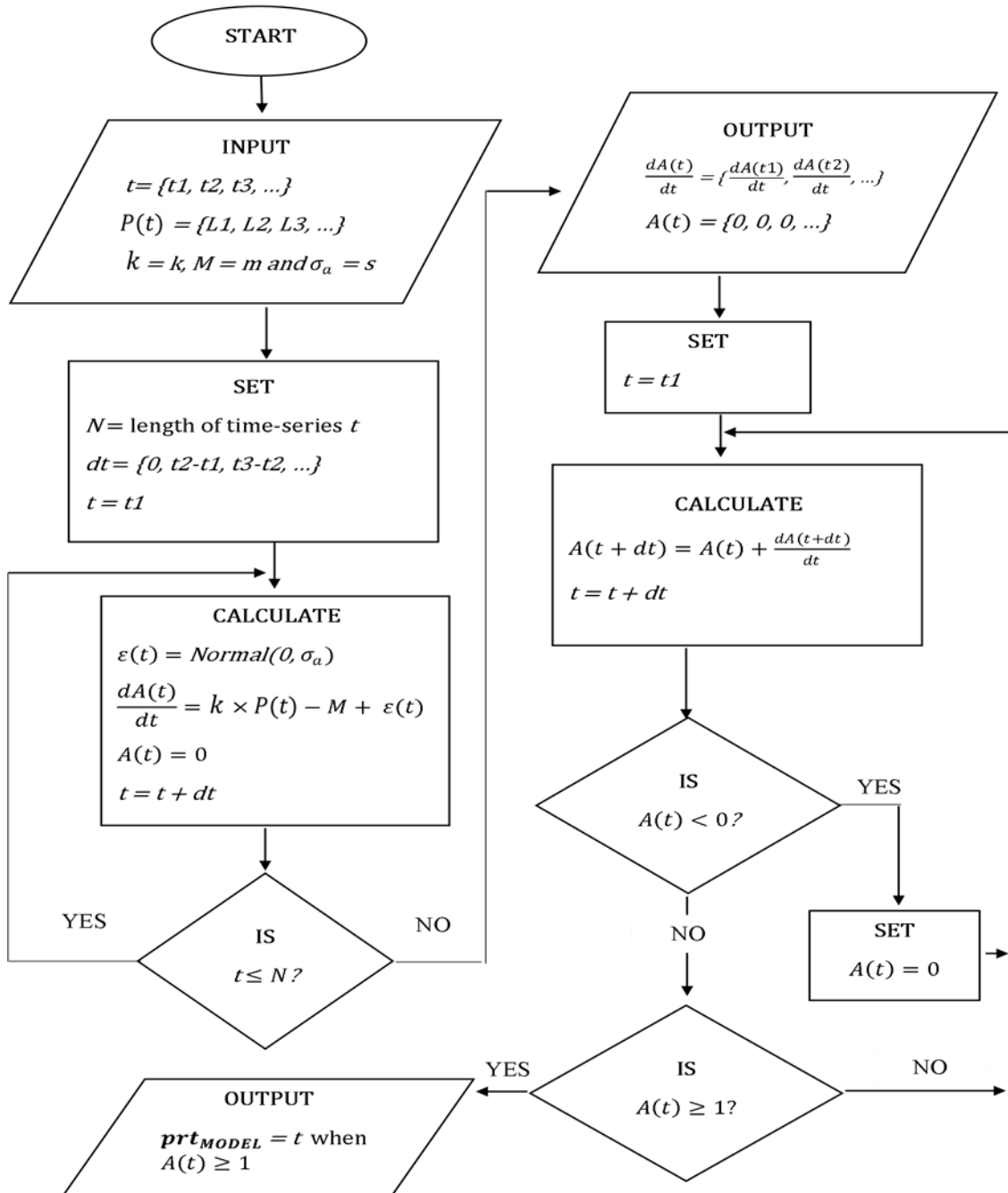


**Fig. 3-5. Algorithm of Accumulator model**

Fig. 3-6 illustrates the variation in control error ($P(t) = \tau_W{}^{-1}$) over time from the start of the lead car's deceleration. The figure shows that the control error increases over time due to the lead car's deceleration. This is because the lead car deceleration increases the speed difference, which increases both angular velocity (Eq. (3-5)) and tau-inverse (Eq. (3-9)).

Due to this increase in control error, the driver in the subject car is expected to detect the deceleration of the lead car after a few seconds, which would prompt a braking response. The algorithm described in Fig. 3-5 predicts the time when the subject driver would start applying the brake after the lead vehicle's deceleration. Therefore, the part of the observed data which corresponds to the actual times of the subject driver's release of the accelerator pedal and braking should not be used as input data in the algorithm. This is because the actual time of braking will be predicted using the algorithm. Moreover, the driver's release of the accelerator pedal and braking alters the increasing values of control error to decreasing values of control error. The decreasing values of control error would not accumulate to a threshold as the control error in this task is positive (i.e., the accumulated evidence for a slower lead vehicle). Hence, the actual control error, i.e., tau-inverse, is replaced with the tau-inverse estimated based on the assumption that the subject car would maintain the current speed (25 m/s in this example). This provides enough input control error data to accurately predict the start time of brake application. Thus, the input tau-inverse trajectory in Fig. 3-6 is the predicted tau-inverse, not the observed tau-inverse.

Moreover, as shown in Fig. 3-6, the time between the lead car brake onset and the subject car brake onset (as predicted by the algorithm) is called Perception-Reaction Time (PRT). The algorithm is run in the following steps:

63
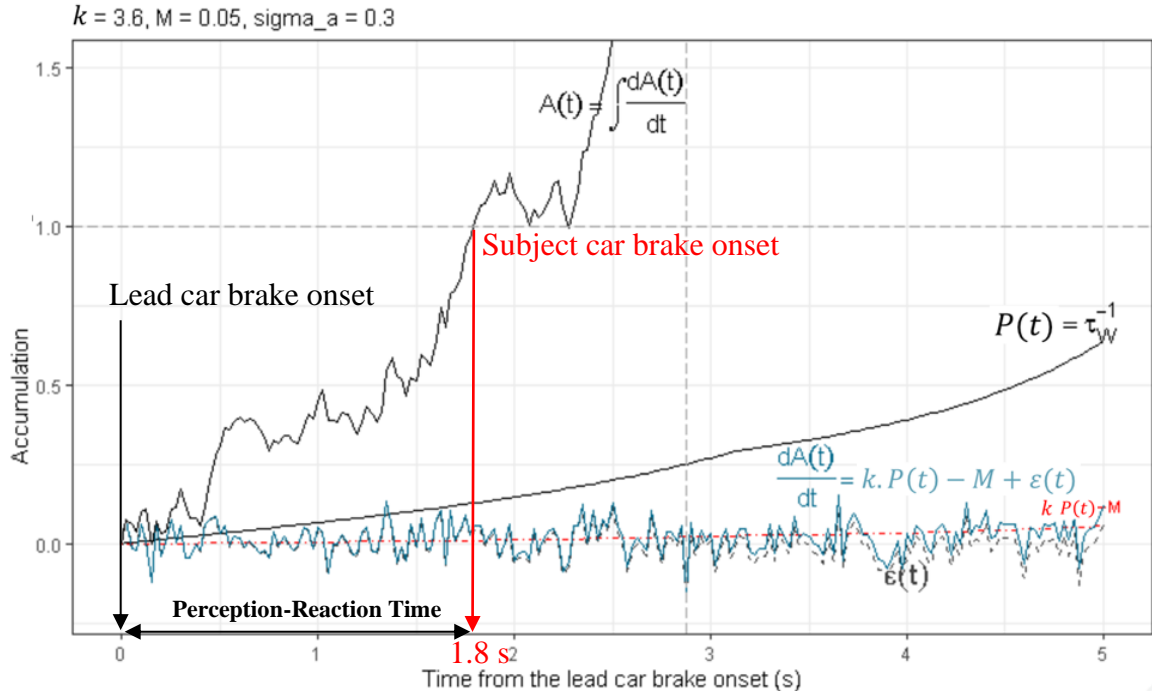
**Fig. 3-6. Example of Accumulator Model**

*Step 1: Import Control Error*

In the beginning of the algorithm (top-left of Fig. 3-5), the control error at time $t$, $P(t)$, is provided as an input. The time $t$ ranges from 0 to 5 seconds and the values of $k$, $M$ and $\sigma_a$ are assumed to be 3.6, 0.05 s$^{-1}$ and 0.3, respectively. Note that the values of these three parameters are arbitrarily selected for the illustrative purpose in this example (Fig. 3-6). These three parameters of the model need to be calibrated. The method of calibrating these parameters is described in Chapter 5: .

*Step 2: Estimate the noise and $dA(t)/dt$*

The length of each time frame (*dt*) is pre-specified in the input time $t$ and the total length of time frames (*N*) is set based on the number of data points in $t$ (Fig. 3-5, left). The length

of time frame *dt* is subjectively determined – a smaller *dt* results in higher accuracy of results but it requires longer calculation time. In this example, *dt* = 0.025 s and *N* = 5 s. Thus, there are a total of 201 values of *t* (= 5 s / 0.025 s + 1 (including the initial value at *t1* = 0)).

In each iteration, $dA(t)/dt$ at time *t* is calculated using Eq. (3-38). In the first iteration, the initial value of time *t* is set to zero, *t1* = 0. The noise term $\varepsilon(t)$ at *t1* is then estimated as a random number drawn from a normal distribution with a mean of 0 and $\sigma_a$ of 0.3 (see CALCULATE, Fig. 3-5, left). Thus, $dA(t)/dt$ at *t1* is calculated using $\tau_W^{-1}$ as control error $P(t)$, $k$ = 3.6 and $M$ = 0.05, and $\varepsilon(t)$ at *t1*. Simultaneously, $A(t)$ at *t1* is set to zero. At the end of each iteration, time is incremented by time frame $dt = 0.025$ s. In this manner, $dA(t)/dt$ and $A(t)$ at each time frame *t* are calculated from $t = 0$ to 5 s (top-right of Fig. 3-5). At this point, $A(t)$ are zero for all time frames. The calculated $\varepsilon(t)$, Eq. (3-38) without $\varepsilon(t)$, and the complete Eq. (3-38) are shown in Fig. 3-6 as the grey dashed line, red dot-dash line and blue solid line, respectively.

*Step 3: Estimate the accumulation of control error and predict PRT*

The final step in the algorithm is to accumulate $A(t)$ over all time frames *t* as follows (also see CALCULATE in Fig. 3-5, right):

$$A(t + dt) = A(t) + \frac{dA(t+dt)}{dt}$$

For instance, at time *t2* = 0.025 s:

$$A(0.025) = A(0) + \frac{dA(0.025)}{dt} = A(0) + k \times P(0.025) - M + \varepsilon(0.025)$$

$$A(0.025) = 0 + 3.6 \times 0.01 - 0.05 + N(0, \sigma_a = 0.3)$$

$$A(0.025) = 0 + 0.036 - 0.05 + (-0.25)$$

$$A(0.025) = -0.264$$

At the end of each iteration, time is incremented by time frame $dt = 0.025$ s. In the first few time frames, the accumulated looming $A(t)$ was a negative value because the noise term $\varepsilon(t)$ and $k \times P(t) - M$ in Eq. (3-38) are negative. The control error $P(t)$ is generally small at a large spacing. A negative value of $A(t)$ means that the accumulation has not started yet because the signal is weaker than the noise. Therefore, if $A(t)$ is negative, it is reset to zero. Without this reset step, the initial few negative values of $\frac{dA(t+dt)}{dt}$ would add up to higher negative values and delay the accumulation process. If $A(t)$ is positive, $A(t)$ is continuously accumulated until $A(t)$ is equal to or greater than 1 (i.e., the threshold $A_{TH}$ in this example) (see the bottom-right of Fig. 3-5).

Initially, $A(t)$ is reset to zero several times due to small control error relative to the noise at a large spacing. But as the signal becomes stronger (i.e., the control error increases), $A(t)$ rapidly increases as shown in Fig. 3-6. Lastly, the algorithm determines the time $t$ immediately after $A(t)$ equals or exceeds 1 when the driver starts braking (see the OUTPUT at the bottom of Fig. 3-5). Thus, the length of time from the start of the lead vehicle's deceleration to this time $t$ is the perception-reaction time (PRT) predicted by the model. Fig. 3-6 shows that $A(t)$ equals 1 at $t = 1.8$ s. This indicate that the driver would start braking 1.8 seconds after the start of the lead vehicle's deceleration.

*Accumulator Model with lead vehicle's brake light*

If the lead vehicle's brake light is considered as extra evidence for braking, then Eq. (3-38) is modified as follows:

$$\frac{dA(t)}{dt} = k \times \epsilon(t) - M + a_{BL} + \varepsilon(t) \tag{3-39}$$

where $a_{BL}$ is the "evidence supported by the lead vehicle's brake light that can help drivers take brake action" (Xue et al., 2018). However, not all drivers consider the lead vehicle's brake light as the extra evidence to decide for braking. The probability that the driver uses the lead vehicle brake light as an additional stimulus is $p_{BL}$. The probability $p_{BL}$ is associated with the use of the term $a_{BL}$ in the model.

Eq. (3-39) can be accumulated using the algorithm described in the Fig. 3-5 with the Eq. (3-39) instead of Eq. (3-38) at the calculation step. The suggested input values for $a_{BL}$ are 0 to 2 with an interval of 0.25, and the suggested input values for $p_{BL}$ are 0 to 1 with an interval of 0.025 (Markkula et al., 2016). The parameters for both Eq. (3-38) and Eq. (3-39) are selected using a genetic algorithm search. The search of parameters is discussed in detail in Chapter 5: .

*Magnitude and shape of control adjustment*

Markkula model assumes that a control adjustment is triggered whenever the accumulated evidence is greater than or equal to the threshold, i.e., $A(t) \geq |A_{TH}|$ (see 'trig' in Fig. 3-4). This control adjustment is pressing a brake pedal when the accumulated evidence is positive (control error is positive: $A(t) \geq A_+$) or pressing an accelerator pedal when the accumulated evidence is negative (control error is negative: $A(t) \leq A_-$ ).

Moreover, the accumulated evidence is reset to zero $A(t) = 0$ (see 'reset' in Fig. 3-4) at the same time when the control adjustment is made.

Furthermore, the Markkula model assumes that the magnitude and shape of the control adjustment are based on the *motor primitives* – a neurobiological concept of human body movement. In this concept, any human body movement can be constructed from a collection of pulses of muscle activation (Giszter, 2015). The amplitude of these muscle activations can be scaled based on the required magnitude of response. For example, the magnitude of deceleration can be increased to reduce a large tau-inverse (evidence or control error).

Markkula et al. (2016) found that in naturalistic driving, the deceleration and the rate of change of deceleration (jerk) linearly varied with the magnitude of tau-inverse at the start of braking. Thus, when the control error is large (e.g., due to a lead vehicle deceleration), the following driver would apply a large jerk. Therefore, deceleration did not increase smoothly and continuously, but it rather rapidly increased in a short time period as shown in the observed control adjustment in naturalistic driving as shown in Fig. 3-7.
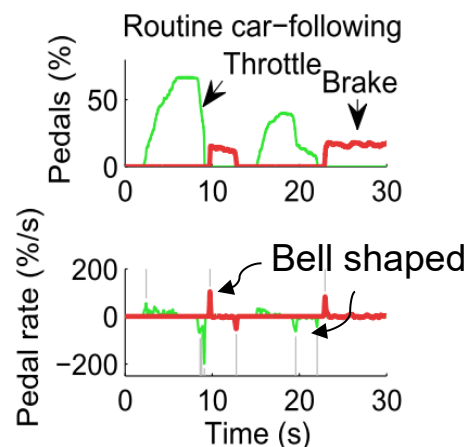


**Fig. 3-7. Driver's brake pedal use in car-following and braking conditions in real traffic** (Source: Markkula, 2014)

In Fig. 3-7, the top figure shows the positions of brake and accelerator pedals (throttle). A pedal position of 100% means that the pedal is fully pressed and 0% means that the pedal is not pressed at all. The bottom figure shows the corresponding rate of change in pedal positions (pedal rate). It was observed that the driver rapidly pressed the accelerator pedal and then held the same pedal position (top figure of Fig. 3-7). It was also found that the pedal rate in the bottom figure of Fig. 3-7 follows a bell-shaped distribution which captures a rapid increase in acceleration in a very short time. According to Svärd et al. (2017), the duration of an individual control ajustment, $\Delta T$, is constant for a driver.

Based on this assumption and empirical evidence from naturalistic driving studies, Markkula et al. (2014) proposed that the *expected* magnitude of the $i^{th}$ control adjustment ($g_i$) is described as a function of control error prediction error as follows:

$$g_i = K\Delta T \cdot \epsilon(t_i)$$

With $K' = K\Delta T$ and $\epsilon(t) = P_r(t) - P_p(t)$:

$$g_i = K'(P_r(t_i) - P_p(t_i)) \tag{3-40}$$

where $K$ is the control gain in the continuous model (Eq. (3-28)), $K'$ is the control gain in the intermittent model, $\Delta T$ is the duration of the control adjustment (e.g., the time elapsed between the start and stop pushing the brake pedal), and $t_i$ is the start time of the $i^{th}$ control adjustment. As discussed in the previous section, the start time of control adjustment $t_i$ is predicted based on the accumulator model.

To illustrate the difference between the control gain of continuous model $K$ and the control gain of intermittent model $K'$, consider a situation where $P_p = 0, \Rightarrow \epsilon = P_r \approx P$.

The intermittent control model will respond to the control error $P$ by applying a magnitude of $g_i = K'P$ in a time duration $\Delta T$. Thus, the average rate of change of control by the intermittent model is $K'P/\Delta T$, which is also the control rate $KP$ applied by the continuous model ($= (K\Delta T)P/\Delta T = KP$).

Larger control adjustments can lead to inaccuracies in the targeted adjustment (e.g., larger deceleration than the intended deceleration). This is called motor noise. The motor noise is also considered in Eq. (3-40). Therefore, the *actual* control adjustment magnitude ($\tilde{g}_i$) is as follows (Markkula et al., 2018):

$$\tilde{g}_i = k \cdot \tilde{\epsilon}_i \tag{3-41}$$
$$\tilde{\epsilon}_i = (1 + m_i) \times \epsilon(t_i)$$

where $m_i$ is the motor noise which is normally distributed with zero mean and variance $\sigma_m{}^2$. The actual magnitude $\tilde{g}_i$ considers the human error in applying the control adjustment by using the motor noise $m_i$ in the applied motor primitive. For example, a driver might apply a slightly larger/smaller brake pedal rate than the required brake pedal rate as per Eq. (3-40).

To replicate the shape of control adjustment as shown in Fig. 3-7, the function $G(t)$ is defined as follows:

$$G(t) = \begin{cases} 0 \text{ for } t \leq \tau_m \\ 1 \text{ for } t \geq \tau_m + \Delta T \end{cases} \tag{3-42}$$

where $t = 0$ is the time when the accumulator model reaches the threshold, and $t = \tau_m$ is the start time of the control adjustment that occurs after the motor delay of $\tau_m$. The motor

delay occurs due to the time it takes between the human body movement and vehicle response. Moreover, $\Delta T$ is the duration of the control adjustment. $G(t)$ corresponds to the shape in the top figure of Fig. 3-7 (shape of pedal position). $G(t)$ is assumed to be an increasing function between $t = \tau_m$ and $t = \tau_m + \Delta T$. Eq. (3-42) is described as follows:

- An individual control adjustment starts at $t = \tau_m$ and ends at $t = \tau_m + \Delta T$. An actual adjustment can start at any time, so $t = \tau_m$ refers to the start time of the $i^{th}$ control adjustment $(t_i)$.

- At $t \leq \tau_m$, $G(t) = 0$ as no control adjustment is made.

- $G(t)$ increases from $G(\tau_m) = 0$ to $G(\tau_m + \Delta T) = 1$.

- At $t \geq \tau_m + \Delta T$, $G(t) = 1$ (i.e., the current pedal position is maintained). If the accumulated evidence $(A(t))$ reaches to a threshold again, a new control adjustment is made.

Eq. (3-42) is illustrated with an example of brake pedal use as control adjustment with the assumed $\tau_m = 0$ (Fig. 3-8). The top figure of Fig. 3-8 (a) shows that the pedal position increased from 0 to 1 during $t = 8.933 - 10.933$ s ($\Delta T = 2$ s). The bottom figure of Fig. 3-8 (a) shows $G(t)$ during the control adjustment. Note that $t = 0$ in this example refers to the start time of the 1$^{st}$ control adjustment $(t_1 = 8.933\ s)$.

Fig. 3-8 (b) shows the rate of change in $G(t)$ which represents the shape of pedal rate. The rate of change in $G(t)$ replicates the bell-shaped distribution of pedal rate as observed in Fig. 3-7. $G(t)$ increases between $t = 0$ and $t = \Delta T$ if it meets the requirements in Eq. (3-42). Markkula used a skewed truncated Gaussian distribution for the rate of change of

71

$G(t)$ (Fig. 3-8 (b)) and integrated it to determine the shape of function $G(t)$ (Fig. 3-8 (a)) (Markkula, 2020).
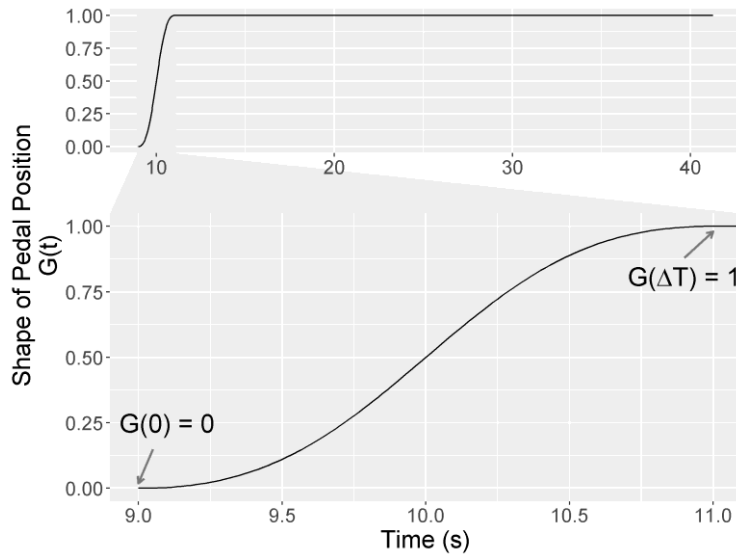


(a) Shape of the brake pedal position described in function $\boldsymbol{G(t)}$
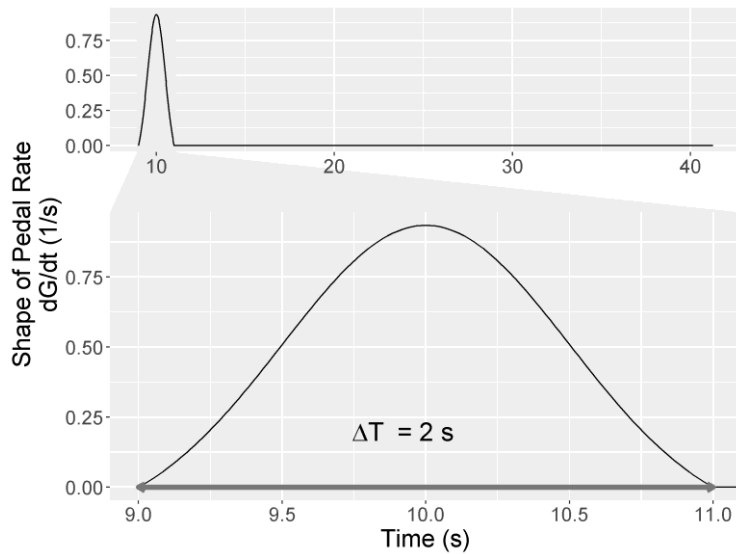


(b) Rate of change of $\boldsymbol{G(t)}$

**Fig. 3-8. Example of shape of control adjustment**

Once the magnitude of control adjustment reaches $\tilde{g}_i$ after the $i^{th}$ control adjustment, the driver is assumed to keep the adjustment at that magnitude until the evidence accumulates again, and a further control adjustment is required. Thus, the total pedal position $C(t)$ is a sum of all individual control adjustments as follows:

$$C(t) = C_0 + \sum_{i=1}^{N} \tilde{g}_i \cdot G(t - t_i)$$

(3-43)

where $N$ is the number of control adjustments during $t_i < t$ and $C_0$ is the initial value of the control.

*Prediction of Control Error*

When a driver makes a control adjustment (e.g., braking) at $t_i$, the driver also makes a prediction $P_p(t)$ of how the control error will decrease over time (Markkula et al., 2018). For instance, if the evidence accumulates at a speed difference of 10 m/s and a spacing of 100 m, the instantaneous control error $P(t_i)$ is $\tau^{-1}(t_i) = \Delta V/S = 10/100 = 0.1\ s^{-1}$. As a result of the accumulated evidence, a driver now *knows* the current magnitude of control error and starts braking. Therefore, the driver would predict that the control error just after the start of braking is equal to the observed control error (Svärd et al., 2017). To reduce this large control error, the driver decelerates at 5 m/s$^2$ and *expects* that the speed difference (and control error) will gradually decrease to zero in the next few seconds. Therefore, $P_p(t)$ becomes equal to the actual control error just after braking starts (i.e., in the next time frame). However, since the speed does not decrease immediately after deceleration because

of inertia, the driver expects that the control error will start to decrease after some time. This expected behaviour is modeled by setting $P_p(t)$ equal to the observed control error for a duration $\Delta T_{p_0}$. Once the speed starts to decrease, it is expected to take a few seconds to decrease the control error to zero. Therefore, after $\Delta T_{p_0}$, the gradual decrease in control error to zero is modeled by decreasing $P_p(t)$ to zero during the time $\Delta T_{p_1}$. The durations $\Delta T_{p_0}$ and $\Delta T_{p_1}$ are explained later in this section.

However, the actual control error $P(t)$ might not decrease as predicted by $P_p(t)$. Therefore, the evidence is not only the control error, but a difference between the control error and the prediction $[P_r(t) - P_p(t)]$. This difference is called the control error prediction error. The magnitude of the predicted control error is directly proportional to the control error prediction error. The prediction function is defined as the sum of individual predictions as follows (Svärd et al., 2017):

$$P_p(t) \ = \ \sum_{i=1}^{N} [\tilde{\epsilon}_i \cdot H(t - t_i)]$$

(3-44)

where $H(t)$ *is* the shape of the prediction which is defined as follows:

$$H(t) = \begin{cases} = 0, for\ t \leq 0\ and\ t \geq \Delta T_p \\ \quad \rightarrow 1, for\ t \rightarrow 0^+ \\ \quad \rightarrow 0, for\ t \rightarrow \Delta T_p \end{cases}$$

(3-45)

where $\Delta T_p$ is a model parameter which controls the duration of the predicted control error $P_p(t)$. At $t_i$, a driver makes the prediction $P_p(t_i)$ and the control adjustment simultaneously (see 'trig' in the 'Superposition of predictive primitives' section of Fig.

3-4). The time $t = 0$ represents the start time of control adjustment $t_i$ in Eq. (3-45). Eqs. (3-44) and (3-45) are explained as follows:

- During the periods $t \leq 0$ and $t \geq \Delta T_p$, $H(t) = 0$ as a driver does not make the prediction and control adjustment.

- $\Delta T_p = \Delta T_{p_0} + \Delta T_{p_1}$

- During $0 < t \leq \Delta T_{p_0}$, $H(t) = 1$. This means that just after the control adjustment is made, $P_p(t)$ is equal to the control error and remains equal to the same error during $\Delta T_{p_0}$.

- During $\Delta T_{p_0} < t \leq \Delta T_p$, $H(t)$ decreases from 1 to zero. This is the duration $\Delta T_{p_1}$.

- $H(t) \rightarrow 1, for\ t \rightarrow 0^+$ indicates that $H(t)$ approaches 1 when time $t$ approaches 0 from positive values.

- $H(t) \rightarrow 0, for\ t \rightarrow \Delta T_p$ indicates that $H(t)$ approaches 0 when time $t$ approaches $\Delta T_p$.

Fig. 3-9 illustrates $H(t)$ for an example of the prediction using assumed values of all parameters. The top figure shows that the prediction begins at 8.933 s ($t = 0$) and $H(t)$ increases to 1 at 8.95 s. During $\Delta T_{p_0} = 0.5\ s$, $H(t) = 1$ as a driver predicts that it will take some time for the control adjustment to start reducing the control error. Afterwards, $H(t)$ gradually decreases to zero during $\Delta T_{p_1} = 8.5\ s$. Thus, the Markkula model predicts that as a result of a control adjustment, the control error prediction error will decrease to zero at 17.95 s (= 8.95 + 0.5 + 8.5).
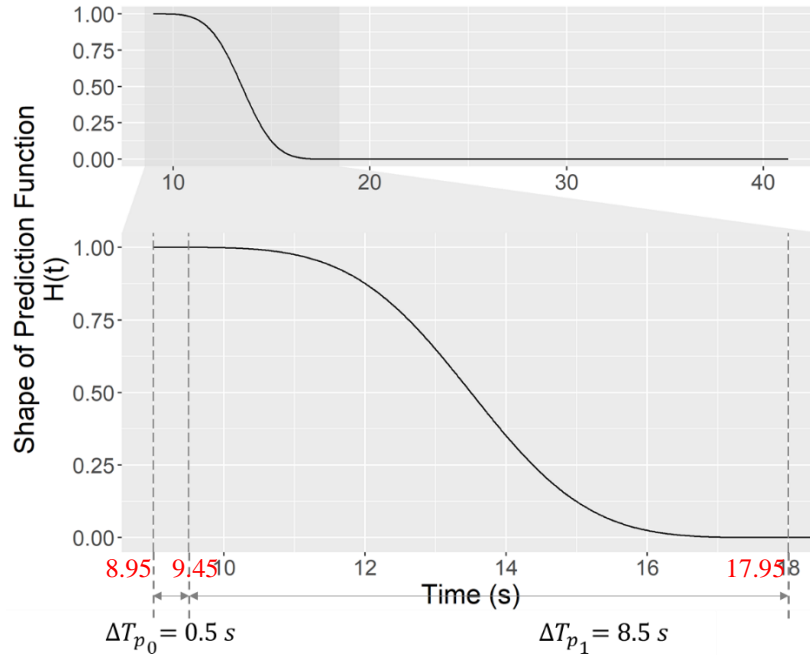
**Fig. 3-9. Shape of Prediction of looming**

Fig. 3-10 shows an example of driver braking behaviour predicted by the Markkula model. Fig. 3-10 (a) shows the observed lead vehicle and subject vehicle deceleration over time. Tau-inverse is the estimated control error $P(t)$ with the assumption that the initial speed difference is zero. Since this example was used to illustrate the model prediction, the parameters were not calibrated. It was assumed that $\varepsilon(t) = 0$, $M = 0.01$, $\tau_p = \tau_m = 0$, $m_i = 0$, and the threshold $A_{TH} = 0.03$.

As shown in Fig. 3-10 (b) and (c), when the control error accumulates to the threshold at $t_1 = 8.933$ s (i.e., when the accumulated evidence $A(t)$ reaches the threshold $A_{TH} = 0.03$), the Markkula model predicts the start time of control adjustment (i.e., brake application) as shown in Fig. 3-10 (d). Simultaneously, a prediction $P_p(t)$ of how the control error would decrease over time (due to the braking) is also calculated using Eqs. (3-44) and (3-45) as shown in Fig. 3-10 (b). The red vertical dashed lines in Fig. 3-10

76

indicate the start times of individual control adjustments. Moreover, the accumulator is reset at $t_i$, i.e., the activity $A(t)$ is reduced from the threshold $A_{TH}$ to a reset value $A_r$ which needs to be calibrated. In this example, $A_r$ was assumed to be 60% of the threshold ($= A_{TH} \times 0.6 = 0.018$).

The figure to the left of Fig. 3-10 (b) shows the zoomed-in part of $P_p(t)$ around the time when $t_i = t_1$, i.e., when the first control adjustment started. As per the function $H(t)$ (Eq. (3-45)), the prediction $P_p(t)$ starts increasing from zero at $t_i = t_1 = 8.933$ s i.e. when $A(t)$ reaches the threshold. Then it starts to approach the value of the observed control error until it becomes equal to the observed control error at 8.95 s. $P_p(t)$ remains equal to the observed control error ($H(t) = 1$) for a duration of $\Delta T_{p_0} = 0.5\ s$ i.e., until 9.45 s. Afterwards, $P_p(t)$ starts decreasing to zero. $P_p(t)$ becomes zero at $t = 17.95$ s as $\Delta T_{p_1} = 8.5\ s$ (9.45 + 8.5 = 17.95 s). However, as $A(t)$ reaches its threshold a second time at $t_i = t_2 = 11.33$ s, $P_p(t)$ increases again as a result of the second control adjustment.

Subsequently, the accumulated evidence $A(t)$ reaches the threshold again and the second control adjustment and the prediction are made at about 11.33 s as shown in Fig. 3-10 (b). As a result, the model replicates the observed step-wise pattern of deceleration as shown in the dashed line in Fig. 3-10 (a).
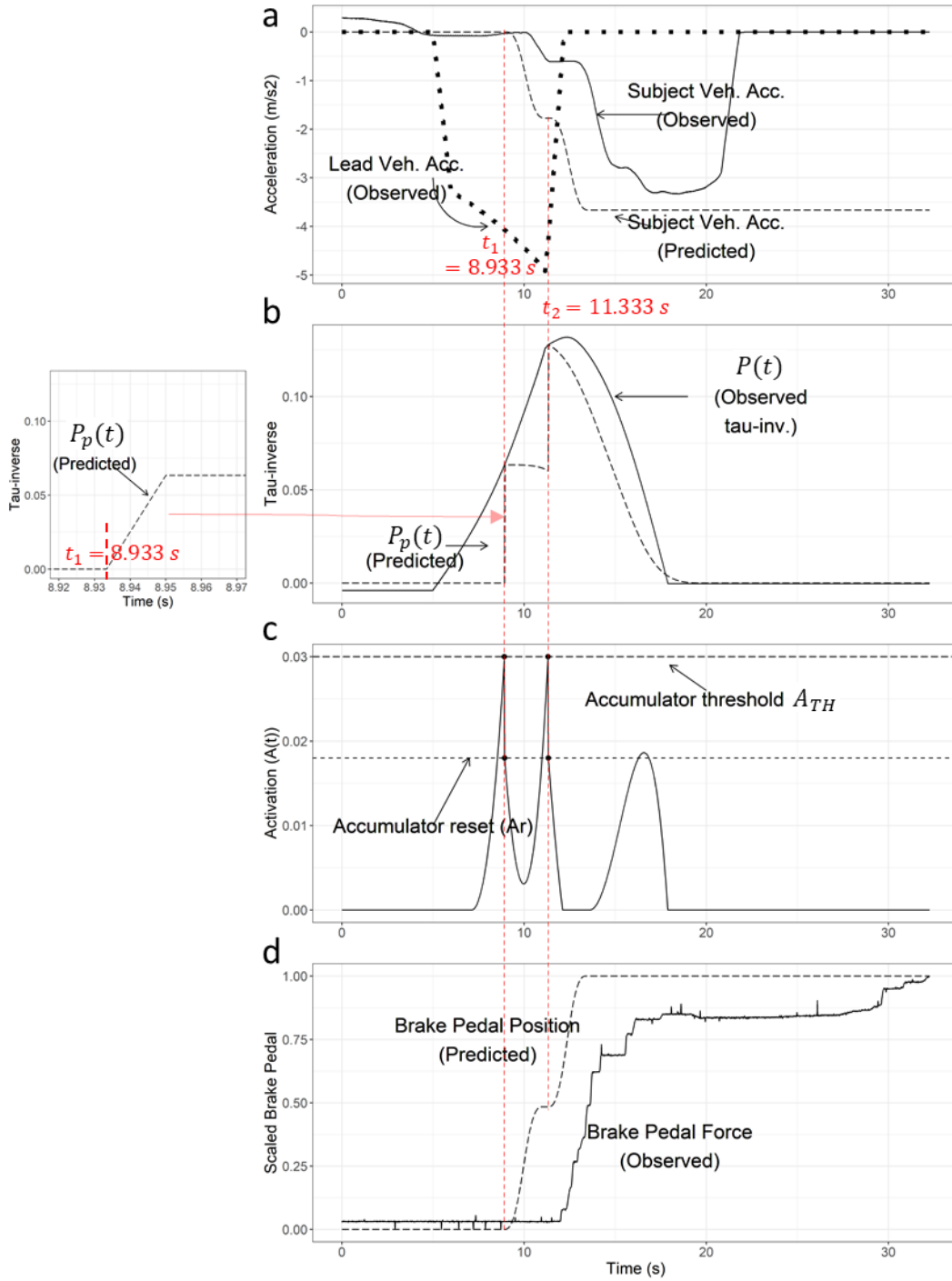
**Fig. 3-10. Prediction of braking behaviour using Markkula Model.**

(Note: Subject vehicle and lead vehicle decelerations were observed from a driving simulator study conducted by the author)

### 3.2.3. Differences between Wiedemann and Markkula Models

The differences between the Wiedemann and Markkula models are summarized as follows:

*Driver Perception and Reaction Time*

Both models consider sensory evidence such as angular velocity and tau-inverse to estimate the start time of driver reaction. Wiedemann model assumes a single value of sensory evidence as a driver-specific perception threshold, while the Markkula model assumes the accumulation of multiple values of the sensory evidence as a reaction threshold. Furthermore, the Markkula model accounts for the noise and other factors such as lead vehicle brake lights. As a result, the Markkula model can account for the variation in the reaction time for the same drivers in different driving conditions. Although the Wiedemann model also accounts for the variation in reaction time using random parameters, it does not explain how the variation occurs.

The Markkula model can also account for other factors that can potentially influence driver perception and reaction time. For instance, higher level of discomfort with following a lead truck compared to a lead car (in addition to a larger width of a lead truck) can potentially decrease reaction time. This factor can be incorporated in the Markkula model in the same manner as the lead vehicle brake light (see Eq. (3-39)). However, the Wiedemann model only accounts for the width of the lead vehicle, but not the type of lead vehicle.

*Driver Reaction*

The Wiedemann model provides equations for acceleration and deceleration as a function of spatiotemporal variables such as speed difference and spacing. The limitation of the Wiedemann model is that it does not account for the observed step-wise deceleration behaviour (see Fig. 3-10 (a)), but rather produces a continuous deceleration profile (see Chapter 3.2.1). Moreover, since the deceleration and acceleration equations are switched whenever the sensory evidence reaches a perception threshold, the jerk (rate of change of acceleration) predicted by the Wiedemann model can be unrealistically large (Lu, Song and Yu, 2018). For instance, when the driving condition changes from the free driving condition to the emergency braking condition, the model predicts a large acceleration in one second but a large deceleration in the next second, which leads to a severe and unrealistic jerk.

The Markkula model predicts deceleration behaviour based on the concepts from neurobiology and empirical evidence and predicts realistic jerk and step-wise deceleration behaviour. However, the Markkula model is not a complete car-following model in the current form as it cannot predict the acceleration in Free-driving and Following conditions. Moreover, in non-emergency situations, drivers generally first release the accelerator and then apply brakes after some time lag. This is the typical behaviour while approaching a slow lead vehicle or braking in non-emergency situations. But Markkula model does not account for this behaviour as it was designed for only emergency deceleration.

The main objective of this thesis is to extend the Markkula model so that it can account for the influence of lead truck on the driver's reaction time and acceleration behaviour in all car-following conditions. To this end, Chapter 4 describes the research hypotheses,

experiment design, and data collection to compare the assumptions of the Wiedemann and Markkula models. Chapter 5 explains the methods to analyze the data and the modifications of the Wiedemann and Markkula models to create a car-following model which realistically predicts the speed, spacing and acceleration in all conditions.

# Chapter 4:  Research Hypotheses and Data Collection

The discussions in the previous chapters elaborated two alternative frameworks of developing car-following models. Chapter 2:  explained the engineering car-following models that use spatiotemporal variables - e.g., spacing and speed difference. Chapter 3: provided the theoretical background of the Wiedemann and Markkula models that use sensory evidence such as angular velocity and tau-inverse. Both spatiotemporal variables and sensory evidence are used in the respective models to predict the time of driver reaction (using either Perception-Reaction Time (PRT) or threshold of sensory evidence) and the magnitude of acceleration.

To develop a car-following model that realistically predicts the start time of drivers' reaction and acceleration rate, it is important to compare the alternative frameworks against the observed behaviour in car-following. Therefore, three hypotheses on PRT were developed to compare the assumptions in the engineering car-following models, Wiedemann model and Markkula model. The next two sections explain these hypotheses and the final section presents the procedures for collecting car-following data which was used for testing the hypotheses.

## 4.1    Hypotheses on the Start Time of Reaction

The time at which a driver starts deceleration (or acceleration) is assumed to be either a function of PRT or a function of a threshold of some sensory evidence. Therefore, in this study, three hypotheses about the definition of PRT were examined. To test these hypotheses, four driving simulator scenarios were tested to measure the driver's perception and reaction thresholds – i.e., minimum detectable tau-inverse or angular velocity - in

approaching and lead vehicle braking conditions. In two of the four scenarios, the drivers were instructed to stop as soon as they felt that the lead vehicle was slow or braking in the absence of lead vehicle brake lights. These "perception scenarios" are called *Perception-in-approaching* and *Perception-in-following* scenarios, respectively. In the other two scenarios, the drivers were instructed to release accelerator or apply brake as they approached the moving or stopped lead vehicle. These "reaction scenarios" are called *Moving-lead-vehicle* (LV) and *Stopped-LV*, respectively.

However, some drivers tend to react immediately when they see the lead vehicle brake lights regardless of spacing and speed difference (Xue et al., 2018). In this case, the drivers are not likely to react based on the visual variables. To test the effect of lead vehicle brake lights on driver reaction in the Moving-LV scenario, equal proportions (50%) of drivers were randomly assigned to lead vehicle brake lights turned ON and OFF cases. However, as some drivers did not complete the experiments, 54% of the experiments were completed with the lead vehicle brake lights turned ON and 46% with the lead vehicle brake lights turned OFF. Each hypothesis of PRT is explained as follows:

### 4.1.1 Hypothesis 1 (H1): Perception and reaction occur at the perception threshold

In this hypothesis, a driver is assumed to release the accelerator or brake as soon as the visual variable reaches the driver's perception threshold. Thus, there is zero or negligible time lag between the perception threshold and the release of the accelerator in approaching condition (or the start of braking in braking condition). This hypothesis was defined as follows:

- For a given driver, tau-inverse or angular velocity at the time of accelerator release/braking is the same in the perception and reaction scenarios.

Therefore, the total PRT can be measured as the time between the first appearance of the lead vehicle (or the start of the lead vehicle deceleration) and the perception threshold (release of accelerator or braking). In this study, tau-inverse was used for the analysis because it normalizes the angular velocity by the visual angle subtended by the lead vehicle width. Also, as truck's width is larger than the car's width, tau-inverse is a better measure for comparison between the lead car and truck cases than angular velocity.

### 4.1.2 Hypothesis 2 (H2): Perception occurs at the perception threshold and the reaction occurs after a reaction time

In this hypothesis, perception occurs when tau-inverse or angular velocity reaches the driver's perception threshold but there is a time lag between perception and reaction (release of the accelerator/braking). This time lag is measured as reaction time. The hypothesis was defined in the following two sub-hypotheses:

- Tau-inverse or angular velocity is significantly higher in the reaction scenarios than the perception scenarios.

  **H2-1:** The time lag between the perception threshold (measured in the perception scenarios) and accelerator release or braking (measured in the reaction scenarios) is the reaction time.

**H2-2:** The time lag between perception threshold and accelerator release or braking is dependent on the reaction threshold, instead of the reaction time. Reaction threshold is also measured by tau-inverse or angular velocity in the reaction scenarios.

Therefore, the PRT consists of the following two components: 1) *Perception Time:* the time between the first appearance of the lead vehicle or the start of lead vehicle deceleration and the time when tau-inverse or angular velocity reaches the driver's perception threshold, and 2) *Reaction Time:* the time between the perception threshold and the release of the accelerator/ braking (H2-1) or the reaction threshold (H2-2).

### 4.1.3 Hypothesis 3 (H3): Reaction occurs as a result of the evidence accumulation process

In this hypothesis, the driver's reaction is more important to characterize the driver behaviour than the driver's perception. Thus, it is hypothesized that a driver reacts after the *evidence* for the need of slowing down (e.g., angular velocity, tau-inverse) is accumulated over time. The evidence will be accumulated faster if the rate of increase in tau-inverse or angular velocity is higher - e.g., due to a decelerating lead vehicle at a short spacing. Consequently, a driver will react faster when the evidence accumulates faster. In this case, the start of reaction is attributed to the rate of accumulation of evidence rather than a driver's perception/reaction thresholds. This hypothesis was defined as follows:

- Tau-inverse or angular velocity at which the driver releases accelerator or brakes is dependent on the accumulation of evidence over time. Therefore, the areas under the

curves of tau-inverse or angular velocity over time is the same for the same driver in the perception and reaction scenarios.

## 4.2    Data Collection

Two sources of data were used in this thesis: 1) driving simulator scenarios and 2) real-world vehicle trajectory data. Driving simulator scenarios were developed by the author. The data obtained from these scenarios were used for testing the hypotheses described above, as well as developing and calibrating a new car-following model. Vehicle trajectory data on a US highway was sourced from an online repository. These trajectory data were used to calibrate and validate the new car-following model developed in this thesis. Both data sources are described in detail as follows.

### 4.2.1    Description of Driving Simulator Scenarios

Two perception scenarios and two reaction scenarios were tested using a driving simulator. For each driver, the reaction scenarios were conducted first because they were normal driving conditions where the driver could control the speed. In the perception scenarios, the speed was controlled by the driving simulator and the drivers were instructed to respond only when they perceived a stimulus. In each scenario, the time, spacing and speed difference at driver response (accelerator push/release or braking) were recorded. Using these data, the angular velocity and tau-inverse were calculated using Eqs. (3-1) and (3-9), respectively.

A total of 50 drivers (33 males and 17 females) participated in this driving simulator study in April and May 2019. The range of their age was 18 to 70 years with 31 participants in the 18-25 years age group. There were 5, 7, 4, 1, and 2 participants in 26-30 years, 31-

40 years, 41-50 years, 51-60 years, and 61-70 years age groups, respectively. Their driving experience varied between 2 to more than 10 years. This study was conducted using the MiniSim ¼ cab driving simulator at the University of Windsor. All drivers drove BMW 330i model to follow a lead vehicle in the simulator scenarios. The simulator experiment was cleared by the University of Windsor Research Ethics Board.

All scenarios were conducted on a 2-lane unidirectional highway with no curve. Drivers were instructed to stay in the right lane only and were prohibited from changing the lane. Drivers did a test run before each scenario until they verbally confirmed that they were comfortable in proceeding. At the start of all scenarios, the subject vehicle was stopped and there was no other vehicle or object nearby. To examine the effect of the lead vehicle size on drivers' perception and reaction, drivers followed either a lead car or a lead truck in two separate scenarios. To avoid any unexpected learning effect, the number of drivers who started with a lead car scenario were balanced with the number of drivers who started with a lead truck scenario.

The order of testing *Moving-LV* (S1) and *Stopped-LV* (S2) scenarios was different for different drivers. However, the drivers always first tested *Perception-in-following* scenario (S3) and then *Perception-in-approaching* scenario (S4). All scenarios were conducted with daytime conditions and low traffic density (only 2 vehicles). The duration of each scenario varied due to different speed of the driver, but it was no more than 7 minutes. Each scenario is explained as follows:

*S1: Moving-LV*

The driver accelerated from a stationary position and drove freely until the speed reached his/her desired speed (>100 km/h in most cases). During free-driving, as soon as

87

the driver passed a fixed location in the scenario, a lead vehicle with a uniform speed of 90 km/h appeared in the same lane at 600 m spacing. As the driver approached the lead vehicle, he/she had to reduce speed to follow the lead vehicle at a safe spacing. After following the lead vehicle for several seconds, the lead vehicle abruptly decelerated at -4 m/s$^2$ and stopped. The lead vehicle started decelerating at the same fixed location for all drivers. Consequently, the driver was further required to decelerate and stop behind the lead vehicle. For example, the speeds of subject and lead vehicles varied over time in this scenario as shown in Fig. 4-1.
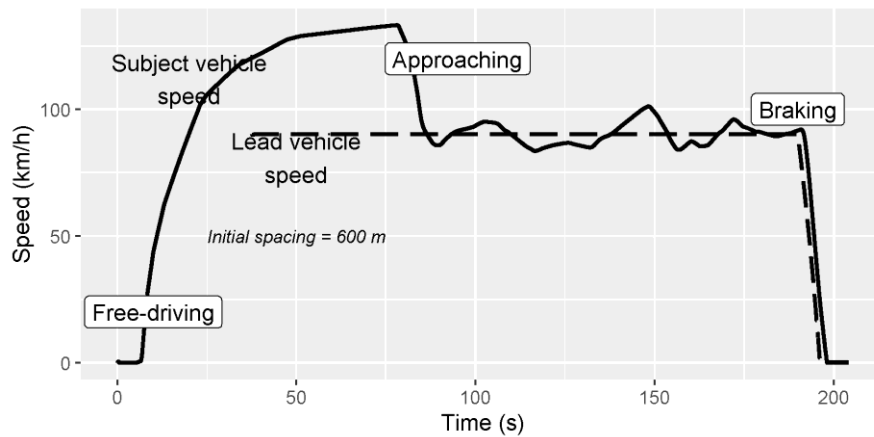


**Fig. 4-1. Temporal variation in speed in the Moving-LV scenario**

As some drivers withdrew (e.g., due to simulator sickness), a total of 49 drivers tested the lead car scenario (26 with the lead vehicle brake lights on and 23 with brake lights off) and a total of 48 drivers tested the lead truck scenario (26 with brake lights on and 22 with brake lights off). Some drivers were influenced by the sudden appearance of the lead vehicle or did not interact with the lead vehicle due to small desired speed (< 90 km/h). Therefore, the data for only 58 cases (29 drivers for lead car/lead truck) were used for the

analysis. Due to the difference in driver's desired speeds, the spacing when the lead vehicle decelerated varied from 15 m to 200 m. This variation in spacing influenced the start time of braking when the lead vehicle decelerated.

*S2: Stopped-LV*

In this scenario, the subject vehicle was approaching the stopped lead vehicle with the brake light off at an initial spacing of 1,200 m and had to reduce speed to stop behind the lead vehicle. Thus, this scenario was designed to capture the driver behaviour when he/she unexpectedly encountered the stopped lead vehicle on a highway. A total of 48 and 49 drivers completed the lead car and lead truck scenarios, respectively.

*S3: Perception-in-following*

The purpose of this scenario was to determine when the drivers perceived that the lead vehicle was slower than the subject vehicle while they were following the lead vehicle at small to medium spacing (50-500 m). The drivers were instructed to increase speed from 0 to 100 km/h. When the speed reached 100 km/h, the cruise control was automatically activated and the drivers were instructed to release the accelerator. Then, a lead car or a lead truck appeared at approximately 50 m, 100 m, or 500 m ahead of the subject vehicle in the same lane.

The lead vehicle initially moved at the same speed as the subject vehicle (100 km/h). Then the drivers were instructed to observe the lead vehicle speed for a few seconds (the "Observe" message was displayed on the screen). At this moment, the lead vehicle started decelerating or accelerating. After the observation of the lead vehicle speed change, the drivers were asked to change their speed (the "Change Speed" message was displayed on

the screen). They could either accelerate by pressing the accelerator if they perceived that the lead vehicle accelerated or decelerate by pressing the brake pedal if they perceived that the lead vehicle decelerated. They could also respond even before the "Change Speed" message was displayed if they perceived the change in the lead vehicle speed. They were required to change speed by the "Change speed" message even if they could not clearly perceive the change in the lead vehicle speed. However, if the drivers pushed the brake or accelerator pedals before the "Observe" message was displayed, the response was discarded, and the experiment was repeated.

In this scenario, the lead vehicle changed speed at an average rate of $\pm 0.15$ m/s$^2$ (max.: $\pm 0.5$ m/s$^2$) for either 1 s (max. speed difference of $\pm 0.5$ m/s), 2 s (max. speed difference: $\pm 1$ m/s), 4 s (max. speed difference: $\pm 2$ m/s) or 6 s (max. speed difference: $\pm 3$ m/s). Four seconds after the lead vehicle reached the new speed, the "Change Speed" message was displayed. The driver accelerated or decelerated based on his/her perceived change in the lead vehicle speed within or at 4 s after the change in speed. The three stages in this scenario are illustrated in Fig. 4-2.

Direction of motion

**1. Cruise control activated**

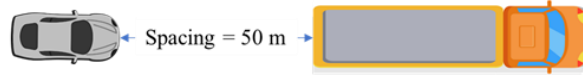Subject vehicle and Lead vehicle
Speed = 100 km/h

Spacing = 50 m
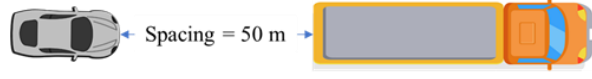
**2. Observe message**

Subject vehicle
Speed = 100 km/h

Lead vehicle
Speed starts to decrease @ -0.5 m/s² for 6 seconds,
Until the new speed = 89.2 km/h

Spacing = 50 m

**3. Change Speed message (appears 4 sec after the new speed is reached)**

Subject vehicle
Participant reduces the speed
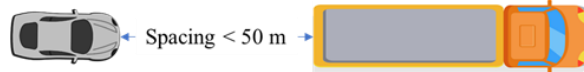
Lead vehicle
Speed = 89.2 km/h

Spacing < 50 m

**Fig. 4-2. Illustration of Perception-in-following scenario (initial spacing = 50 m, maximum speed difference = -3 m/s)**

Source: Truck - https://www.dreamstime.com/stock-illustration-truck-top-view-flat-style-vector-icon-lorry-container-illustration-isolated-white-background-cargo-transportation-image86583281

Car - http://www.clipartpanda.com/categories/truck-clipart-top-view

There were a total of 48 cases of car-following (= 3 spacing × 8 speed differences × 2 lead vehicle types). However, testing 48 cases for each driver was not desirable due to driver fatigue. To reduce the number of cases for each driver, the driver was tested for 3 spacings and both lead vehicle types but 6 speed differences only (i.e., 36 cases per driver). A set of cases for each driver was randomly selected in the manner that each combination of spacing and speed difference for each lead vehicle type was run for at least 4 different

drivers. A total of 46 drivers completed both lead car and lead truck scenarios. Each driver tested both lead vehicle acceleration/deceleration because he or she might be able to easily anticipate changes in the lead vehicle speed if the lead vehicle consistently accelerates or decelerates in multiple runs.

*S4: Perception-in-approaching*

The purpose of this scenario was to determine when the drivers first perceived that the lead vehicle was slower than the subjective vehicle while they were approaching the lead vehicle at a larger spacing. The drivers accelerated from zero speed to 100 km/h, at which the cruise control was automatically activated, and they released the accelerator. Then, a lead car or a lead truck which was moving at the speed of 70 km/h appeared at a spacing of 1,000 m in the same lane. If the drivers perceived that the lead vehicle was slower than the subject vehicle, they were instructed to press the brake pedal to indicate their perception. Otherwise, they could continue driving without any response. A few drivers were removed from the data because they mistakenly pressed the accelerator during this scenario. Thus, a total of 90 cases (44 drivers for the lead car scenario and 46 drivers for the lead truck scenario) were used for the analysis.

The PRTs were estimated according to the hypotheses 1 and 2 using the data collected from the four scenarios in the driving simulator experiment. The start and end points of PRT in approaching and braking conditions are explained in Table 4-1.

**Table 4-1. Definitions of PRT in Hypotheses 1 and 2**

| Hypothe-sis | Car-following Condition | Scenario | Definition of PRT |
|---|---|---|---|
| **H1** | Approaching | Approaching part in both reaction scenarios (S1 and S2) | *Start:* time when driver first sees the lead vehicle in the same lane (i.e., time when the lead vehicle appears)<br>*End:* time when driver releases the accelerator (the tau-inverse at this point must be similar to the tau-inverse at the accelerator release in the Perception-in-approaching scenario (S4)). |
| | Braking | Braking to a decelerating LV (Braking part of S1) | *Start:* time at the start of lead vehicle braking<br>*End:* time when driver starts braking (the tau-inverse at this point must be similar to the tau-inverse at braking in the Perception-in-following scenario (S3)) |
| | | Braking to a stopped LV (S2) | *Start:* time when driver released the accelerator to reduce speed during approaching<br>*End:* time at start of braking (the tau-inverse at this point must be similar to the tau-inverse at braking in the Perception-in-following scenario (S3)) |
| **H2** | Approaching | Approaching part in both reaction scenarios (S1 and S2) | Perception Time:<br>*Start:* time when driver first sees the lead vehicle in the same lane<br>(i.e., time when the lead vehicle appears)<br>*End:* time when tau-inverse reaches the driver's perception threshold (i.e., the value of tau-inverse estimated in the Perception-in-approaching scenario (S4))<br><br>Reaction Time:<br>*Start:* time when tau-inverse reaches the driver's perception threshold<br>*End:* time when driver releases the accelerator<br><br>PRT = Perception Time + Reaction Time |
| | Braking | Braking to a decelerating LV (Braking part of S1) | Perception Time:<br>*Start:* time at the start of lead vehicle braking<br>*End:* time when tau-inverse reaches the driver's perception threshold (i.e., the value of tau-inverse at the accelerator release in the Perception-in-following scenario (S3))<br><br>Reaction Time:<br>*Start:* time when tau-inverse reaches the driver's perception threshold<br>*End:* time when driver starts braking<br><br>PRT = Perception Time + Reaction Time |
| | | Braking to a stopped LV (S2) | Perception Time:<br>*Start:* time when driver released the accelerator to reduce speed during approaching<br>*End:* time when tau-inverse reaches the driver's perception threshold<br><br>Reaction Time:<br>*Start:* time when tau-inverse reaches the driver's perception threshold<br>*End:* time when driver starts braking<br><br>PRT = Perception Time + Reaction Time |

### 4.2.2　Description of Vehicle Trajectory Data

In addition to the vehicle trajectory data from the driving simulator, real-world vehicle trajectory data were also used for the calibration and validation of the new car-following model. Vehicle trajectory data were obtained from a segment of the Interstate-80 (I-80) in San Francisco, California on April 13, 2005. The data were collected under Federal Highway Administration's Next Generation Simulation  (NGSIM) project which aims at developing behavioural algorithms for microsimulation modeling and validation (FHWA, 2015). The original data are available in the Research Data Exchange (RDE) website (FHWA, 2016).

Seven cameras mounted on a high-rise building captured vehicle movements and the resulting images were transcribed into data at the resolution of one tenth of a second. The raw data sets consisted of lead and following vehicle IDs, longitudinal and lateral positions, velocities, accelerations, vehicle types, lane numbers, headway and spacing. However, the original NGSIM data had significant positional measurement errors which yielded unrealistic distributions of velocities and accelerations (Montanino and Punzo, 2015). Consequently, they used a four-step method to remove the errors and reconstructed the data collected during 4:00-4:15 pm. These data are available from Montanino and Punzo (2015). Therefore, only the reconstructed dataset for the duration 4:00 - 4:15 pm was used in this thesis, instead of the original data.

# Chapter 5: Methods

This chapter describes the development of a new car-following model that reflects the intermittent nature of driver reaction as discussed in the previous chapters. The chapter also describes the methods of calibration and validation of the new and existing car-following models using the driving simulator data and the Interstate-80 data.

## 5.1   New Car-Following Model: Intermittent Intelligent Driver Model

The proposed new car-following model – the Intermittent Intelligent Driver Model (IIDM) – was developed based on the Markkula's Framework of Sensorimotor Control in Sustained Motion Tasks. as explained in Chapter 3.2.2. Following sections describe the new model in detail.

### 5.1.1   Control Error $P(t)$

The control error $P(t)$ represents the need for control in each car-following condition. Car-following conditions include *free-driving*, *approaching* a slow lead vehicle, *following* closely, and *braking*. Previous studies have demonstrated $P(t) = \tau^{-1}$ as an appropriate control error for the braking condition (Markkula, 2014). However, using $\tau^{-1}$ as the control error $P(t)$ only represents the need for deceleration while approaching a slow lead vehicle and braking. Therefore, $\tau^{-1}$ is insufficient to represent the need for control in maintaining a desired distance with the lead vehicle in the following condition. Separate models are required to represent the need for acceleration in the free-driving and the following conditions. However, calibrating the model for two different conditions is not practical.

Therefore, $P(t)$ must include a combination of speed difference and spacing with a desired time gap or a desired spacing to represent the need for control (acceleration or deceleration) in all car-following conditions. Thus, a *complete* car-following model which predicts acceleration (positive and negative) in all car-following conditions was used to define the control error $P(t)$. An example of a complete car-following model is the Intelligent Driver Model (IDM) (Treiber and Kesting, 2013).

The IDM was used as the control error because the model does not have any existing parameter for reaction time. Therefore, the start time of reaction can be predicted using the accumulator model in this framework (explained in the next section), while the IDM only predicts the required acceleration/deceleration. Other complete car-following models such as the Gipps Model and the Wiedemann Model were not used because the models predict the start time of reaction either by using a constant reaction time (Gipps Model) or a constant perception threshold (Wiedemann Model). Thus, the Accumulator model cannot be incorporated into the Gipps Model and the Wiedemann model without significant modification of the original model specifications.

The acceleration, $a_{IDM}$, is calculated using the equation of IDM as follows:

$$a_{IDM} = A_i \left[ 1 - \left( \frac{v}{v_0} \right)^\delta - \left( \frac{s^*}{s} \right)^2 \right] \tag{5-1}$$

$$s^* = s_0 + \max \left( 0, vT + \frac{v \Delta v}{2 \sqrt{A_i b}} \right)$$

where $A_i$ is the maximum acceleration when starting from zero speed, $v$ is the subject vehicle speed, $v_0$ is the desired speed of subject vehicle in free-driving, $s$ is the spacing

between rear bumper of the lead vehicle and front bumper of the subject vehicle, $s_0$ is the standstill spacing, $T$ is the time gap in following, $\Delta v$ is the relative speed (subject vehicle speed minus lead vehicle speed), $b$ is the comfortable deceleration, and $s^*$ is the desired spacing in the following condition. Note that there is no reaction time term in the IDM.

Fig. 5-1 shows the speed, spacing, acceleration and jerk predicted using the calibrated IDM for a single run of Moving-LV scenario (as described in Chapter 4: ).
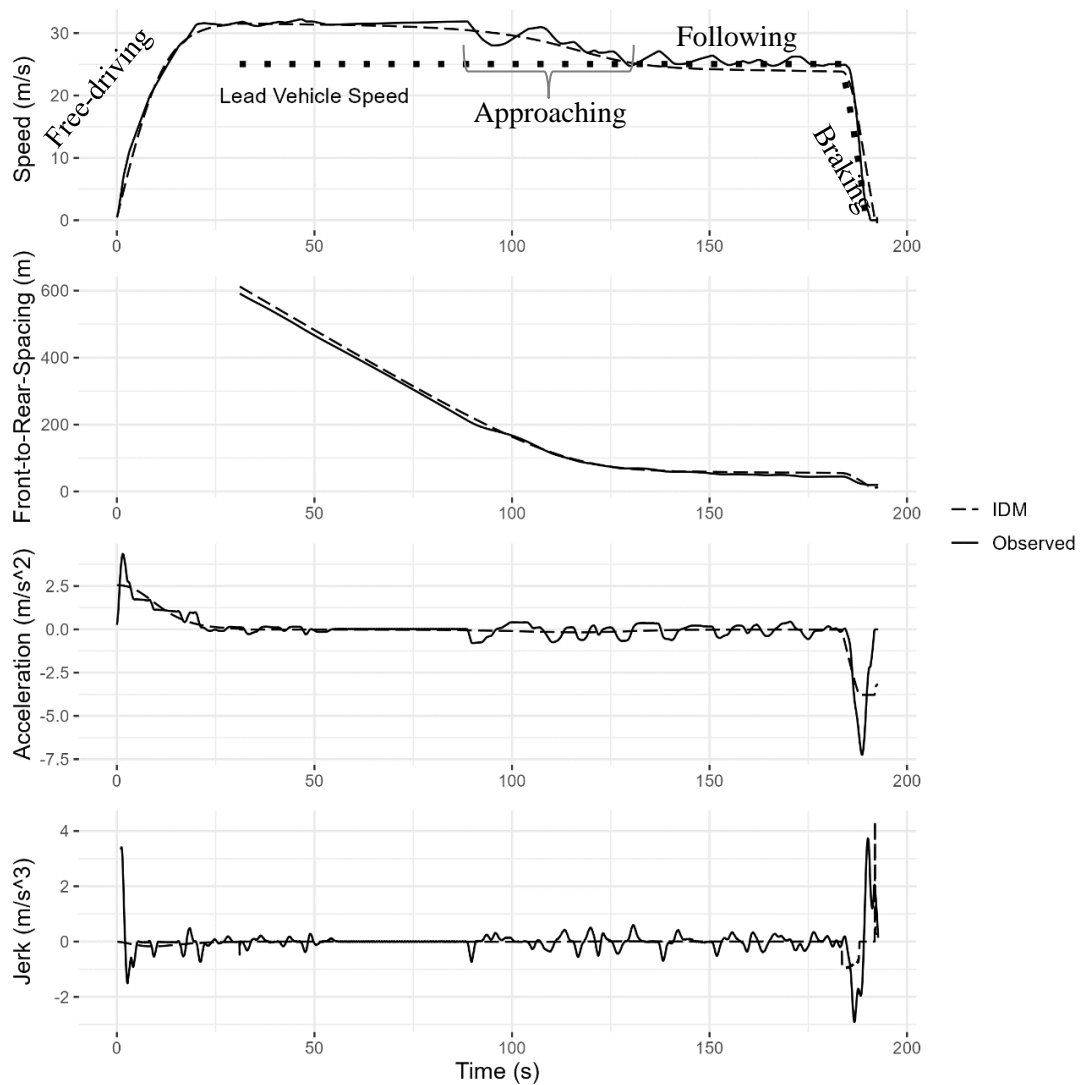


**Fig. 5-1. Predicted trajectories of the calibrated Intelligent Driver Model (IDM)**

The IDM predicts the acceleration in each car-following condition as follows:

*Free-driving*

The term $A_i \left[ 1 - \left( \frac{v}{v_0} \right)^\delta \right]$ in Eq. (5-1) controls the acceleration in free-driving. The maximum acceleration $A_i$ is used when the speed $v$ of the subject vehicle is zero. The acceleration generally decreases as the speed approaches the desired speed $v_0$. The rate of decrease in acceleration is regulated by the parameter $\delta$ (smaller values of $\delta$ such as 1 lead to smoother acceleration profiles). The acceleration is zero when the speed reaches the desired speed $v_0$. Fig. 5-1 shows that the IDM predicts an initial acceleration of 2.5 m/s$^2$ when starting from zero speed and the acceleration reduces to zero after the speed reaches the desired speed of 32 m/s.

*Following*

Drivers generally maintain a minimum spacing while following a lead vehicle in the steady-state traffic (all vehicles have nearly identical speeds). The IDM models this minimum spacing using a standstill spacing $s_0$ and a desired time gap $T$ in the desired distance expression $(s_0 + vT)$ in Eq. (5-1). Thus, in the steady-state condition, the IDM predicts acceleration when the desired distance $(s_0 + vT)$ is less than the current spacing $s$ or deceleration when the desired distance is longer than the current spacing.

*Approaching and Braking*

The IDM uses an "intelligent braking strategy" for predicting deceleration in approaching and braking conditions (Treiber and Kesting, 2013). This braking strategy depends on the kinematic deceleration, $\frac{v^2}{2s}$, i.e., the minimum deceleration required to avoid a collision. To

focus on the use of the kinematic deceleration in the IDM, the desired distance ($s_0 + vT$) and the free-driving acceleration ($A_i \left[ 1 - \left( \frac{v}{v_0} \right)^\delta \right]$) terms are set to zero. Moreover, as the lead vehicle is assumed to stop, $\Delta v = v$ (Treiber and Kesting, 2013). Then the deceleration is calculated based on the intelligent braking strategy using the following equation:

$$a_{intelligent} = -A_i \left[ \left( \frac{s^*}{s} \right)^2 \right]$$

$$a_{intelligent} = -A_i \left[ \left( \frac{v \cdot v}{2\sqrt{A_i b} \cdot s} \right)^2 \right]$$

$$a_{intelligent} = -A_i \left[ \frac{v^4}{4A_i b s^2} \right]$$

$$a_{intelligent} = -\left( \frac{v^2}{2s} \right)^2 \times \frac{1}{b} \qquad (5\text{-}2)$$

Deceleration in approaching and braking conditions (urgent and non-urgent) is determined using Eq. (5-2). In non-urgent braking or approaching condition, the required deceleration to avoid collision, $\left( \frac{v^2}{2s} \right)$, is smaller than the comfortable deceleration ($b$). Therefore, Eq. (5-2) predicts $a_{intelligent}$ which is less than the kinematic deceleration $\left( \frac{v^2}{2s} \right)$.

In the urgent braking situation, the required deceleration to avoid collision $\left( \frac{v^2}{2s} \right)$ is greater than the comfortable deceleration. Therefore, the predicted deceleration $a_{intelligent}$ is greater than the required deceleration to overcompensate for the urgent situation and regain control of the situation (Treiber and Kesting, 2013).

Fig. 5-1 shows the IDM deceleration in approaching and braking conditions (non-urgent). Compared to the observed deceleration, the IDM predicted early deceleration due to no reaction time in the model. This means that IDM continuously predicted acceleration and deceleration (and jerk) with smaller magnitude than the actual magnitude of acceleration/deceleration. The actual magnitude of deceleration was larger due to the delay caused by the accumulation of evidence by the driver (discussed in the next section).

Therefore, implementing the IDM in the intermittent framework by Markkula can lead to a realistic car-following behaviour where the start time of reaction is predicted by the accumulator model and acceleration/deceleration are predicted by the IDM at the start of reaction. This can be done by including $a_{IDM}$ in the control error $P(t)$.

Based on the moving target tracking example discussed in Chapter 3.2.2, the control error $P(t)$ for car-following was defined as the difference between the target acceleration $a_{IDM}(t)$ (Eq. (5-1)) and the current acceleration $a(t)$ as follows:

$$P(t) = C_T(t) - C(t) = a_{IDM}(t) - a(t) \tag{5-3}$$

$$P(t) = A_i \left[ 1 - \left( \frac{v(t)}{v_0} \right)^\delta - \left( \frac{s^*(t)}{s(t)} \right)^2 \right] - a(t)$$

where $C_T(t)$ is the target control and $C(t)$ is the actual control represented as $a_{IDM}(t)$ and $a(t)$, respectively. Using Eq. (5-3), the model applies a control rate $\dot{a}(t)$ (i.e., rate of change of acceleration) such that $a(t)$ equals $a_{IDM}(t)$ or the control error equals zero. Then Eq. (3-28) is re-written as follows:

$$\dot{a}(t) = K \cdot P(t - \tau_d) \tag{5-4}$$

where $K$ is control gain and $\tau_d$ is the sum of delays at perceptual, control decision and motor stages as discussed in Chapter 3.2.2.

### 5.1.2 Start Time of Driver Reaction

The continuous model of Eq. (5-4) does not reflect human drivers' intermittent time of reaction (i.e., drivers do not continuously change acceleration over time). Therefore, the accumulator model was used to predict the start time of reaction at intermittent time intervals - i.e., the driver reacts only when the accumulated evidence $A(t)$ exceeds the threshold $A_{TH}$. The instantaneous evidence $\epsilon(t)$ or 'control error prediction error' is:

$$\epsilon(t) = P_r(t) - P_p(t) \tag{5-5}$$

$$P_r(t) = P(t - \tau_p)$$

where $P_p(t)$ is the brain-predicted control error and $\tau_p$ is the perceptual delay (see Chapter 3.2.2 for details). The accumulator model is expressed as follows:

$$\frac{dA(t)}{dt} = \gamma\left[\eta\big(\epsilon(t)\big)\right] - \lambda A(t) + a_{BL} + \varepsilon(t) \tag{5-6}$$

where $A(t)$ is the accumulated evidence, $-\lambda A(t)$ represents the leakage of evidence, $k$ is the accumulator gain, $a_{BL}$ is the effect of lead vehicle brake lights, and $\varepsilon(t)$ is random background noise. Moreover, $\eta(\epsilon) = k\epsilon$, and $\gamma(\eta)$ is defined as follows (refer to Eq. (3-38)):

$$\gamma(\eta) = sign(\eta) \times \max(0, |\eta| - M) \tag{5-7}$$

where $M$ is the minimum gating below which accumulation does not start, and $sign(\eta)$ is +1, -1 or 0 when $\eta$ is positive, negative or zero, respectively.

Since deceleration condition is more critical than the acceleration condition, the threshold $A_{TH}$ is not the same for both conditions, but rather two thresholds $A_-$ and $A_+$ for negative and positive accumulated evidence in Eq. (5-6), respectively.

### 5.1.3 Acceleration Rate and Predicted Control Error

The magnitude of the $i^{th}$ control adjustment (acceleration or deceleration) ($g_i$) is expressed as follows (refer to Eq. (3-40)):

$$g_i = K'\epsilon(t_i) \tag{5-8}$$

where $K'$ represents the control gains in the intermittent model. Similar to the control error for the steering wheel angle rate model described in Chapter 3.2.2 (Eq. (3-30)), $P(t)$ described in Eq. (5-3) contains its own calibration parameters (e.g., $A$, $b$, etc.). Therefore, the control gain $K'$ is set to 1 and Eq. (5-8) is expressed as follows:

$$g_i = \epsilon(t_i) \tag{5-9}$$

$$g_i = P_r(t_i) - P_p(t_i)$$

$$g_i = A_i\left[1 - \left(\frac{v(t_i - \tau_p)}{v_0}\right)^\delta - \left(\frac{s^*(t_i - \tau_p)}{s(t_i - \tau_p)}\right)^2\right] - a(t_i - \tau_p) - P_p(t_i)$$

Adding the motor noise $m_i$ to Eq. (5-9) yields:

$$\tilde{g}_i = \tilde{\epsilon}_i \tag{5-10}$$

$$\tilde{\epsilon}_i = (1 + m_i) \times \epsilon(t_i)$$

where $m_i$ is the motor noise which is normally distributed with zero mean and variance $\sigma_m^2$. The shape of the control adjustment is provided by the function $G(t)$ (refer to Eq. (3-42)) is as follows:

$$G(t) = \begin{cases} 0 \ \text{for } t \leq \tau_m \\ 1 \ \text{for } t \geq \tau_m + \Delta T \end{cases} \tag{5-11}$$

where $t = 0$ is the time when $A(t) \geq A_+$ or $A(t) \leq A_-$, $t = t_i = \tau_m$ is the time of the $i^{th}$ control adjustment, $\tau_m$ is the motor delay, and $\Delta T$ is duration of acceleration/deceleration.

As discussed in Chapter 3.2.2, the prediction of control error $P_p(t)$ is defined as follows (refer to Eqs. (3-44) and (3-45)):

$$P_p(t) = \sum_{i=1}^{N} [\tilde{\epsilon}_i \cdot H(t - t_i)] \tag{5-12}$$

$$H(t) = \begin{cases} = 0, for\ t \leq 0\ and\ t \geq \Delta T_p \\ \rightarrow 1, for\ t \rightarrow 0^+ \\ \rightarrow 0, for\ t \rightarrow \Delta T_p \end{cases}$$

where $H(t)$ is the shape of prediction.

Based on the magnitude and shape functions, each acceleration/deceleration adjustment is controlled by the following intermittent control rate as follows:

$$\dot{a}(t) = \sum_{i=1}^{N} \tilde{g}_i \cdot \dot{G}(t - t_i) \tag{5-13}$$

where $N$ is the total number of acceleration and deceleration adjustments. The IIDM predicts the acceleration $a(t)$ in all car-following conditions as follows (refer to Eq. (3-43)):

$$a(t) = a_0 + \sum_{i=1}^{N} \tilde{g}_i \cdot G(t - t_i) \tag{5-14}$$

where $a_0$ is the initial acceleration, $\tilde{g}_i$ is the magnitude of control adjustment, $G(t)$ is the shape of control adjustment, and $N$ is the total number of adjustments.

Fig. 5-2 illustrates how the IIDM uses the control error and the accumulator model to make predictions on a single scenario run from the Moving-LV scenario. Fig. 5-2 (e) show the times when the model reaches the positive and negative thresholds. At these times, the model predicts acceleration or deceleration as shown in Fig. 5-2 (b). Fig. 5-2 (d) shows a zoomed-in part of Fig. 5-2 (c) for the duration 130 – 150 s to illustrate samples of control error $P(t)$ and its prediction $P_p(t)$ for both acceleration and deceleration adjustments.
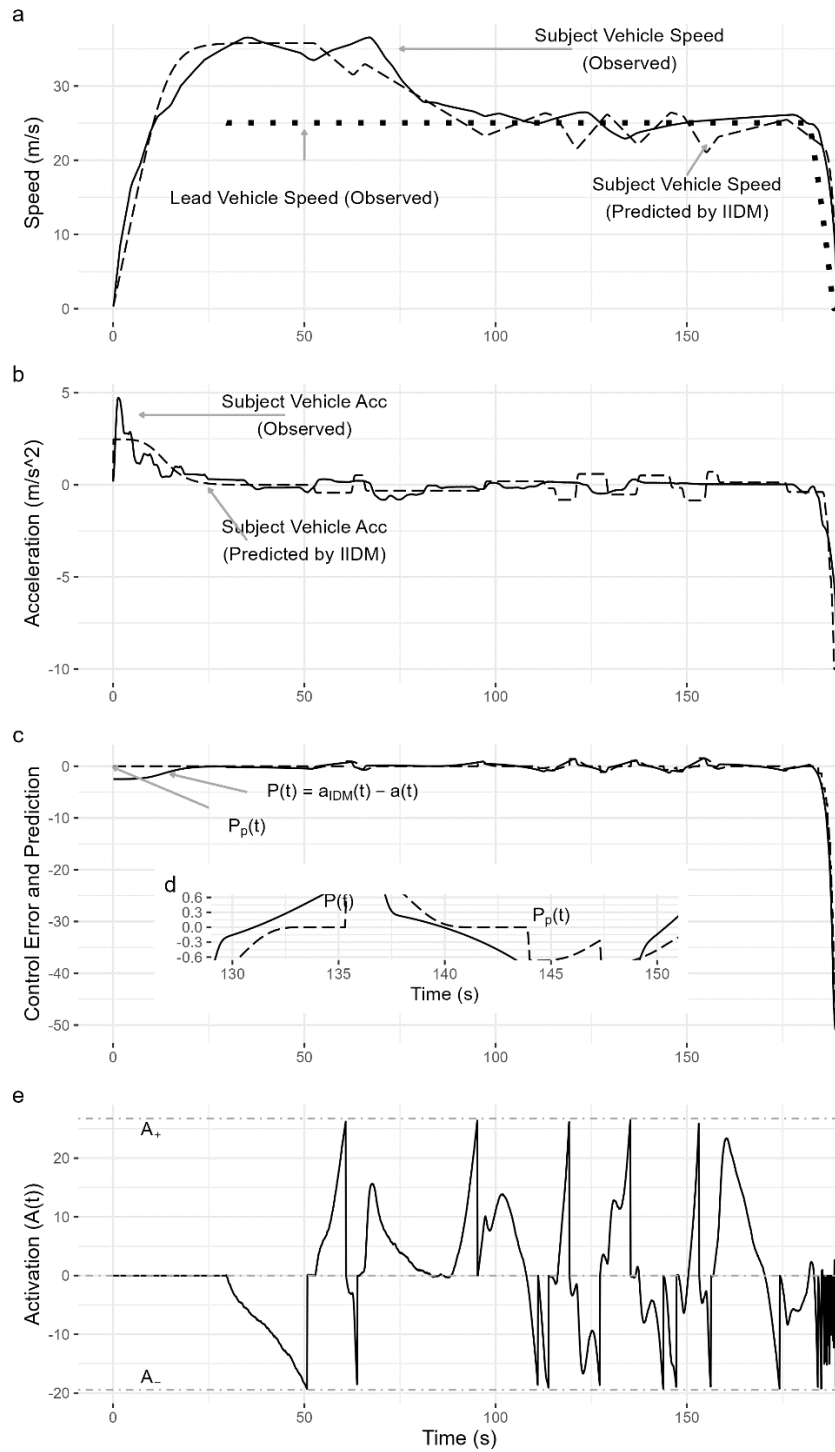
**Fig. 5-2. Prediction of Car-following Behaviour using the Intermittent IDM**

## 5.2    Assessment of Model Performance

The new car-following model, IIDM, was evaluated to assess if it can better predict car-following behaviour than the three existing car-following models that are most frequently used for microscopic simulation – 1) the Gipps Model (Gipps, 1981), 2) the Intelligent Driver Model (IDM) (Treiber and Kesting, 2013), and 3) the original Wiedemann Model (Wiedemann and Reiter, 1992).

Since two different types of data were used in this thesis, the models were calibrated at different levels of granularity. The driving simulator data consisted of individual scenario runs as opposed to the same traffic in the I-80 dataset. Therefore, each scenario run from the driving simulator data was individually used to calibrate the car-following models. The model performance was then assessed by visually comparing the predicted and observed speed, acceleration, jerk, and spacing. Moreover, the model performance was also quantitatively assessed by comparing the distributions of the above variables, as well as the minimum Time to Collision (TTC) and Deceleration Required to Avoid Crash (DRAC).

For the I-80 dataset, only the trajectory data for a pair of vehicles longer than 70 s were used. There were 60 car-following-car pairs which satisfy this requirement (pairs with heavy-vehicles were shorter than 70 s). Seventy and 30 percents of these 60 pairs were randomly assigned to the *calibration* data set (42 pairs) and the *validation* data set (18 pairs), respectively. The car-following models were calibrated using the calibration data. Thus, a single set of optimal parameters was determined for each model. The optimal parameters were then used to predict the car-following behaviour using the validation data. The predicted trajectories were then assessed qualitatively and quantitatively as described

above. The methods of calibrating the car-following models for both datasets are explained in the next section.

## 5.3     Model Calibration

### 5.3.1    Driving Simulator Data

Fig. 5-3 shows the procedure of calibration of the car-following models. The models were calibrated using the data collected from the *Moving-LV* and *Stopped-LV* scenarios as described in Chapter 4: Each step of the calibration is explained in details as follows.
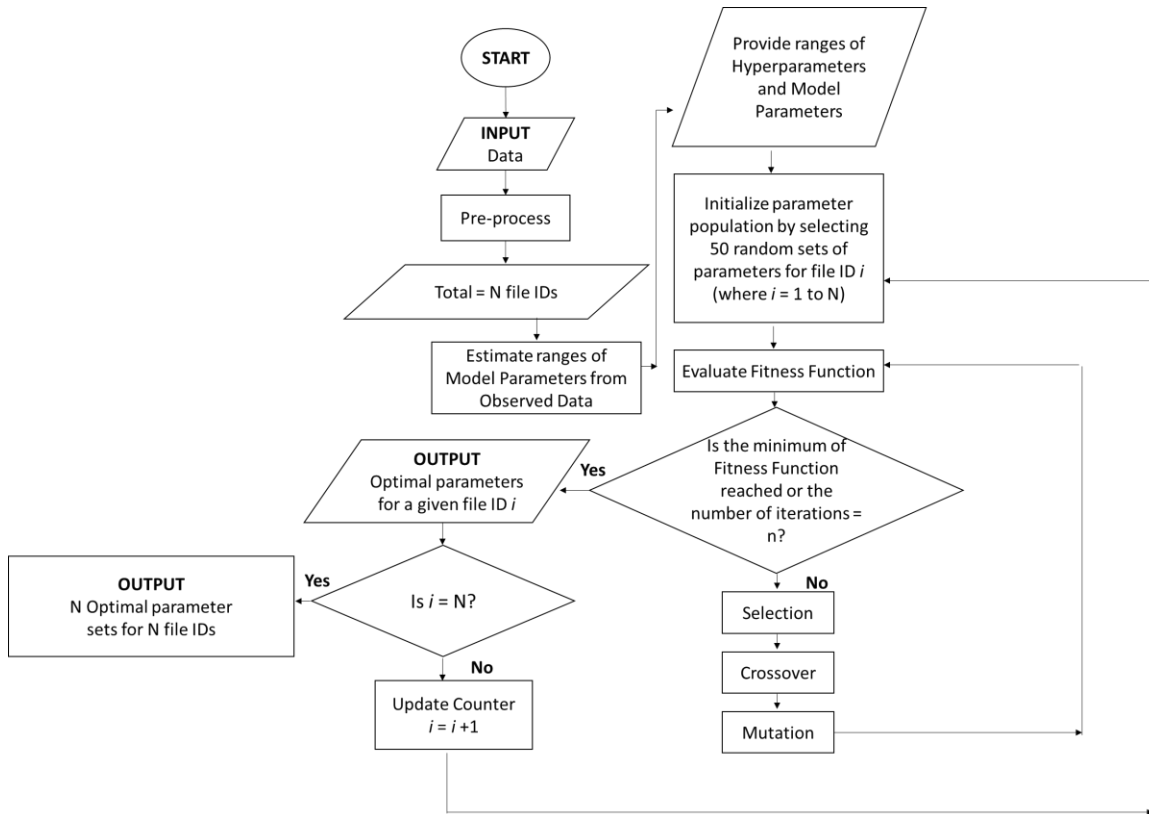


**Fig. 5-3. Procedure for calibration of car-following models for driving simulator data**

107

*Data Pre-processing*

In some cases, drivers reduced their speeds when they first saw the lead vehicle in the scenario, but later maintained or increased their speeds to drive at their desired speeds in Free-driving. Since Free-driving condition is not the focus of this study, the data collected during initial speed reduction and acceleration to reach the desired speed were not used.

Each run of a scenario was labelled as a 'file ID' which is described in terms of the driver, lead vehicle type and the reaction scenario type. For example, a driver who drove the *Moving-LV* scenario with the lead car was labelled as the file ID 'car_following_<driver_name>'.

*Calibration*

The calibration process was divided into two steps as shown in Fig. 5-3. First, most of the parameters of Gipps model, IDM, Wiedemann model, and IIDM were estimated from the driving simulator data. Other parameters of the models could not be directly estimated from the data. These were called "hyperparameters". After a preliminary investigation of these hyperparameters, the ranges of both model parameters and hyperparameters were provided as an input to the genetic algorithm with a fitness function. Second, the genetic algorithm determined the optimal set of parameters for a given file ID (combination of driver, lead vehicle type, reaction scenario type). Other approaches such as grid testing were also used to determine the optimal parameters but the genetic algorithm provided results faster. Each calibration step is described in detail below.

The equations of Gipps model, IDM, Wiedemann model, and IIDM with their calibration parameters (marked in grey) are listed in Table 5-1. The equations of the Wiedemann model do not include the random parameters as they were not required to calibrate the model for individual file IDs. This methodology was based on Higgs, Abbas and Medina (2011) study that removed the random parameters (RND and NRND) to analyze the Wiedemann model for different individual drivers' speeds. Following sections discuss the calibration procedure in different car-following conditions.

**Table 5-1. Calibration Parameters in Gipps Model, IDM, Wiedemann Model, and IIDM**

| Models / Thresholds | Equations (parameters for calibration are marked in grey) | Definition of calibration parameters |
|---|---|---|
| Gipps Model | $v_i(t + \tau_i)$ <br><br> $= min \begin{cases} v_i(t) + 2.5A_i\tau_i\left(1 - \dfrac{v_i(t)}{v_0}\right)\sqrt{0.025 + \dfrac{v_i(t)}{v_0}} \\ \qquad\qquad if\ free\ flow \\ -b_i\tau_i + \sqrt{b_i^2\tau_i^2 - b_i\left[-v_i(t)\tau_i - \dfrac{v_{i-1}^2(t)}{B_{i-1}} - 2l_{i-1} + 2s_i(t)\right]} \\ \qquad\qquad if\ following \end{cases}$ | $A_i$ is the maximum desired acceleration starting from standstill, $\tau_i$ is reaction time (hyperparameter), $v_0$ is the desired speed, $b_i$ is the comfortable maximum deceleration of subject vehicle, $B_{i-1}$ is the deceleration of lead vehicle, $l_{i-1}$ is the length of lead vehicle and $s_i$ is the front-to-front spacing |
| Intelligent Driver Model (IDM) | $a_i = A_i\left[1 - \left(\dfrac{v_i}{v_0}\right)^{\delta} - \left(\dfrac{s^*}{s}\right)^2\right]$ <br><br> $s^* = s_0 + max\left(0, vT + \dfrac{v\Delta v}{2\sqrt{A_i b}}\right)$ | $\delta$ is a hyperparameter, $s^*$ is the desired front-to-rear spacing, $s_0$ is the minimum standstill spacing, and $T$ is the front-to-rear time headway. |

**Table 5-1. Calibration Parameters in Gipps Model, IDM, Wiedemann Model, and IIDM (Continued)**

| Models / Thresholds | Equations (parameters for calibration are marked in grey) | Definition of calibration parameters |
|---|---|---|
| Wiedemann Model | | |
| Perception thresholds of spacing in Following | $AX = L + AXadd$ <br> $ABX = AX + (BXadd \times \sqrt{V})$ <br> $EX = EXadd$ <br> $SDX = AX + (EX \times BXadd \times \sqrt{V})$ | $AXadd$ is the minimum standstill front-to-rear spacing, $BXadd$ is the effect of speed on the following distance $ABX$, and $EXadd$ is a hyperparameter. |
| Perception thresholds of speed difference in Approaching | $SDV = \left(\dfrac{DX - AX}{CX}\right)^2, CX = \sqrt{\dfrac{W}{\dot{\theta}_{W(TH)}}}$ | $\dot{\theta}_{W(TH)}$ is the angular velocity threshold in Approaching. |
| Perception thresholds of speed difference in Following | $CLDV = SDV \cdot EX^2$ <br><br> $OPDV = CLDV \times (-OPDVadd)$ | $OPDVadd$ is a hyperparameter. |
| Acceleration to reach desired speed in Free-driving | $BMAX = BMAXmult \times (V_{MAX} - V \times FaktorV)$ <br><br> $FaktorV = \dfrac{V_{MAX}}{V_{DESIRED} + FAKTORVmult \cdot (V_{MAX} - V_{DESIRED})}$ <br><br> $V_{MAX} = 44$ m/s is the maximum speed of the following vehicle. | $BMAXmult$ is a function of max. acceleration when starting from zero speed, $V_{DESIRED}$ is the drivers' desired speed, and $FAKTORVmult$ is a hyperparameter. |
| Acceleration and deceleration to maintain speed in Following | $BNULL = BNULLmult$ | $BNULLmult$ is the absolute acceleration that controls the unintended oscillation in speed. |
| Deceleration in Approaching | $B(i)_{App} = \dfrac{1}{2} \times \dfrac{DV^2}{ABX - DX} + B(i - 1)$ | |
| Deceleration in Emergency Braking | $B(i)_{Emg} = \dfrac{1}{2} \times \dfrac{DV^2}{AX - DX} + B(i - 1) + BMIN \dfrac{(ABX - DX)}{(ABX - AX)}$ <br><br> $BMIN = -8$ m/s$^2$ | $BMIN = -8$ m/s$^2$ based on the observed maximum deceleration in the data. |

**Table 5-1. Calibration Parameters in Gipps Model, IDM, Wiedemann Model, and IIDM (Continued)**

| Models / Thresholds | Equations (parameters for calibration are marked in grey) | Definition of calibration parameters |
|---|---|---|
| Intermittent Intelligent Driver Model (IIDM) | | |
| Control Error | $$P(t) = A_i \left[ 1 - \left( \frac{v(t)}{v_0} \right)^\delta - \left( \frac{s^*(t)}{s(t)} \right)^2 \right] - a(t)$$ $$s^* = s_0 + \max \left( 0, vT + \frac{v\Delta v}{2\sqrt{A_i b}} \right)$$ | All parameters defined for IDM above |
| Control Error Prediction Error | $$\epsilon(t) = P_r(t) - P_p(t)$$ $$P_r(t) = P(t - \tau_p)$$ | $\tau_p$ is the perceptual delay |
| Accumulator Model | $$\frac{dA(t)}{dt} = k \times \epsilon(t) - M - \lambda A(t) + a_{BL} + \varepsilon(t)$$ $A_+$ and $A_-$ are the thresholds of the accumulator model $a_{BL}$ is used with a probability $p_{BL}$ $$\varepsilon(t) \sim N(0, \sigma_a)$$ | $k$ is the accumulator gain, $\lambda$ controls the evidence leakage, $a_{BL}$ is the effect of the lead vehicle brake light, $M$ is the minimum gating below which the accumulation does not start, and $\sigma_a$ is the standard deviation of the noise term $\varepsilon(t)$ |
| Magnitude of Acceleration | $$\tilde{g}_i = \tilde{\epsilon}_i$$ $$\tilde{\epsilon}_i = (1 + m_i) \times \epsilon(t_i)$$ $$m_i \sim N(0, \sigma_m)$$ | $m_i$ is normally distributed motor noise with a standard deviation of $\sigma_m$ |
| Shape of Control Adjustment | $$G(t) = \begin{cases} 0 \text{ for } t \leq \tau_m \\ 1 \text{ for } t \geq \tau_m + \Delta T \end{cases}$$ | $\tau_m$ is the motor delay, and $\Delta T$ is the duration of the control adjustment |
| Shape of Predicted Control Error | $$H(t) = \begin{cases} = 0, \text{ for } t \leq 0 \text{ and } t \geq \Delta T_p \\ \rightarrow 1, \text{ for } t \rightarrow 0^+ \\ \rightarrow 0, \text{ for } t \rightarrow \Delta T_p \end{cases}$$ | $\Delta T_p$ is the total duration of predicted control error per adjustment. It consists of $\Delta T_{p_0}$ and $\Delta T_{p_1}$ as explained above |

*Free-driving*

Desired speed in Free-driving is expressed as $v_0$ or $V_{DESIRED}$ in different models (see Table 5-1). The data contained two parts of Free-driving. In the first part, the speed increases from a zero speed to a driver-specific desired speed. In the second part, the speed becomes stable at the desired speed with minor variation. These two parts of Free-driving were

identified using a changepoint algorithm in the R programming language (Killick and Eckley, 2014). The changepoint algorithm detects the change in the mean and variance of the distribution of a time-dependent variable. Since the variance of the speed significantly decreases after the driver reaches the desired speed, the changepoint algorithm can determine the time when the desired speed is achieved.

Fig. 5-4 shows the estimated desired speed from Free-driving data of a single driver using the changepoint method. The changepoint detected with this method indicated that there was no significant change in the mean and variance of speed after the desired speed was achieved. Thus, the driver had maintained his/her desired speed after the changepoint. The median value of the speeds after the changepoint was estimated as the desired speed for a given file ID.
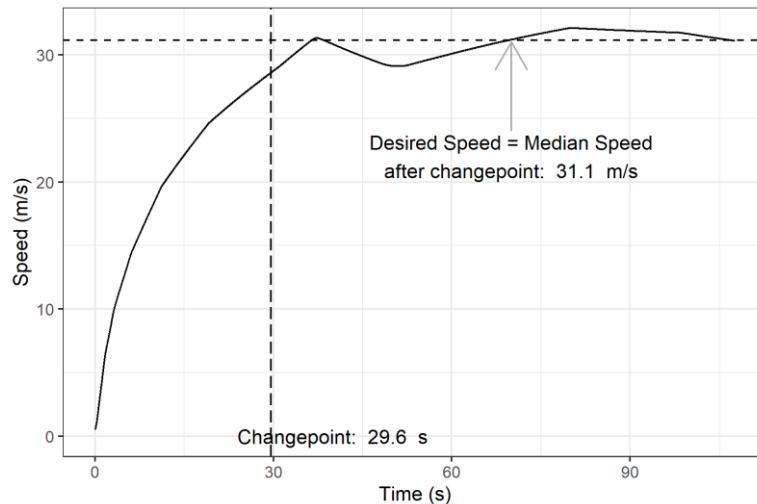


**Fig. 5-4. Estimation of Desired Speed from Free-driving part of the Calibration Data**

The acceleration when starting from zero speed was expressed as $A_i$ or ($BMAXmult \times V_{MAX}$) in different models. Therefore, the maximum acceleration $A_i$ for each file ID was obtained as the maximum acceleration in the Free-driving data. Then $BMAXmult$ was estimated as the maximum acceleration divided by $V_{MAX}$ (the maximum speed of the subject vehicle). Since all drivers used the same car model in the driving simulator, $V_{MAX} = 44$ m/s. Fig. 5-5 shows the distributions of the parameters for all file IDs in the Free-driving data.

$FaktorV$ depends on $V_{DESIRED}$, $V_{MAX}$ and $FAKTORVmult$ in the Wiedemann model. Since $FAKTORVmult$ and $\delta$ in the IDM and IIDM could not be estimated from the data, a range of values was tested by randomly selecting a few values. This range was then provided to genetic algorithm in the next step.
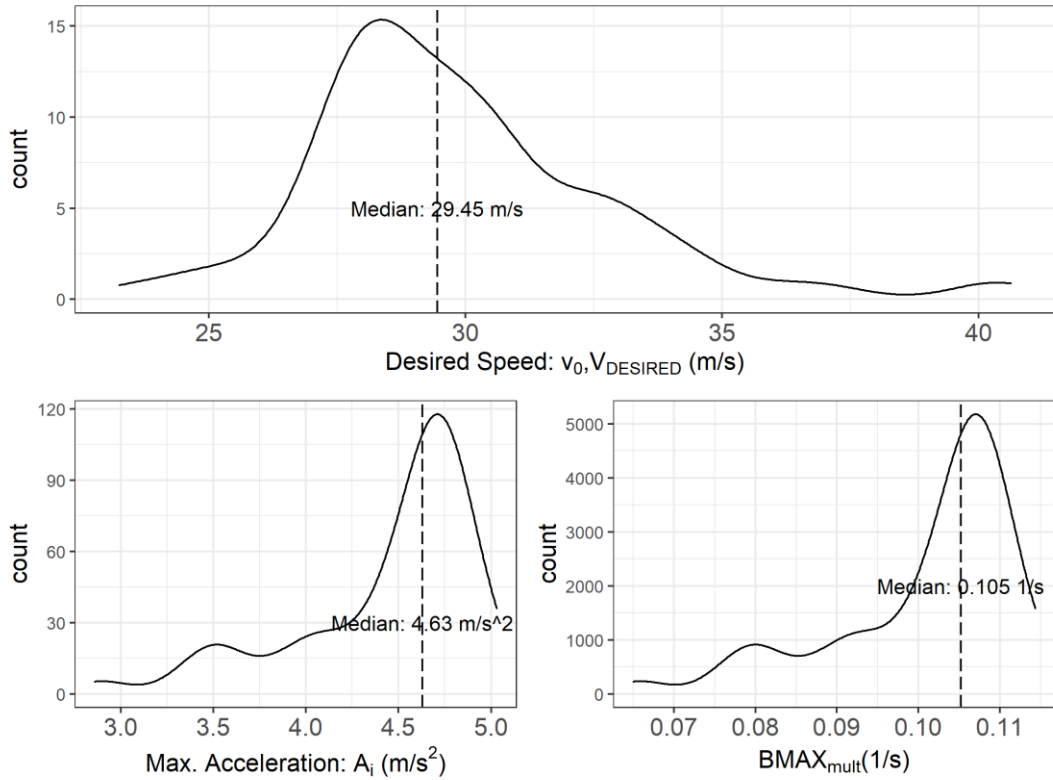
**Fig. 5-5. Distributions of Parameters in Free-driving Condition**

*Approaching and Following*

Gipps model and IDM do not have a perception threshold of Approaching condition. But the Wiedemann model considers the angular velocity threshold $\dot{\theta}_{W(TH)}$ as the start of Approaching condition. Therefore, $\dot{\theta}_{W(TH)}$ was estimated as the value of $\dot{\theta}_W$ when the driver first released the accelerator while approaching from a large spacing. The parameter *CX* depends on $\dot{\theta}_{W(TH)}$ as shown in Table 5-1.

   The deceleration due to accelerator release is modeled as $B(i)_{App}$ in the Wiedemann model, which is a function of the following distance *ABX*. The

following distance is the spacing kept by the following vehicle when both vehicles are moving at the same speed. Therefore, *ABX* = *L* + *AXadd* + *(BXadd* ×√*V)* depends on the front-to-rear standstill spacing *AXadd,* and *BXadd* is the effect of speed on *ABX*. The following distance in the IDM is $s^* = s_0 + \max\left(0, vT + \frac{v\Delta v}{2\sqrt{Ab}}\right)$, where $s_0 = AXadd$ and $T$ = the effect of speed on $s^*$.

*AXadd* and $s_0$ were estimated as the front-to-rear spacing when the speeds of both vehicles were less than 0.5 m/s, as not all drivers completely stopped at the end of scenarios. $BXadd$ and $T$ were calculated for each file ID using the estimated *AXadd* and $s_0$ in the above equations. The data used for calculating $BXadd$ and $T$ were only from the Following condition, i.e., when the speeds of lead and following vehicles were almost the same (22-28 m/s). *CX* was then estimated based on the above estimated parameters. Fig. 5-6 shows the distributions of the parameters for Approaching and Following conditions obtained from the data.
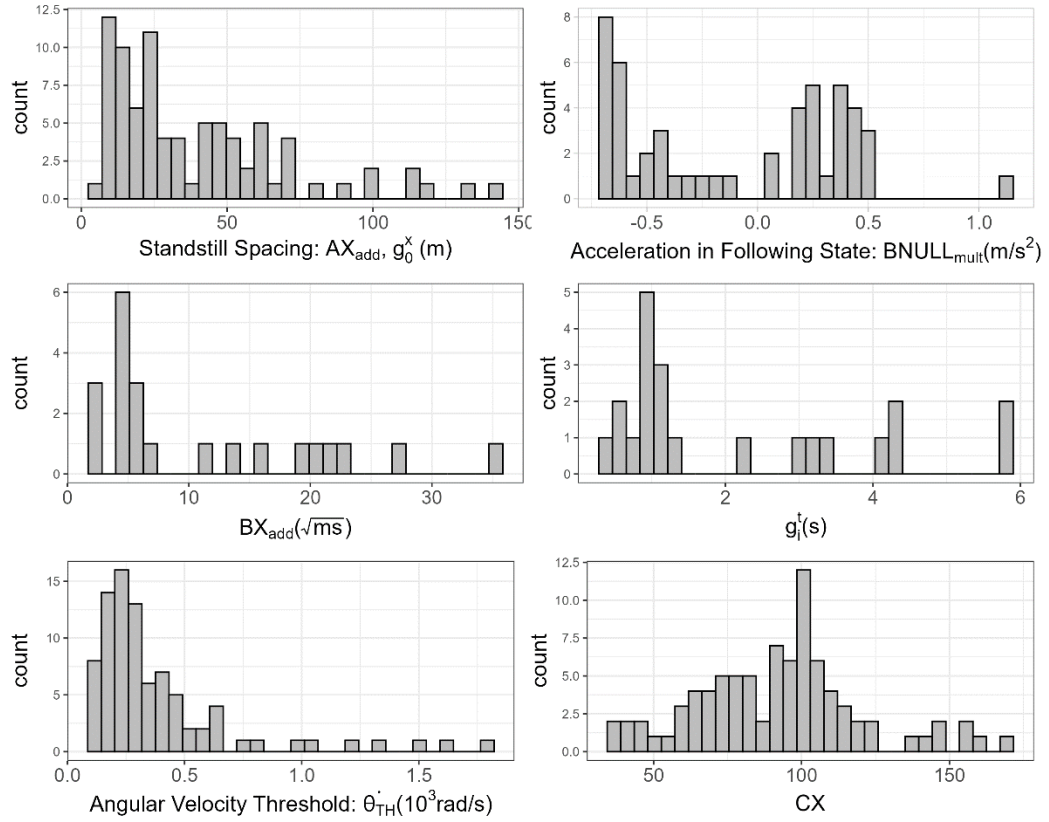
**Fig. 5-6. Distributions of Parameters in Approaching Condition**

The hyperparameters, $\tau_i$, $EXadd$ and $OPDVadd$, were optimized in the next step. The suggested values are 0.1-2.5 s for $\tau_i$, 2 for $EXadd$, and larger than 1 for $OPDVadd$ (Wiedemann and Reiter, 1992; Treiber and Kesting, 2013).

The thresholds $A_+$ and $A_-$ in the IIDM were also hyperparameters. The initial absolute values for the threshold were 0.001 to 5000. The leakage parameter and the noise terms had the initial ranges of $0 - 1$ and $0 - 0.5$ respectively, $a_{BL}$ $0 - 2$, $p_{BL}$ $0 - 1$, $M$ $0 - 5$, $\tau_p$ and $\tau_m$ $0 - 0.05$, $\Delta T$ $0.1 - 5$, $\Delta T_{p_0}$ $0 - 0.9$, and $\Delta T_{p_1}$ $1 - 10$.

*Braking*

The maximum comfortable deceleration is a function of vehicle model and drivers' desire to use it. It is represented as $b_i$ in the Gipps model, and $b$ in the IDM and the IIDM. In the Wiedemann model, $B(i)_{Emg}$ is used in a more urgent situation when the following distance *ABX* is violated. The upper bound of deceleration in braking, *BMIN*, was -10 m/s$^2$ based on the observed data. Fig. 5-7 shows the distribution of deceleration in the data. Based on this distribution, an initial absolute range of $1 - 10$ was used for $b_i$ and $b$.
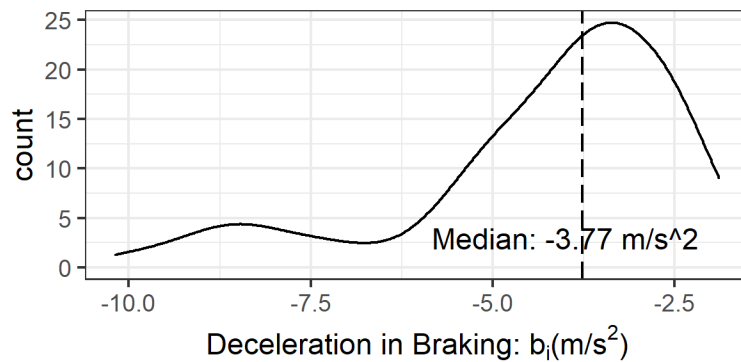


**Fig. 5-7. Distribution of *b***

*Optimization of Parameters using Genetic Algorithm*

Genetic algorithm was used for the non-linear optimization of the acceleration and speed functions of the models described in Table 5-1. As shown in Fig. 5-3, the optimal parameters were determined for each file ID using genetic algorithm. The package GA in the R programming language was used for the optimization of parameters in this study (Scrucca, 2013). The procedure of optimization is briefly explained below. Fig. 5-8 shows an example of using genetic algorithm for determining the optimal parameters of the Gipps

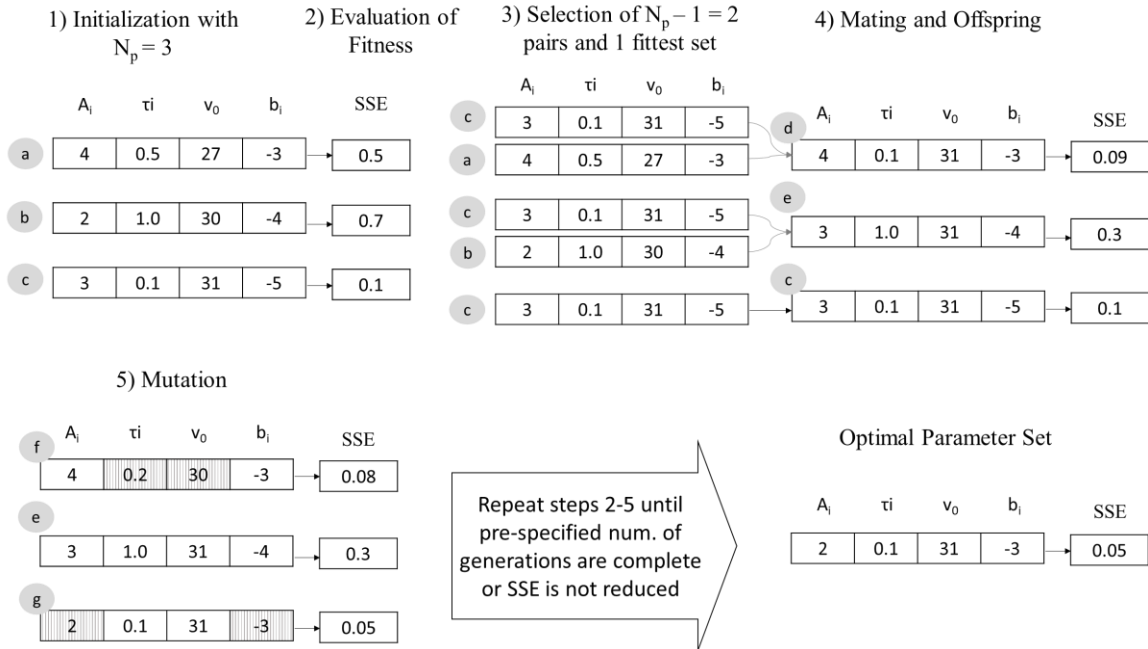model. More details of the procedure can be found in Chapter 16 of Treiber and Kesting (2013).



**Fig. 5-8. Procedure of Estimating Optimal Parameters using the Genetic Algorithm**

*Initialization:*

Create $N_p$ parameter sets for a given car-following model. For example, for Gipps model, $N_p$ sets of four calibration parameters $\{A_i, \tau_i, v_0, b_i\}$ were created. The value of each parameter was randomly selected from the observed range of values in the previous step. In this study, the number of parameter sets, $N_p$, was set to 50. As an example, Fig. 5-8 shows the initialization of $N_p = 3$ parameter sets (a, b, c) for the Gipps model in step 1.

*Evaluation of Fitness*

For each parameter, the sum of squared errors (SSE) for each file ID was calculated as follows:

$$SSE = \frac{\sum_{i=1}^{n}(\hat{y}_i - y_i^{data})^2/y_i^{data}}{\sum_{i=1}^{n}y_i^{data}} \qquad (5\text{-}15)$$

where $i = 1$ to $n$ represents the time frames (second) $i = 1, 2, 3, \dots, n$ with n as the last time frame per file ID. $\hat{y}_i$ and $y_i^{data}$ are the simulated and observed front-to-rear spacing, respectively. This SSE can account for both large and small front-to-rear spacing because it is a combination of absolute and relative errors which are sensitive to large and small spacing, respectively (Kesting and Treiber, 2008).

Moreover, optimizing the parameters with respect to front-to-rear spacing can also reduce the differences between the simulated and observed speed. However, "this does not hold the other way round, as the error in the front-to-rear spacing may incrementally grow when optimizing with respect to differences in simulated and observed speed" (Kesting and Treiber, 2008).

At the end of this step, N values of SSE were obtained for a given car-following model and file ID. This is illustrated in the example shown in Fig. 5-8 where the SSE for the parameter set c was the lowest (most fit) in step 2.

*Selection*

$N_p$-1 pairs of parameter sets were selected from the population of $N_p$, such that the parameter sets with lower SSE were chosen with a higher probability (lower SSE = higher fitness). A pair consisted of 2 parameter sets (parents), and a given parameter set could be part of more than one pair. The fittest parameter set from the evaluation step was also added to this selection.

The example in Fig. 5-8 illustrates the selection procedure in step 3 where the $N_p$-1 = 2 selected pairs were made of parameter sets c-a and c-b. Since parameter set c had the lowest SSE in step 2, it was also selected.

*Mating and Offspring*

New parameter sets (offspring) were created per pair by randomly combining the parameters from each parent. For instance, a pair of $\{A_{i_1}, \tau_{i_1}, v_{0_1}, b_{i_1}\}$ and $\{A_{i_2}, \tau_{i_2}, v_{0_2}, b_{i_2}\}$ was randomly combined to create $\{A_{i_1}, \tau_{i_2}, v_{0_1}, b_{i_2}\}$. The offspring of the fittest parameter set was itself. Then SSE was estimated for each offspring. This procedure is illustrated in step 4 of Fig. 5-8 where pairs of parameter sets c-a and c-b generated new offspring parameter sets d and e. Parameter set c was its own offspring.

*Mutations*

Since the car-following model equations are non-linear functions, the optimization procedure can lead to local minima of SSE instead of reaching a global minimum. To avoid this issue, some of the parameters of all offspring were randomly varied and SSE was estimated. The example in Fig. 5-8 shows random variation in two out of the three

parameter sets (d and c) that led to new parameter sets f and g. The randomly varied parameters are highlighted. Parameter set g produced the lowest SSE among the three parameter sets.

*Termination*

The previous steps were repeated for a fixed maximum number of generations (100 in this study) to obtain the minimum possible SSE. The algorithm stopped when no further improvements in SSE were found for a few consecutive generations. This is shown in Fig. 5-8 where parameter g was the fittest and no further reduction in SSE was observed after running the steps 2-5 several times.

### 5.3.2 Calibration and Validation of the Interstate-80 (I-80) Vehicle Trajectory Data

Previous section described the calibration with individual scenario runs. This individual-run calibration procedure is useful in understanding the model performance by visually comparing the predicted trajectories among different models and the observed trajectories. However, this method is time-intensive and not useful practically when calibrating traffic trajectories. Therefore, for the I-80 data, the complete data were used for calibration as described below.

Fig. 5-9 shows the procedure for calibrating and validating the car-following models using the I-80 data. This procedure is similar to the one described for the driving simulator data. But unlike the driving simulator data, the calibration of models was performed simultaneously on all the car-following vehicles in the calibration data (42 pairs). This was done by providing a given set of parameters (chosen by the genetic algorithm from the

initial ranges provided) to a given model (Fig. 5-9 top-right). This same set of the parameters was then used to generate the speed, acceleration and spacing trajectories for all 42 car-following-car pairs. Then, the following fitness function was evaluated:

$$SSE = \frac{\sum_{i=1}^{n} (\hat{y}_i - y_i^{data})^2 / y_i^{data}}{\sum_{i=1}^{n} y_i^{data}} \tag{5-16}$$

where $i = 1$ to $n$ represents the time frames (second) $i = 1, 2, 3, ..., n$ with n as the last time frame. $\hat{y}_i$ and $y_i^{data}$ are the simulated and observed front-to-rear spacing, respectively of the 42 pairs in the calibration data, stacked by rows. The remaining procedure was the same as discussed in the previous section.

The optimal parameter set per model was then used to evaluate the model performance on the validation data (18 pairs).
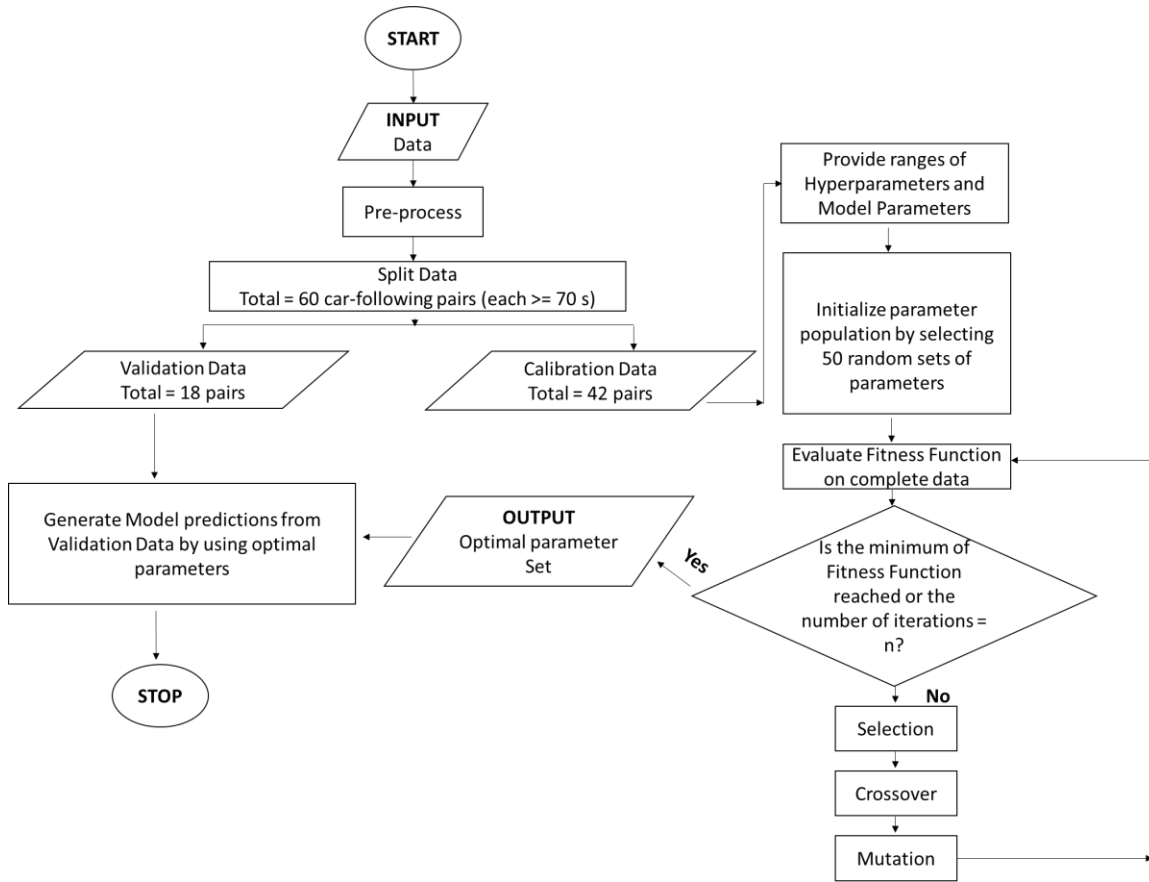
**Fig. 5-9. Procedure for calibration of car-following models for I-80 data**

## 5.4    Effect of Lead Vehicle Type on the Start Time of Driver Reaction

Previous sections discussed the development of the Intermittent Intelligent Driver Model (IIDM) and the methods of calibrating the model. The IIDM adapts the IDM with the Accumulator Model which reflects the driver's intermittent reactions. However, the IDM does not explicitly consider the effects of the lead vehicle types on car-following behaviour. It is expected that drivers initiate the deceleration earlier when they follow a larger lead vehicle than following a smaller lead vehicle.

Since the IDM does not consider the lead vehicle size, the effect on the start time of driver reaction can be estimated using perceptual cues such as the angular velocity and tau-inverse in the Accumulator Model only. The Accumulator Model was calibrated separately for approaching and braking conditions, scenario type (Moving-LV and Stopped-LV), and each vehicle type (car and truck). Since the height of lead truck is larger than its width and it potentially has more influence on drivers, angular velocity due to the LV height ($\dot{\theta}_H$) was also considered as a looming variable for the lead truck case. The equation and parameters of the Accumulator Model were explained in section 3.2.2.

The data from the Moving-LV and Stopped-LV scenarios were combined to build the calibration data (87 runs only). The Accumulator model was run 100 times for each file ID in the calibration data with a given set of parameters chosen by genetic algorithm. The fitness function for genetic algorithm was based on the likelihood of obtaining the observed reaction time for given model parameters (Xue et al., 2018). The observed reaction times in approaching and braking conditions were defined in Table 4-1. The log-likelihood function is shown as follows:

$$
\begin{aligned}
\text{Log-Likelihood}(\theta) \qquad\qquad\qquad\qquad\qquad\qquad &\text{(5-17)} \\
= \log\left[p\big(RT_{OBS_1}\big|\theta\big)\right] + \log\left[p\big(RT_{OBS_2}\big|\theta\big)\right] + \cdots & \\
+ \log\left[p\big(RT_{OBS_N}\big|\theta\big)\right] &
\end{aligned}
$$

**Table 5-2. Equations of Accumulator Model**

| Model | Equations (parameters for calibration are marked in grey) | Definition of calibration parameters and the range of values | | |
|---|---|---|---|---|
| | | | Approach | Brake (LV brake lights OFF) |
| Base | $\dfrac{dA(t)}{dt} = K \times L(t) - M + \varepsilon(t)$ <br> $L(t)$ is looming ($\dot{\theta}$ or $\tau^{-1}$) <br> $A(t)$ is activation <br><br> $\varepsilon(t) \sim N(0, \sigma_a)$ | $K$ ($L(t) = \dot{\theta}$) | {50, 13000} | {5, 6000} |
| | | $K$ ($L(t) = \tau^{-1}$) | {1, 300} | {1, 300} |
| | | $M$ | {0, 0.5} | {0, 0.5} |
| | | $\sigma_a$ | {0, 0.5} | {0, 0.5} |
| | | | Brake (LV brake lights ON) | |
| Brake Light | $\dfrac{dA(t)}{dt} = K \times L(t) - M + a_{BL} + \varepsilon(t)$ <br> used with a probability $p_{BL}$ | $K$ ($L(t) = \dot{\theta}$) | {10, 1000} | |
| | | $K$ ($L(t) = \tau^{-1}$) | {1, 100} | |
| | | $M$ | {0, 0.5} | |
| | | $\sigma_a$ | {0, 0.5} | |
| | | $a_{BL}$ | {0.5, 5} | |
| | | $p_{BL}$ | {0.6, 1} | |

In the calibration process, the optimal model parameters in all conditions were determined. The goodness-of-fit of the models was evaluated based on Akaike Information Criterion (AIC) which is estimated as follows:

$$AIC = 2k - 2\ln(\hat{L}) \tag{5-18}$$

where $k$ is the number of parameters in the model and $\hat{L}$ is the likelihood. Smaller AIC values indicate better model fit.

# Chapter 6:  Results and Discussion

## 6.1     Hypotheses on Start Time of Reaction

Chapter 4: presented three hypotheses on the start time of deceleration in approaching and braking conditions. These three hypotheses were tested using the data collected from the four driving simulator scenarios also discussed in Chapter 4. These scenarios were Perception-in-approaching, Perception-in-following, Moving-LV and Stopped-LV. The former two scenarios are referred to as perception scenarios while the latter two are referred to as reaction scenarios in the discussion of the results as follows.

### 6.1.1    Perception and reaction in approaching condition

Fig. 6-1 shows the distribution of tau-inverse at the times when drivers released accelerator in Perception-in-approaching and reaction scenarios while approaching a slow or stopped lead car (left figure) and truck (right figure) from a large spacing. Each data point in Fig. 6-1 represents the value of tau-inverse in a scenario run by a driver. The values of tau-inverse for the same driver were connected using straight lines. The darker lines correspond to the data within the inter-quartile range (IQR) (= $75^{th}$ percentile – $25^{th}$ percentile) of the perception scenario, which eliminates outliers.
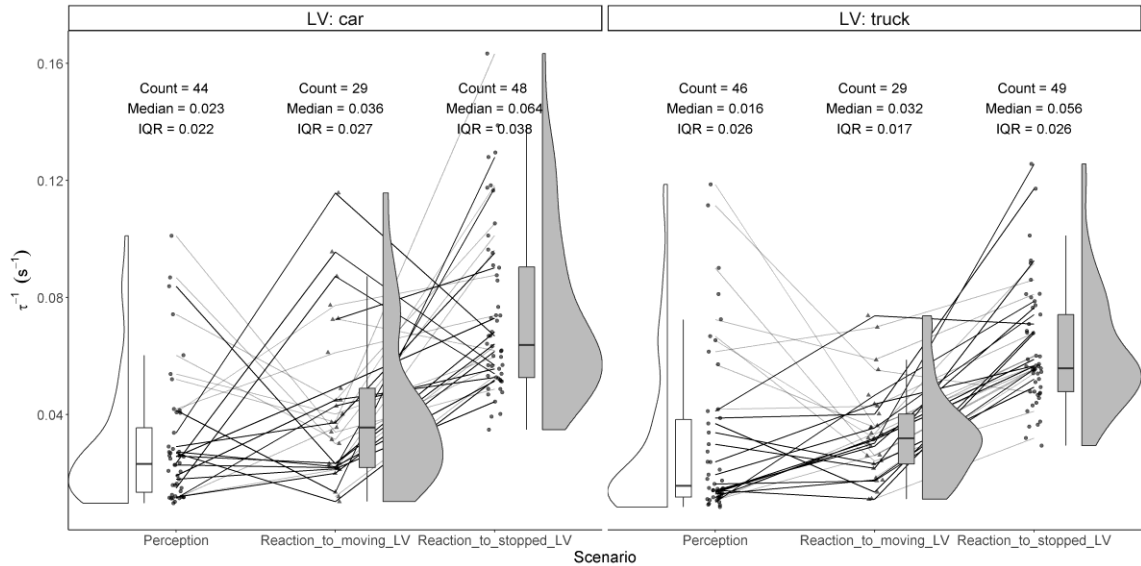
**Fig. 6-1. Distribution of tau-inverse at the time of accelerator release in approaching condition**

The three hypotheses were evaluated to understand the driver behaviour in approaching a slow or stopped lead vehicle. In the hypothesis H1, a driver is assumed to release accelerator as soon as tau-inverse reaches the driver's perception threshold. This assumption was used in psychophysical car-following models such as the Wiedemann car-following model (Wiedemann and Reiter, 1992). Therefore, if this assumption were correct, the distributions of tau-inverse values must have been similar in the perception and reaction scenarios. However, Fig. 6-1 shows that the tau-inverse values are generally higher for the reaction scenarios than the perception scenario. The result of Mann-Whitney U Test shows that the distributions of tau-inverse were statistically different between perception and reaction scenarios at a 95% confidence level. Thus, the hypothesis H1 was rejected.

In the hypothesis 2, a driver is assumed to detect the lead vehicle motion when tau-inverse reaches the driver's perception threshold and then react after a driver-specific

reaction time. Because of the reaction time, the tau-inverse at the time of releasing accelerator (i.e., the reaction threshold) will be greater than the perception threshold. Higher values of tau-inverse for the reaction scenarios than the perception scenario in Fig. 6-1 supports this hypothesis. The distributions of perception time and reaction time determined to according to the definitions in Table 1 were compared in Fig. 6-2. The figure only shows the data in the inter-quartile range in the Perception-in-approaching scenario.
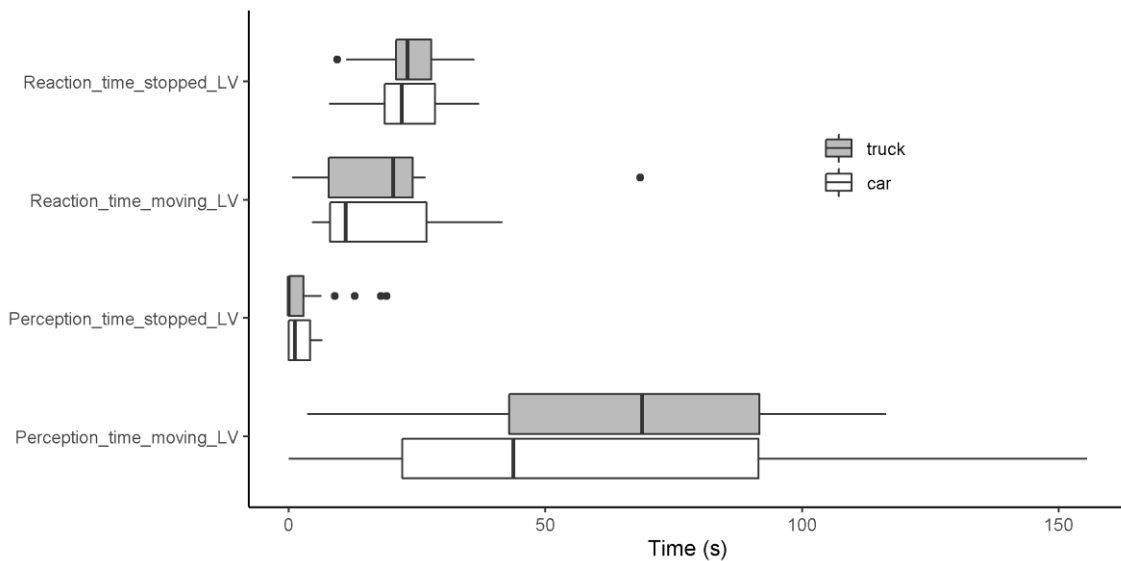


**Fig. 6-2. Perception time and reaction time in approaching condition in hypothesis H2**

To accept the hypothesis H2-1, the perception time and the reaction time should be similar for the same driver in different approaching conditions. However, Fig. 6-2 clearly shows that the perception time and the reaction time varied significantly between the Moving-LV and Stopped LV scenarios. Also, the values of PRT (= perception time + reaction time) were greatly larger than the typical values of 1.5-2.5 s in the literature (Green, 2017b). To accept the hypothesis H2-2, drivers must react at the reaction threshold rather than after the reaction time. However, Fig. 6-1 shows that the distributions of tau-

inverse are different between the two reaction scenarios. These results imply that driver reaction is not dependent on the reaction time or reaction threshold. Therefore, the hypothesis H2 (both H2-1 and H2-2) was also rejected.

The hypothesis H3 assumes that drivers react based on the accumulation of the evidence (represented by tau-inverse) over time. Fig. 6-3 shows the increase in tau-inverse over time (illustrated in the accumulation curve) in the perception and reaction scenarios of approaching condition for 3 drivers. It was found that the areas under the accumulation curves for different drivers were generally similar across all three scenarios for a given lead vehicle type (car/truck). The areas under the accumulation curves were estimated using the trapezoidal rule implemented in the "bayestestR" package in the R programming language (Makowski et al., 2019).
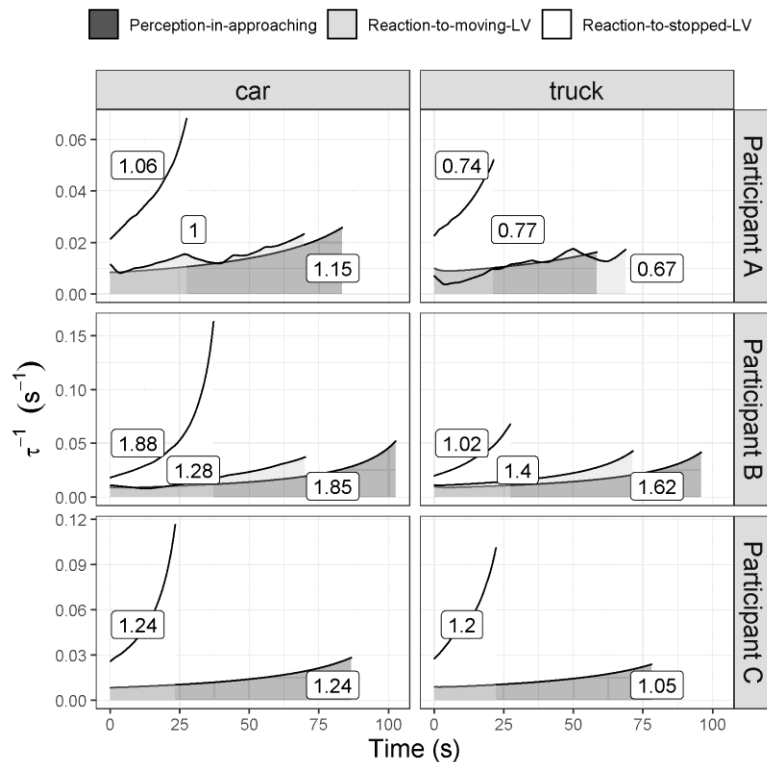


**Fig. 6-3. Increase in tau-inverse over time in approaching condition**

Note: The numbers inside the boxes denote the area under the curves.

In general, tau-inverse increased rapidly in the Reaction-to-stopped-LV scenario due to a large speed difference. This leads to a faster accumulation of evidence for reaction to slow down. In contrast, tau-inverse accumulated more slowly in the Perception-in-approaching scenario, which resulted in slower response. Therefore, the evidence accumulation process seems to be the best hypothesis to explain the driver behaviour in approaching condition. The evidence accumulation framework has been implemented as a model and tested on braking condition in previous studies (Xue et al., 2018). Thus, this study demonstrated that the evidence accumulation framework can also explain the driver behaviour in approaching a lead vehicle from a large spacing.

Fig. 6-3 also shows that the lead truck has larger influence on driver reaction than the lead car as indicated by smaller areas under the curves in the lead truck case. This indicates that drivers reacted earlier to the lead truck potentially because of either larger height of trucks or driver's discomfort with following the truck.

### 6.1.2 Perception and reaction in braking condition

Fig. 6-4 shows the perception thresholds in braking condition (i.e., the value of tau-inverse at the start of braking) in the Perception-in-following scenario. This figure includes the data for the speed differences of 2 and 3 m/s in the spacing of 20-100 m only because over 80% of drivers correctly judged the speed difference in this spacing range. The data from the drivers who did not correctly judge speed differences were discarded. Fig. 6-4 shows that the drivers generally detected the lead vehicle at a smaller tau-inverse in longer spacing. Also, they detected the lead truck at a smaller tau-inverse than the lead car. Thus, driver behaviour in braking condition is dependent on speed difference and spacing.
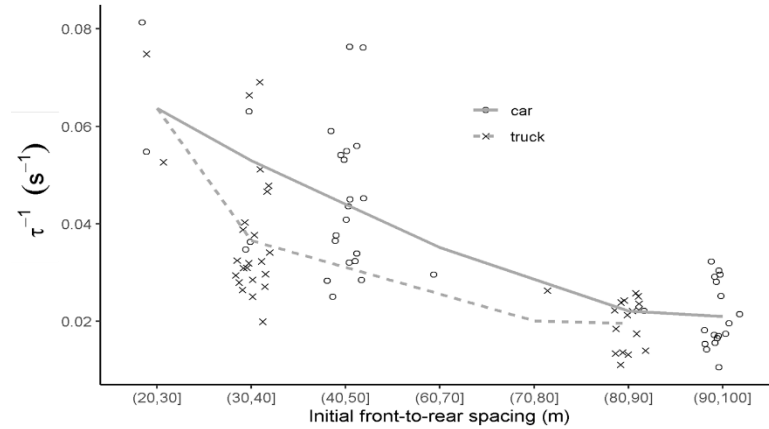
**Fig. 6-4. Perception threshold in Perception-in-following scenario (speed difference of 2-3 m/s)**

Fig. 6-5 shows the distributions of tau-inverse at the start of braking behind a decelerating or stopped lead car and lead truck. The Moving-LV data were further divided into the drivers who saw the lead vehicle brake lights (triangle markers) and the drivers who did not (circle markers). The lead vehicle brake lights were always turned off in the Stopped LV scenario.
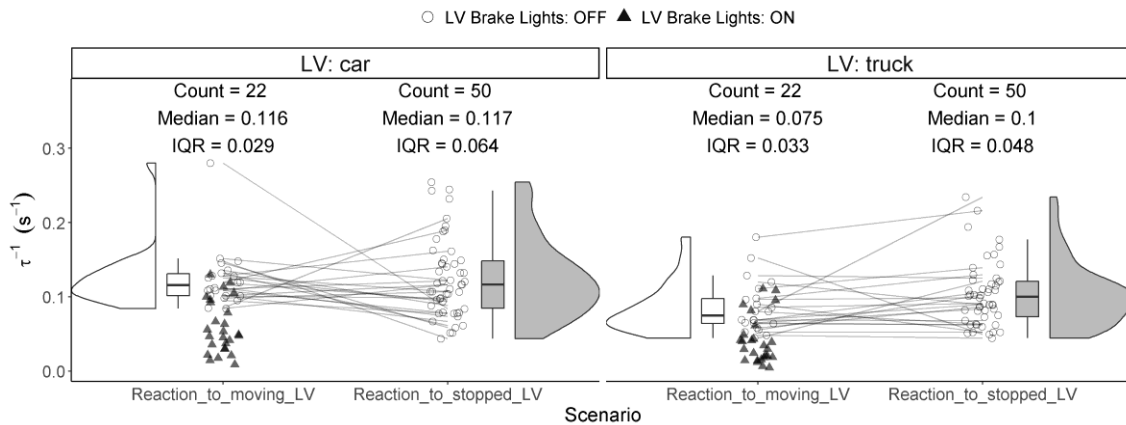


**Fig. 6-5. Distribution of tau-inverse at the start of braking in braking condition**

Note: Circle markers and triangle markers represent the lead vehicle brake lights off and brake lights on conditions, respectively.

It is evident from Fig. 6-5 that when the drivers did not see the lead vehicle brake lights, they relied on the visual variables and applied brakes at higher tau-inverse. Since the tau-inverse at the start of braking (Fig. 6-5) was greater than the tau-inverse in the Perception-in-following scenario (Fig. 6-4), the hypothesis H1 (a driver perceives and reacts at the same threshold) was rejected.

Fig. 6-5 also shows that tau-inverse was slightly greater in the Stopped-LV scenario than the Moving-LV scenario (lines were connected for the lead vehicle brake lights off cases only). But these distributions of tau-inverse were not statistically different between the two scenarios at a 95% confidence level. However, when the lead vehicle brake lights on cases were included, the distributions were statistically different at a 95% confidence level. If the drivers indeed reacted after a reaction time or at a specific value of tau-inverse, their reaction threshold must have been similar in both lead vehicle brake lights on and off cases. However, the values of tau-inverse at the start of braking were generally higher in the lead vehicle brake lights off case than the lead vehicle brake lights on case in the Moving-LV scenario as shown in Fig. 6-5. Therefore, the hypothesis H2 (driver reacts after a reaction time or at a reaction threshold) was also rejected.

Fig. 6-6 shows the increase in tau-inverse in braking conditions of reaction scenarios for three drivers (lead vehicle brake lights off cases). The areas under the accumulation curves were not similar between the Moving-LV (labelled as Decelerating_LV) and Stopped-LV scenarios because of the different start time of accumulation for each scenario. The time starts when drivers released accelerator in the Stopped-LV scenario whereas the time starts when the lead vehicle started braking in the Moving-LV scenario.
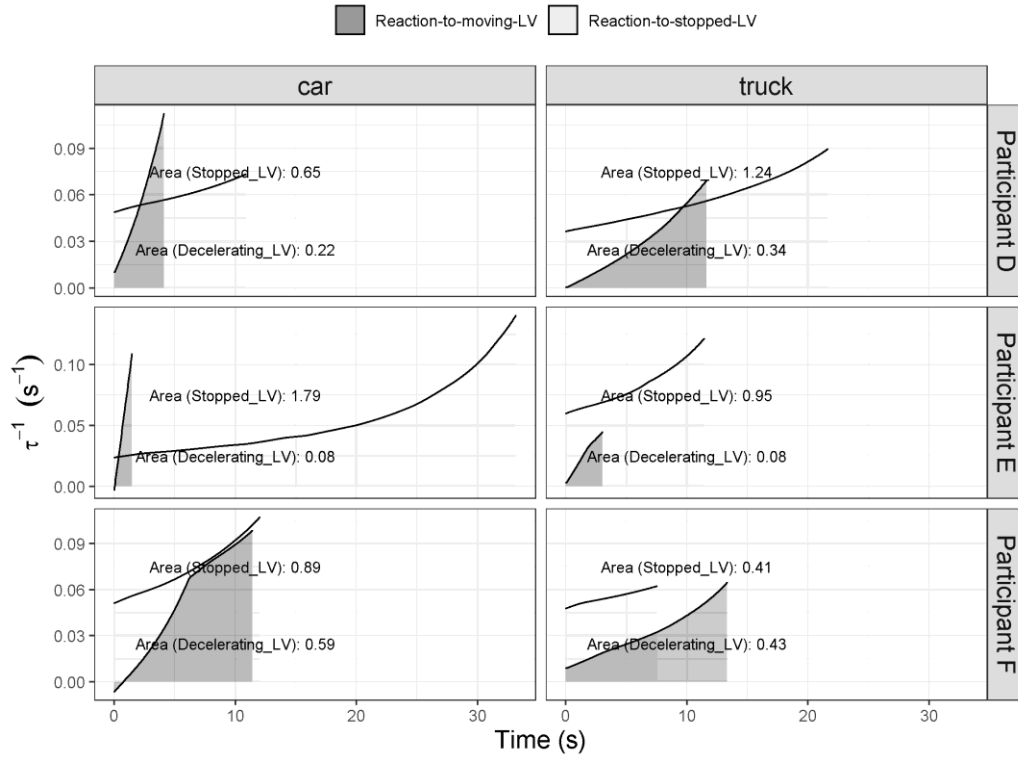
**Fig. 6-6. Increase in tau-inverse over time in braking condition**

Moreover, unlike the approaching condition, the areas under the curves were not consistently smaller for the lead truck case than the lead car case. This is because the initial speed difference and/or spacing were not necessarily the same in both lead car and lead truck cases for the same driver. For this reason, the values of tau-inverse when the lead vehicle started braking were different between the two cases.

Nevertheless, the patterns of increase in tau-inverse were similar to the approaching condition (Fig. 6-3). A slower increase in tau-inverse over a longer time results in a slower start of braking whereas a faster increase in tau-inverse over a shorter time results in a faster start of braking.

In summary, the theoretical concept of the evidence accumulation framework provides plausible explanation on the time of releasing accelerator and applying brakes in both approaching and braking conditions for different types of lead vehicle (car and truck). This demonstrates that the time of driver reaction can be better predicted based on the evidence accumulation of control error (e.g., tau-inverse) rather than the fixed value of PRT or the PRT value randomly drawn from a situation-independent empirical distribution, as used in the engineering car-following models. Thus, the assumption of the Wiedemann model that the driver reaction starts when a perceptual variable reaches a fixed threshold, does not reflect the actual driver behaviour.

These findings suggest that a car-following model needs to account for the variation in the start time of reaction based on the evidence accumulation of an appropriate control error. In this regard, the Intermittent Intelligent Driver Model (IIDM) proposed in this study is a better alternative to the conventional car-following models.

## 6.2    Calibration of Accumulator Model

To predict the driver's start time of reaction based on the evidence accumulation, the IIDM incorporates the Accumulator model (see Chapter 3.2.2) in the model framework. The parameters of the Accumulator model were calibrated as follows.

The Accumulator model accounts for the effect of the type of the lead vehicle as a parameter $a_T$ which represents the effect of lead truck in Eq. (5-6). This parameter $a_T$ does not only represent the effect of larger size of truck, but also the effect of driver's discomfort and/or unsafe feeling associated with following a large truck (Peeta et al., 2005). However, $a_T$ did not result in any improvement in model results.  Instead, the effect of the lead

vehicle type was captured using different perceptual variables for different lead vehicle type – e.g., the angular velocity due to the height of lead vehicle for the lead truck case.

Fig. 6-7 shows the AIC values for the Accumulator model with different perceptual variables. The minimum AIC (i.e., the best model fit) in each case is also shown in dark bars. Fig. 6-7 (a) shows that angular velocity due to the width of lead vehicle produced the best model for the approach reaction time in the Moving-LV scenario (left figures). However, tau-inverse produced the best model fit in the lead car case of the Stopped-LV scenario (top right figures of Fig. 6-7). This is potentially because the drivers are more sensitive to the tau-inverse in more urgent condition when approaching a stopped LV than approaching a moving LV. Interestingly, the angular velocity due to the height produced the best model fit in the lead truck case of the Stopped-LV scenario (bottom right figure of Fig. 6-7). This is in contrast with the assumption in the literature that drivers are more sensitive to horizontal dimension (width) than vertical dimension (height) (Green, 2017a)

In case of the brake reaction time, tau-inverse produced the best model fits for the Moving-LV scenario (left figures of Fig. 6-7 (b)) while angular velocity produced best model fits for the Stopped-LV scenario (right figures of Fig. 6-7 (b)) when LV brake lights were off. This contradicts the best model fit of the approach reaction time with angular velocity in the lead car case. This indicates that the drivers are more sensitive to tau-inverse in more urgent condition of braking than approaching a moving LV. Similarly, previous studies found that in urgent braking conditions, tau-inverse produced better model fit than angular velocity due to the width (Maddox and Kiefer, 2012). Again, angular velocity due to the height produced the best model fit in the lead truck case of the Stopped-LV scenario.
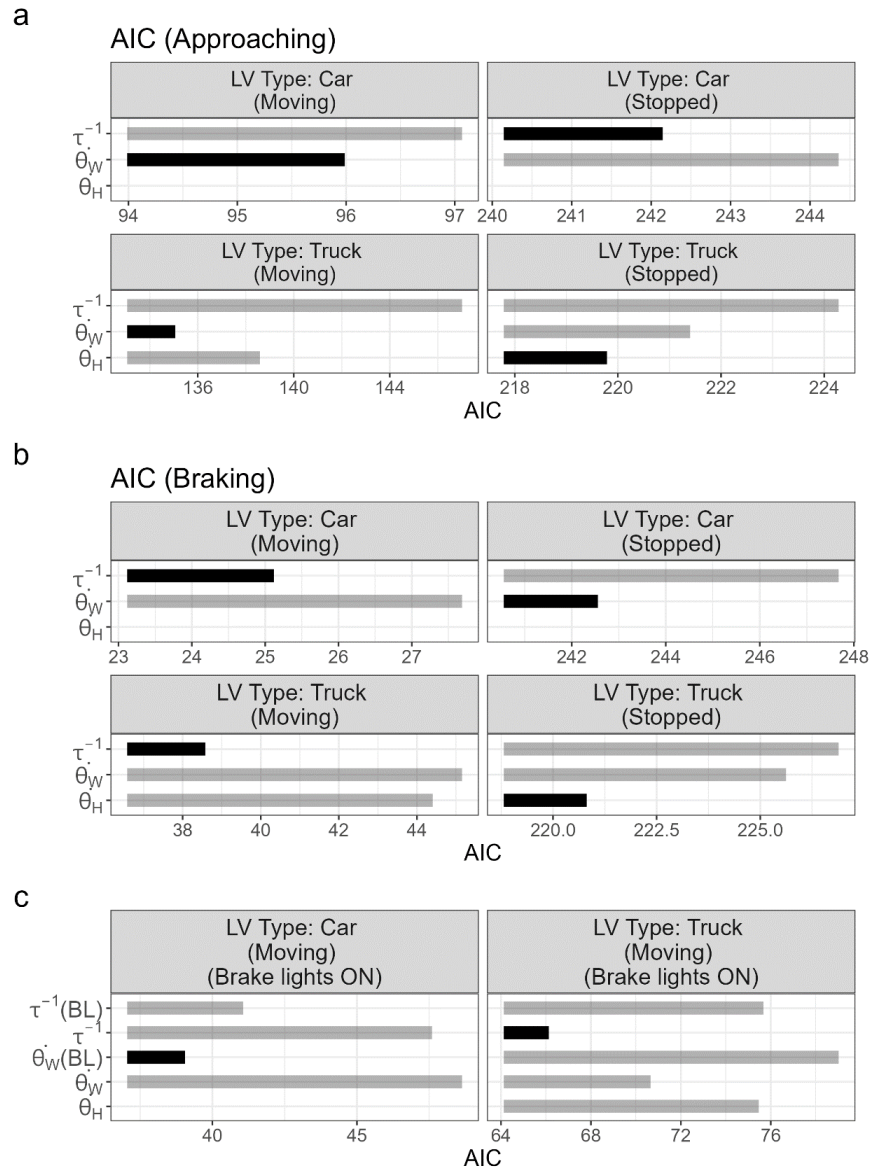
**Fig. 6-7. Akaike Information Criterion (AIC) of Accumulator models with different perceptual variables and the lead vehicle brake light parameter**

When lead brake lights were on, the Accumulator Model with angular velocity due to the width and the LV brake light parameter produced the best model fit in the lead car case as shown in Fig. 6-7 (c). However, the lead vehicle brake lights parameter did not improve the model fit. This is because the lead vehicle brake lights helped the drivers detect the lead

136

car's deceleration, which prompted their early brake application. In the lead truck case, the drivers did not apply brakes earlier even if they could better detect the lead vehicle with brake lights on because they released the accelerator earlier and they had more time to brake.

Based on the comparison of AIC, the values of calibrated parameters which produced the best fitted Accumulator models were determined as shown in Table 6-1. These results indicate that a control error in the IIDM which incorporates the perceptual cues for both acceleration and deceleration adjustments can help predict the start time of driver reaction more realistically.

**Table 6-1. Calibrated Parameter Values of Accumulator Model**

| Condition | Scenario type | Lead vehicle type | Lead vehicle brake lights | Best fit with | Parameters |
|---|---|---|---|---|---|
| **Approaching** | Moving-LV | Car | Off | $\dot{\theta}_W$ | $K = 2057, M = 0.34, \sigma_a = 0.19$ |
| | | Truck | Off | $\dot{\theta}_W$ | $K = 1407, M = 0.34, \sigma_a = 0.16$ |
| | Stopped-LV | Car | Off | $\tau^{-1}$ | $K = 9, M = 0.35, \sigma_a = 0.11$ |
| | | Truck | Off | $\dot{\theta}_H$ | $K = 1587, M = 0.36, \sigma_a = 0.10$ |
| **Braking** | Moving-LV | Car | Off | $\tau^{-1}$ | $K = 11, M = 0.34, \sigma_a = 0.24$ |
| | | Car | On | $\dot{\theta}_W$ | $K = 391, M = 0.33, \sigma_a = 0.10,$ $a_{BL} = 0.97, \ p_{BL} = 0.71$ |
| | | Truck | Off | $\tau^{-1}$ | $K = 9, M = 0.43, \sigma_a = 0.20$ |
| | | Truck | On | $\tau^{-1}$ | $K = 11, M = 0.35, \sigma_a = 0.44$ |
| | Stopped-LV | Car | Off | $\dot{\theta}_W$ | $K = 666, M = 0.36, \sigma_a = 0.24$ |
| | | Truck | Off | $\dot{\theta}_H$ | $K = 223, M = 0.19, \sigma_a = 0.17$ |

## 6.3    Comparison of Car-Following Model Performance

To evaluate the performance of the IIDM, four car-following models – the Gipps Model, the IDM, the Wiedemann Model, and the IIDM (with and without the lead vehicle brake lights (BL)) – were fit to the driving simulator data (Moving-LV and Stopped-LV scenarios) as well as the Interstate-80 (I-80) data. Optimal values of model parameters were

obtained using a fitness function in a genetic algorithm such that the error between the observed and predicted spacing is minimized. Each model was fit to an individual driving simulator run to estimate the optimal parameter set for each individual run. This generates the distributions of optimal parameters obtained from the individual runs.

To validate the performance of these models, the real-world trajectory data from the I-80 was used. The data were divided into calibration and validation data. Each model was fit to car-following-car pairs in the complete calibration data instead of individual pairs of lead and following vehicles. Then a single set of optimal parameters was determined for each car-following model. This optimal parameter set was used to evaluate the model performance with the validation data.

The following sections compare the model performance both quantitatively and qualitatively. The last subsection compares the model parameter values between the lead car and lead truck cases in the driving simulator data.

### 6.3.1 Speed Distribution

Fig. 6-8. Observed and Predicted Speed Distributions shows the distributions of observed and predicted speeds in the three datasets. Fig. 6-8 (a) shows that the IIDM with and without BL has the best fit for the Moving-LV data compared to the Wiedemann Model, the Gipps Model and the IDM which overestimated the speeds around 21-22 m/s and underestimated the speeds around 25 m/s. The speed of 25 m/s was the speed of the lead vehicle. This means that these models generally predicted lower speeds while following the lead vehicle. This will be discussed further in the qualitative comparison of the models in the next section.
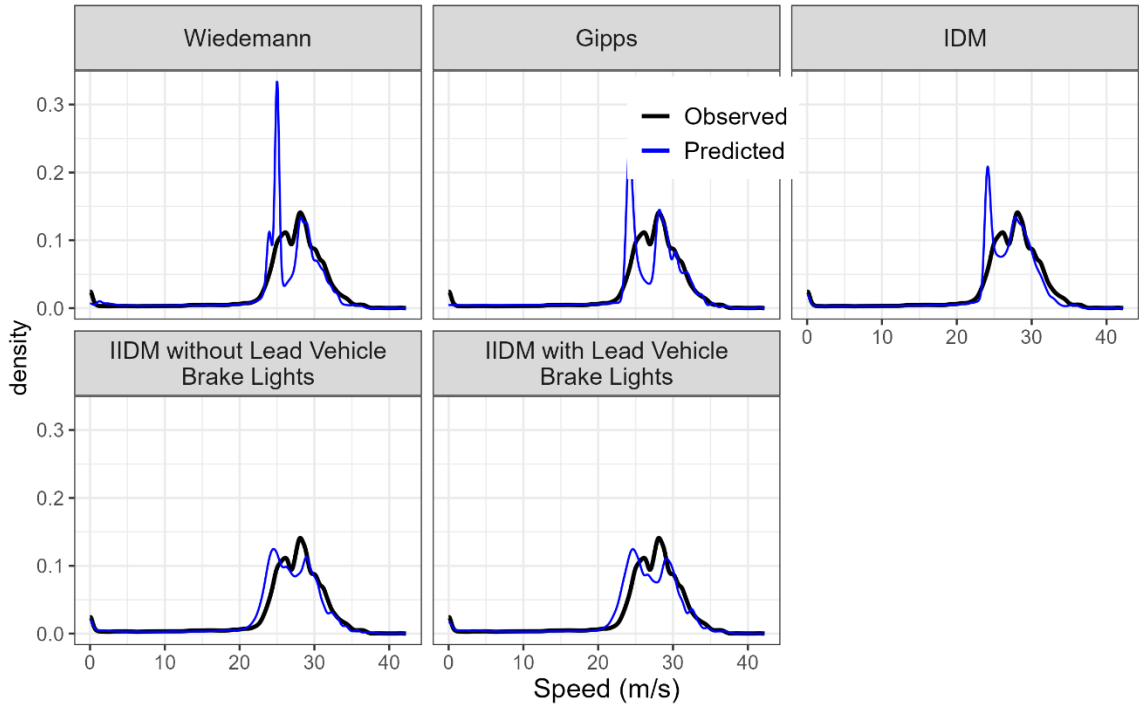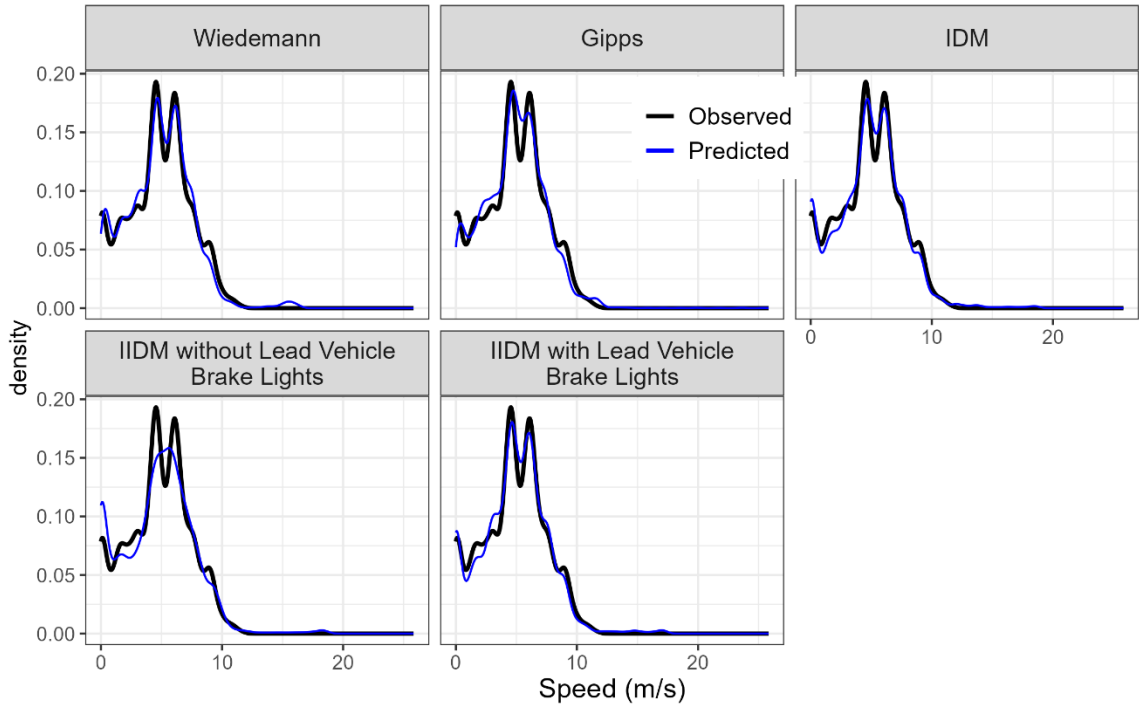
(a) Moving-LV scenario
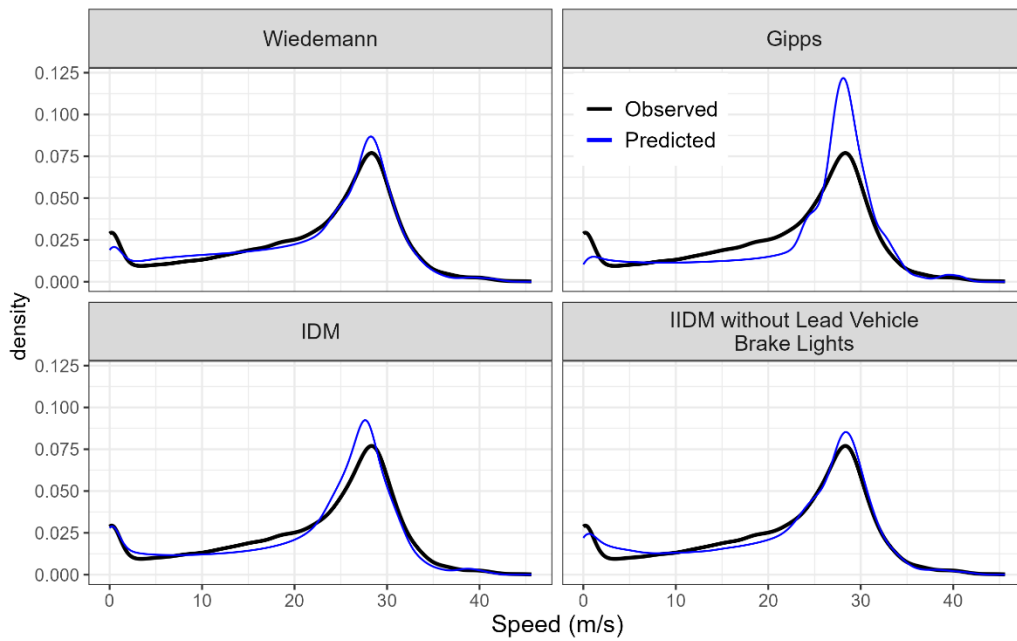


(b) Stopped-LV scenario

**Fig. 6-8. Observed and Predicted Speed Distributions**

(c) I-80 data

**Fig. 6-8. Observed and Predicted Speed Distributions (Continued)**

However, for the Stopped-LV data, the predicted speed distribution from the Wiedemann model also provided a good fit to the observed speed distribution as the IIDM (Fig. 6-8. Observed and Predicted Speed Distributions (b)). The IIDM with BL was not used as the brake lights of the stopped lead vehicle were turned off.

In case of the I-80 data, all models provided similar fit to the observed speed distribution as shown in Fig. 6-8. Observed and Predicted Speed Distributions (c). Overall, the IIDM predicted the speed distributions more accurately than the other models in all the datasets.

### 6.3.2    Acceleration Distribution

Fig. 6-9 compares the acceleration distributions among different models. For the Moving-LV and the Stopped-LV scenarios, the IIDM with and without BL predicted the accelerations (positive, negative, and zero) more accurately than the other models as shown in Fig. 6-9 (a) and (b).
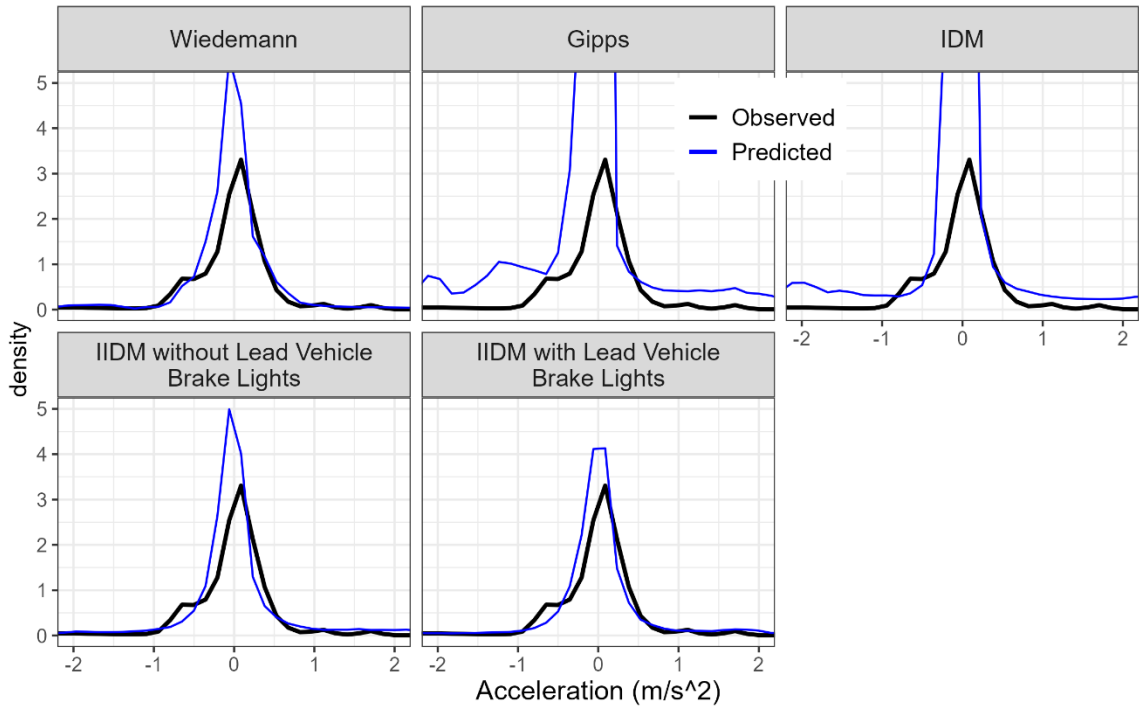


(a)  Moving-LV Acceleration Distributions

**Fig. 6-9. Observed and Predicted Acceleration Distributions**
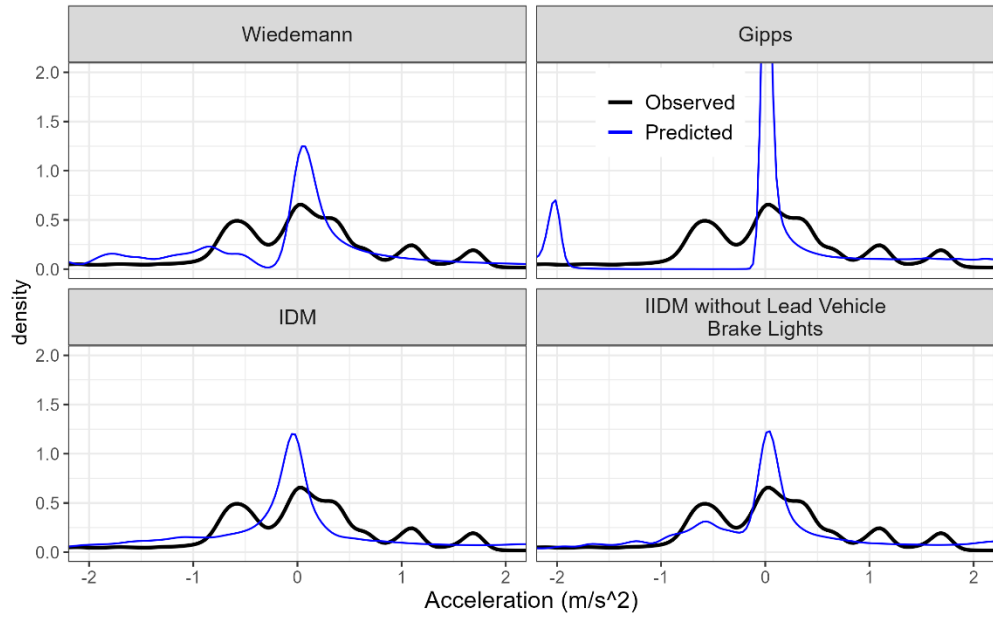
(b) Stopped-LV Acceleration Distributions
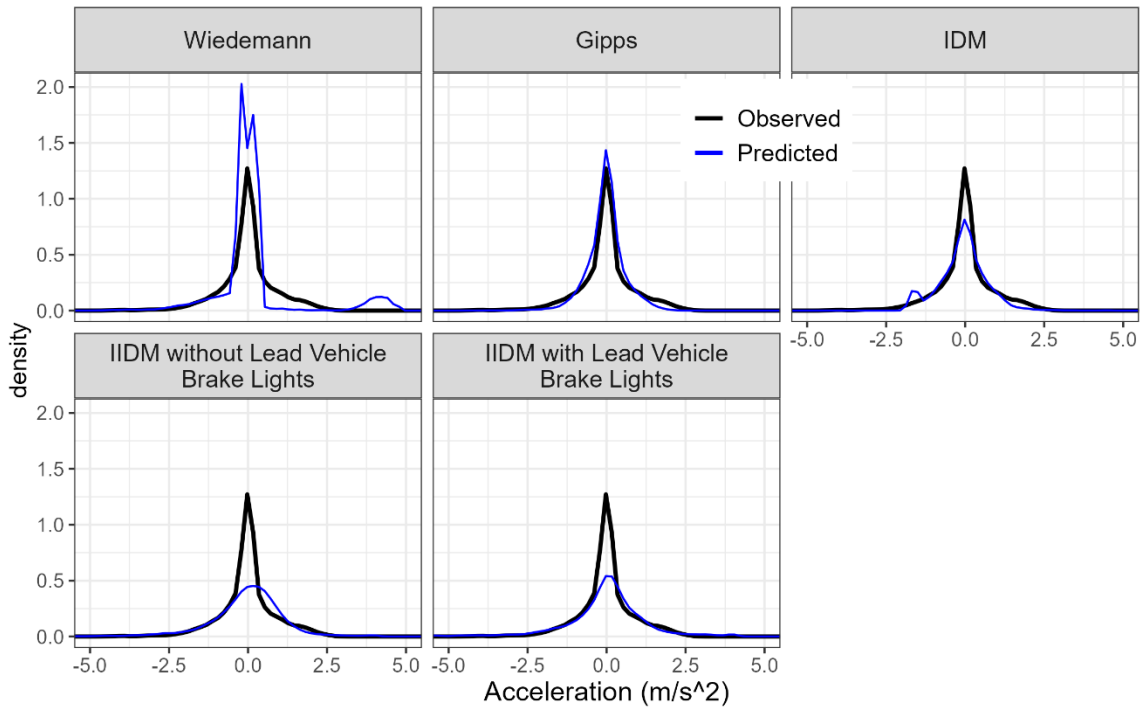


(c) I-80 Acceleration Distributions

**Fig. 6-9. Observed and Predicted Acceleration Distributions (Continued)**

For the I-80 data, the Gipps Model and the IDM produced more similar acceleration distributions to the observed acceleration distributions than the other models as shown in Fig. 6-9 (c)). The Gipps Model and the IDM also provided good fits for predicting speed as shown in Fig. 6-8 (c). However, although the Wiedemann Model, the Gipps Model and the IDM predicted the accelerations closer to zero similar to the observed data, they underestimated the accelerations greater or less than zero. On the other hand, the IIDM predicted the acceleration in this range more accurately than the Wiedemann Model and the Gipps Model.

### 6.3.3   Trajectory-level Comparison

The distributions of speed and acceleration in the previous section compared the aggregated performance of the car-following models. However, they did not reveal the model performance at the individual subject vehicle level. For instance, the acceleration distributions in Fig. 6-9 do not show how the observed and predicted acceleration varied for individual runs/vehicles. Thus, the observed and predicted trajectories of speed, acceleration, jerk and spacing were also compared among different car-following models.

Examples of the observed vehicle trajectories for one run in each driving simulator scenario and one pair in the I-80 data are shown in Fig. 6-10. The ranges of acceleration and jerk trajectories in the observed data (Fig. 6-10). The acceleration varied between +4 to -5 $m/s^2$ while the jerk varied between +5 to -5 $m/s^3$ with an outlier at -10 $m/s^3$ in I-80 data. To clearly show the patterns of vehicle trajectories with different ranges of value for the Moving-LV, Stopped-LV, and I-80 data, different scales were used in Fig. 6-10.

The following figures compare the trajectories predicted using individual car-following models to the observed trajectories for one run in each driving simulator scenario and one pair in the I-80 data. A total of 178 trajectories generated by the four car-following models were compared for each driving simulator scenario or pair. A sample of 15 trajectories are shown in Appendix A.
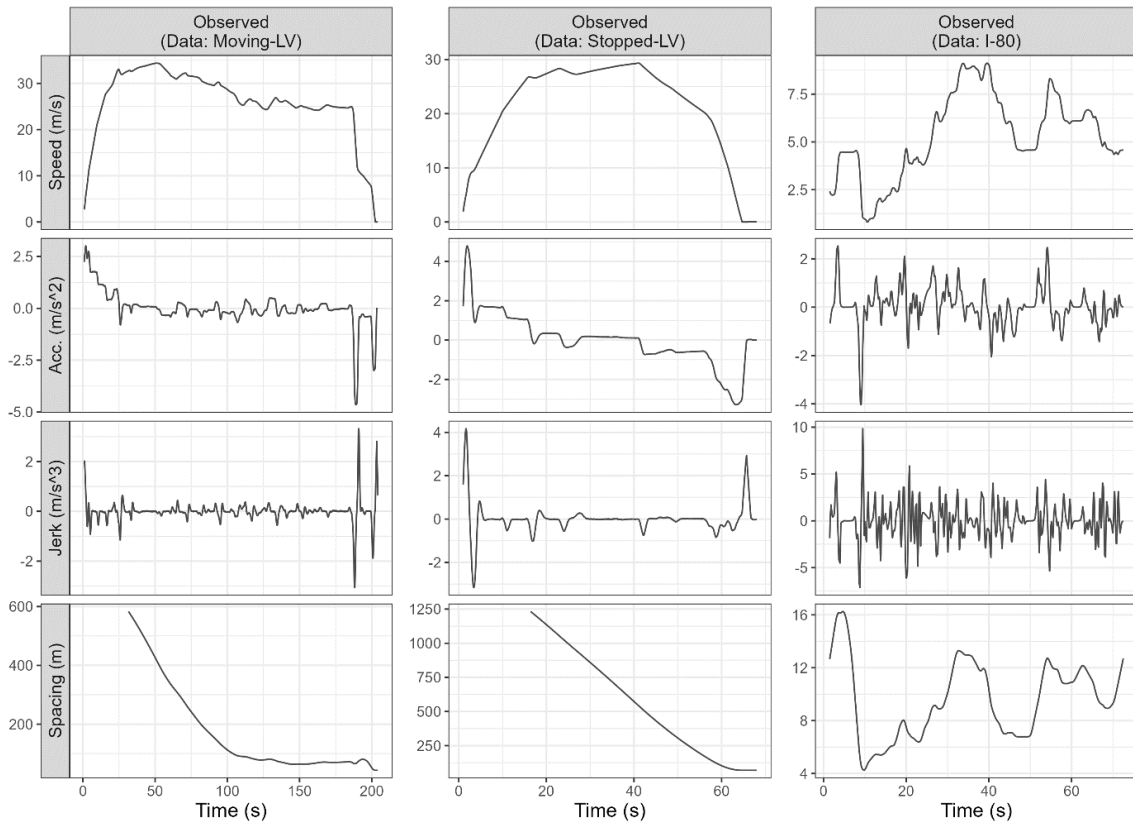


**Fig. 6-10. Example of Observed Trajectories of Speed, Acceleration, Jerk and Spacing**

Fig. 6-11 compares the trajectories predicted using the Wiedemann Model to the observed trajectories. Although the predicted speed profiles from the Wiedemann model were closer to the observed speed profiles, the acceleration and jerk profiles were

144

significantly different. The reason for large spikes in the predicted acceleration and jerk is that the Wiedemann Model does not assume the driver's continuous reaction to the lead vehicle motion. As discussed in Chapter 3.2.1, the Wiedemann Model determines the car-following condition in a given instance by comparing the instantaneous speed difference and spacing with the estimated perception thresholds. As a result, the predicted acceleration abruptly changed whenever the driving conditions switched between free-driving and following as well as following and emergency-braking conditions. Since jerk is the rate of change of acceleration, this large variation in acceleration resulted in unrealistically large jerk of -10 $m/s^3$. According to Lu et al. (2018), the "discrete regime [conditions] structure" of the Wiedemann Model also creates the steep decrease in acceleration ("acceleration cliff"), which produced large estimation errors of vehicle emissions (Lu et al., 2018).

Furthermore, the predicted spacing was generally larger than the observed spacing due to large deceleration. This means that the Wiedemann Model predicted unrealistically safer driving behaviours (i.e., keep larger spacing).
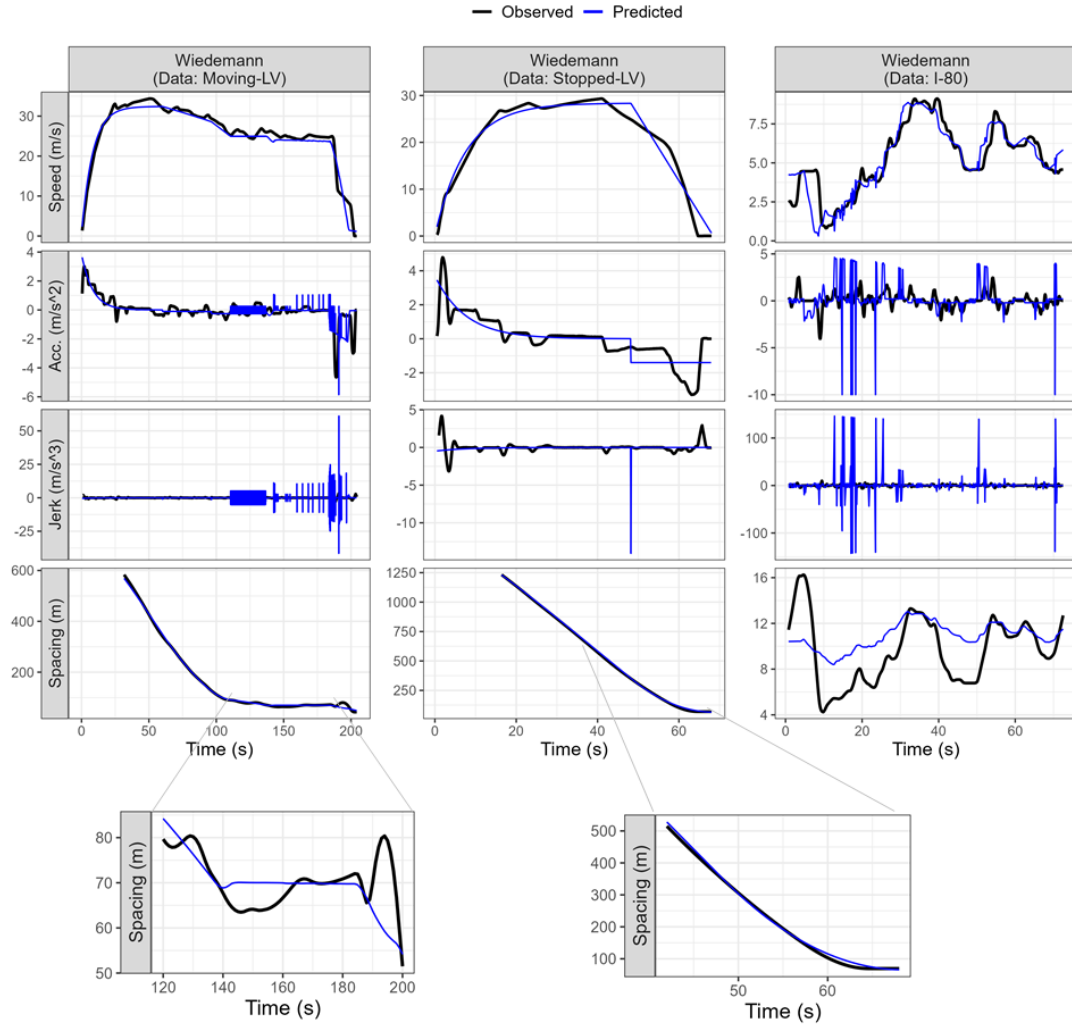
**Fig. 6-11. Observed and Predicted Trajectories (Wiedemann Model)**

Fig. 6-12 shows the trajectories predicted using the Gipps Model. The Gipps Model assumes a "true reaction time" and a "safety reaction time" that is equal to the half of the true reaction time (Gipps, 1981). Due to this assumption, the model predicts that the subject vehicle starts deceleration earlier to avoid a collision with a slow or stopped lead vehicle.

The Gipps Model generally predicted smoother speed and acceleration and smaller jerk than the observed data. This is because the Gipps Model assumes that the driver

continuously react to the lead vehicle motion instead of irregularly reacting based on perception thresholds unlike the Wiedemann Model.
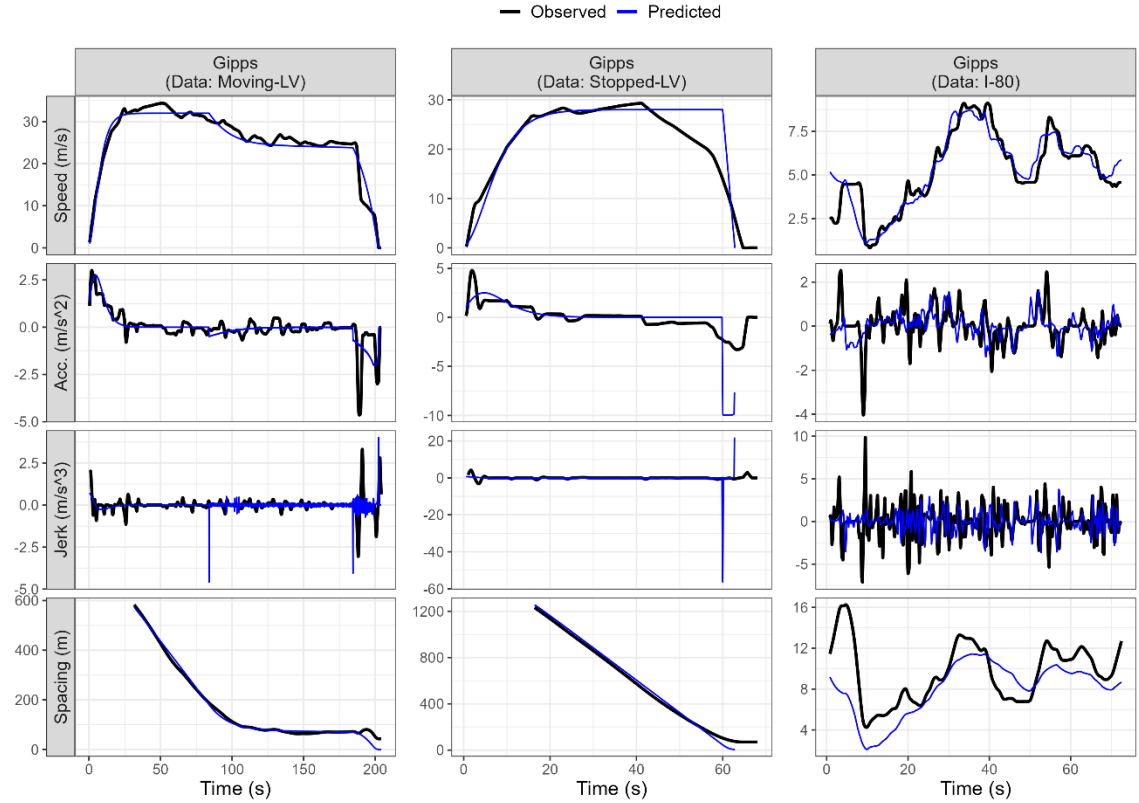


**Fig. 6-12. Observed and Predicted Trajectories (Gipps Model)**

Similar to the Gipps Model, the IDM produced reasonable trajectories compared to the observed trajectories as shown in Fig. 6-13. However, the IDM also predicted smooth speed and acceleration profiles and mostly zero jerk for the driving simulator data (left and middle figures in Fig. 6-13). This is because the IDM also assumes the driver's continuous reaction similar to the Gipps Model. The difference between the two models is that the IDM assumes that the driver reacts with zero delay (no reaction time) and the Gipps Model assumes that the driver reacts after fixed-time delay. However, human drivers adjust

acceleration and deceleration after intermittent time delays, i.e., only after the evidence for those adjustments accumulates to a threshold (Markkula, 2014).
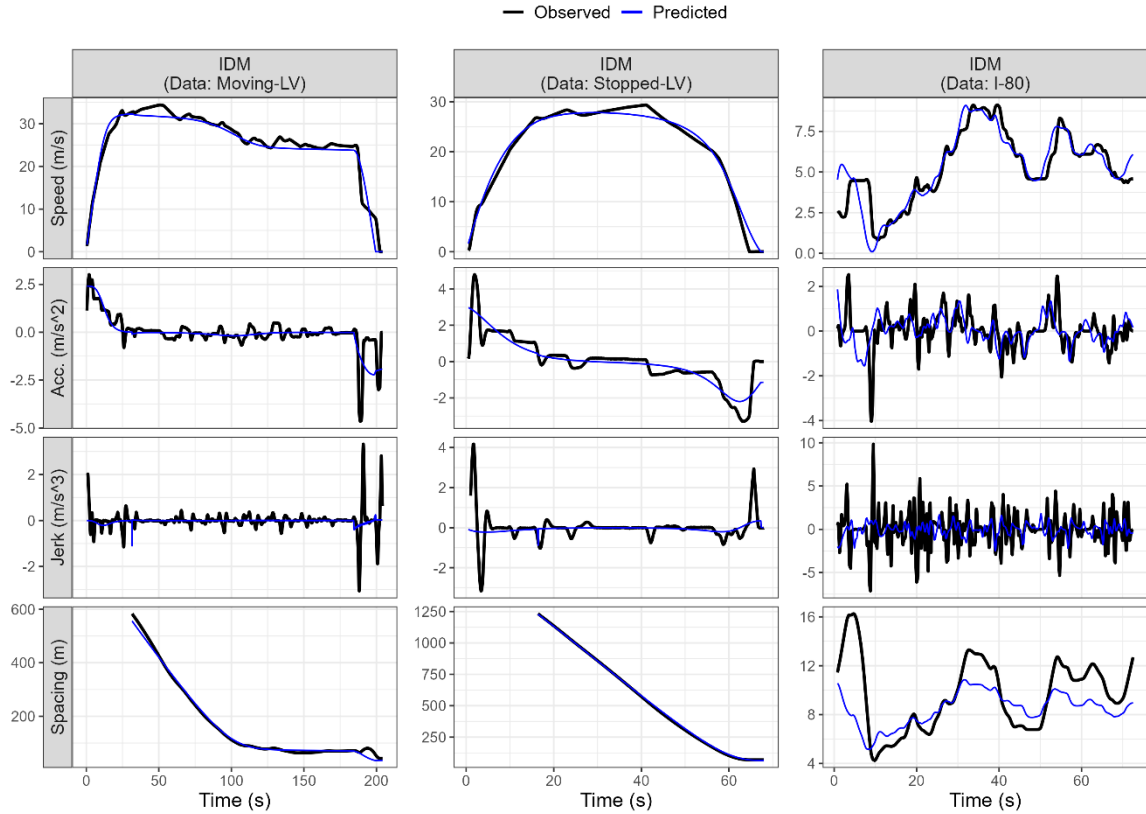


**Fig. 6-13. Observed and Predicted Trajectories (Intelligent Driver Model)**

On the other hand, the IIDM assumes that the driver adjusts acceleration and deceleration only after the accumulated evidence over time exceeds a threshold and thereby captures the intermittent time delay for reaction.

As a result, the IIDM with and without BL reasonably reproduced the observed vehicle trajectories as shown in Fig. 6-14 and Fig. 6-15, respectively. The figures demonstrate that the IIDM better predicted the observed car-following behaviours than the Wiedemann

Model, the Gipps Model, and the IDM for all car-following conditions in both free-flow and congested conditions.
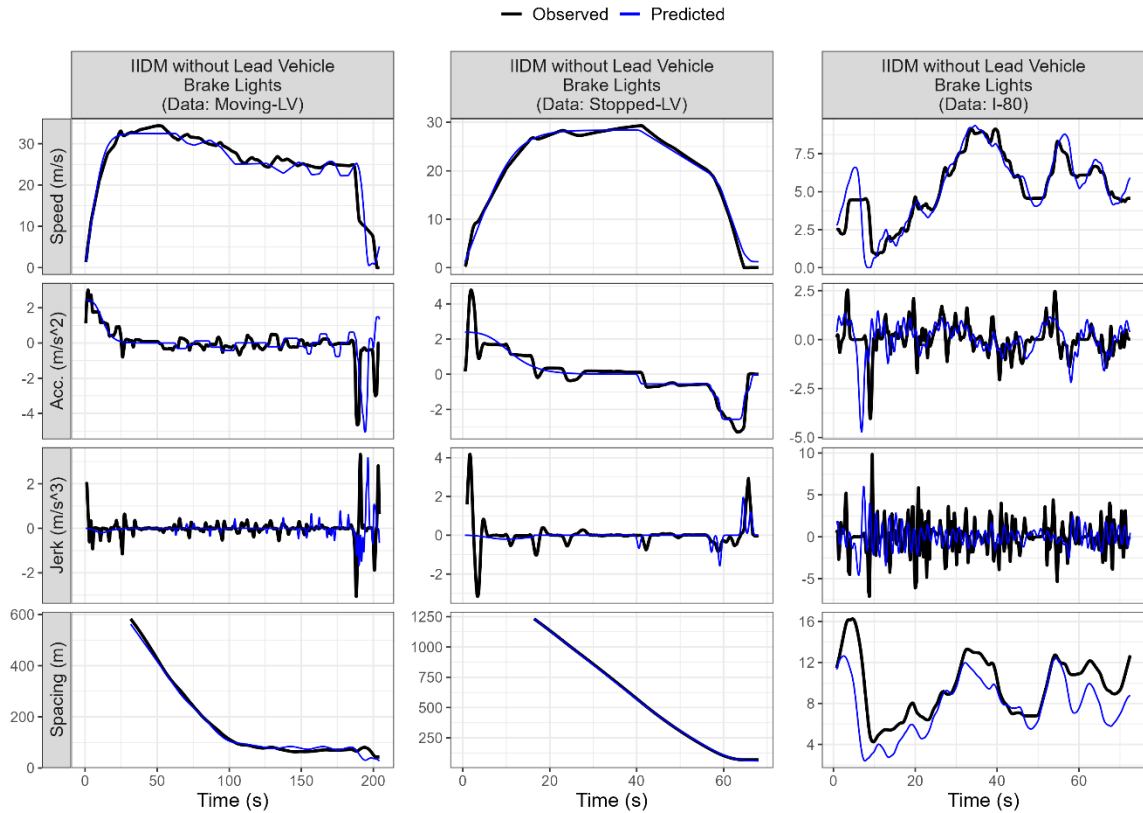


**Fig. 6-14. Observed and Predicted Trajectories (Intermittent Intelligent Driver Model without Lead Vehicle Brake Lights)**
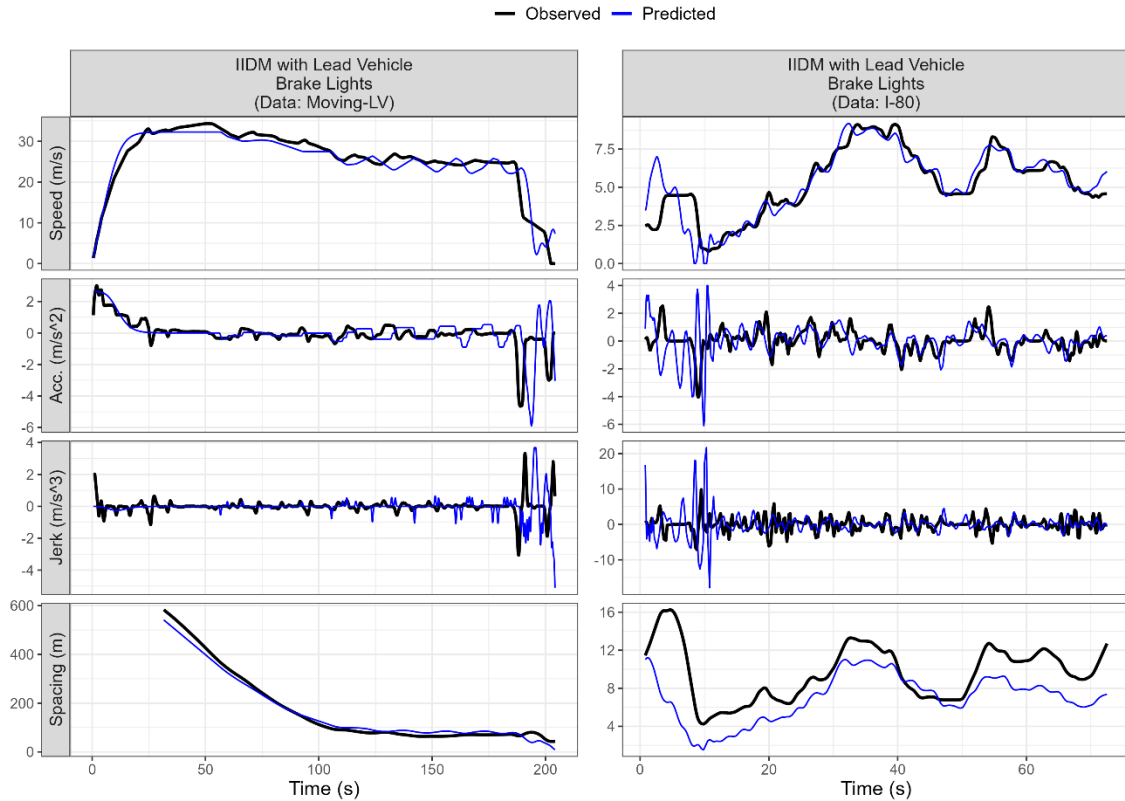
**Fig. 6-15. Observed and predicted trajectories (Intermittent Intelligent Driver Model with Lead Vehicle Brake Lights)**

More accurate prediction of the IIDM than the other models is also because the IIDM uses more realistic shape and duration of acceleration adjustments. For instance, Fig. 6-16 compares speed, acceleration, and jerk among the four car-following models for a time interval of 40 – 45 seconds. As shown in the enlarged figures in the right, the IIDM predicted the shapes of the acceleration and jerk profiles as the function $G(t)$ and its rate of change, respectively, as discussed in Chapter 5.1.3. Due to this specification of the shape and duration, the IIDM produced acceleration and jerk profiles more similar to the observed profiles than the other car-following models.
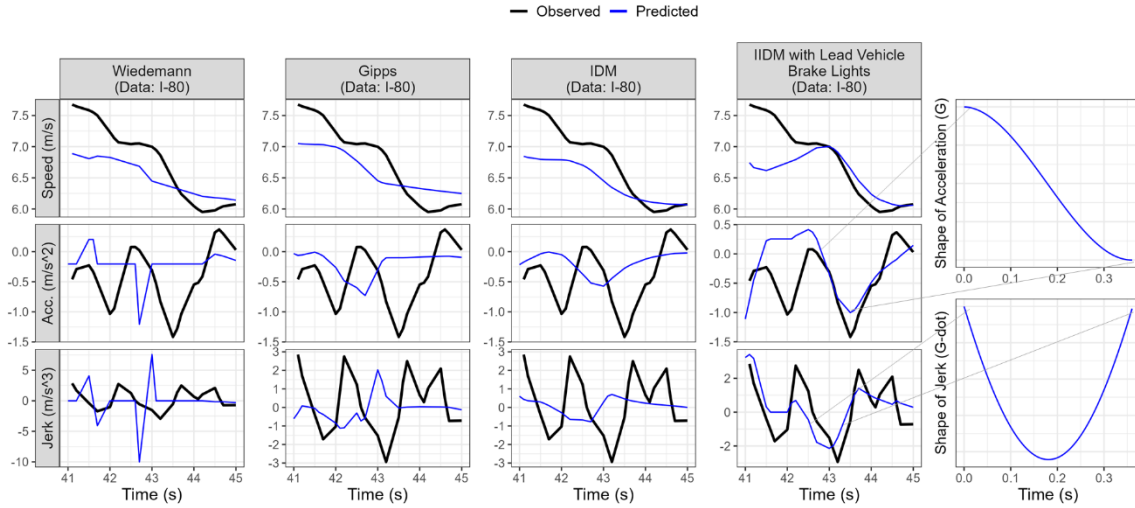
150

**Fig. 6-16. Observed and predicted shape and duration of acceleration and jerk for different car-following models**

Table 6-2 shows the calibrated parameters of the IIDM with and without BL for the Stopped-LV and Moving-LV scenarios. These values are the mean $\pm$ standard deviation of all the calibrated values for individual scenario runs. The first six parameters ($T, A_i, b, v_0, \delta, and s_0$) were generally similar in both Stopped-LV and Moving-LV scenarios. However, the accumulator gain $k$ was smaller in the Stopped-LV scenario compared to the Moving-LV scenario. The absolute values of the thresholds ($A_+$ and $A_-$) were also larger in the Stopped-LV scenario than the Moving-LV scenario. These differences are due to different requirement of deceleration between the scenarios. In the Moving-LV scenario, the parameter values were also generally similar between the IIDM without BL than the IIDM with BL. The value of $p_{BL} = 0.40$ indicates that drivers were likely to use the additional effect of lead vehicle brake lights with a probability of 0.40 on average.

151

**Table 6-2. Calibrated parameters of the IIDM for different datasets**

| Parameter | Stopped-LV scenario* | Moving-LV scenario* | | I-80 | |
|---|---|---|---|---|---|
| | Without LV Brake Lights | Without LV Brake Lights | With LV Brake Lights | Without LV Brake Lights | With LV Brake Lights |
| $T$ | 5.32 $\pm$ 3.02 | 3.03 $\pm$ 1.83 | 3.25 $\pm$ 2.19 | 1.04 | 0.97 |
| $A_i$ | 2.78 $\pm$ 0.43 | 2.45 $\pm$ 0.47 | 2.29 $\pm$ 0.61 | 1.43 | 3.83 |
| $b$ | 5.87 $\pm$ 1.28 | 7.33 $\pm$ 3.69 | 6.78 $\pm$ 4.20 | 2.66 | 2.83 |
| $v_0$ | 30.42 $\pm$ 3.16 | 31.83 $\pm$ 2.82 | 31.81 $\pm$ 2.75 | 28 | 28 |
| $\delta$ | 2.88 $\pm$ 0.90 | 3.56 $\pm$ 0.89 | 3.54 $\pm$ 0.93 | 3.13 | 1.29 |
| $s_0$ | 26.58 $\pm$ 11.89 | 24.39 $\pm$ 10.92 | 23.04 $\pm$ 8.90 | 1.19 | 1.07 |
| $k$ | 25.76 $\pm$ 7.63 | 31.89 $\pm$ 6.55 | 30.78 $\pm$ 7.69 | 2,724.91 | 2,626.37 |
| $A_+$ | 24.73 $\pm$ 6.70 | 20.96 $\pm$ 8.27 | 20.14 $\pm$ 10.55 | 22.96 | 32.36 |
| $A_-$ | −26.03 $\pm$ 7.54 | −21.00 $\pm$ 9.97 | −21.21 $\pm$ 9.06 | -29.84 | -10.37 |
| $\lambda$ | 0.52 $\pm$ 0.16 | 0.41 $\pm$ 0.17 | 0.94 $\pm$ 0.32 | 0.55 | 0.47 |
| $a_{BL}$ | - | - | 0.51 $\pm$ 0.14 | - | 1.2 |
| $p_{BL}$ | - | - | 0.40 $\pm$ 0.18 | - | 0.23 |
| $M$ | 2.47 $\pm$ 0.69 | 2.14 $\pm$ 0.87 | 2.40 $\pm$ 0.82 | 2.26 | 2.19 |
| $\tau_p$ | 0.03 $\pm$ 0.01 | 0.02 $\pm$ 0.01 | 0.03 $\pm$ 0.01 | 0.02 | 0.02 |
| $\tau_m$ | 0.02 $\pm$ 0.01 | 0.03 $\pm$ 0.01 | 0.02 $\pm$ 0.01 | 0.02 | 0.02 |
| $\sigma_n$ | 0.25 $\pm$ 0.07 | 0.24 $\pm$ 0.07 | 0.23 $\pm$ 0.08 | 0.15 | 0.34 |
| $\sigma_m$ | 0.26 $\pm$ 0.08 | 0.26 $\pm$ 0.08 | 0.24 $\pm$ 0.07 | 0.17 | 0.31 |
| $\Delta T$ | 2.57 $\pm$ 0.99 | 3.13 $\pm$ 1.39 | 3.25 $\pm$ 1.47 | 0.74 | 0.36 |
| $\Delta T_{p0}$ | 0.44 $\pm$ 0.14 | 0.46 $\pm$ 0.14 | 0.45 $\pm$ 0.12 | 0.28 | 0.08 |
| $\Delta T_{p1}$ | 5.82 $\pm$ 1.61 | 5.79 $\pm$ 1.06 | 5.33 $\pm$ 1.70 | 2.16 | 1.26 |

\* The values are mean $\pm$ standard deviation.

Furthermore, the calibrated parameters from the I-80 data are also listed in Table 6-2. Some of the parameter values for the I-80 data were significantly different from those for the driving simulator data. This was due the difference in traffic conditions. The driving simulator scenarios were run for individual drivers with only one lead vehicle several hundred meters away in the beginning. However, in the I-80 data, there were many vehicles and traffic conditions were mostly congested. The calibrated value of the accumulator gain $k$ was significantly higher in the I-80 data than the driving simulator data because the evidence was accumulated faster in congested traffic. Moreover, the duration parameters, $\Delta T$, $\Delta T_{p0}$, and $\Delta T_{p1}$, were smaller in the I-80 data than the driving simulator data due to faster adjustment of acceleration and deceleration in congested traffic.

### 6.3.4   Estimated Surrogate Measures of Safety

This section compares the combination of two trajectories, speed difference and spacing, in the form of two surrogate measures of safety, Time-to-Collision (TTC) and Deceleration to Avoid Crash (DRAC) to evaluate model performance. TTC is the time remaining until a faster subject vehicle collides with a lead vehicle when both vehicles maintain their speed. TTC is estimated in each time instant as the ratio of the front-to-rear spacing to the speed difference from the lead vehicle. Therefore, the minimum value of TTC in each car-following segment indicates highest risk of rear-end collision throughout the car-following.

DRAC is the minimum *deceleration* rate required to come to a complete stop behind a slow/stopped lead vehicle. According to American Association of State Highway and Transportation Officials (AASHTO), DRAC greater than 3.4 m/s$^2$ indicates a conflict

(AASHTO, 2001). DRAC is estimated by dividing the square of speed difference by front-to-rear spacing.

*Start Time and Pattern of Deceleration in Crash Cases*

One of the objectives of using car-following models in a microscopic simulation is to use the predicted trajectories for evaluating traffic safety. Various past studies have indicated a long reaction time and/or an insufficient deceleration rate lead to rear-end crash and near-crashes (Green, 2017b). Therefore, this section discusses the start time, pattern of deceleration, TTC and DRAC in two crash cases from the Moving-LV (lead car) and Stopped-LV (lead truck) scenarios.

Fig. 6-17 (a) and (b) show trajectories of speed, acceleration, spacing, TTC, and DRAC for the approaching condition and the braking condition, respectively, for the same driver. The points on the trajectories indicate the start of deceleration. Since DRAC is deceleration or negative acceleration, the sign of values of DRAC in Fig. 6-17 is negative (i.e., higher deceleration denotes higher absolute value of DRAC).
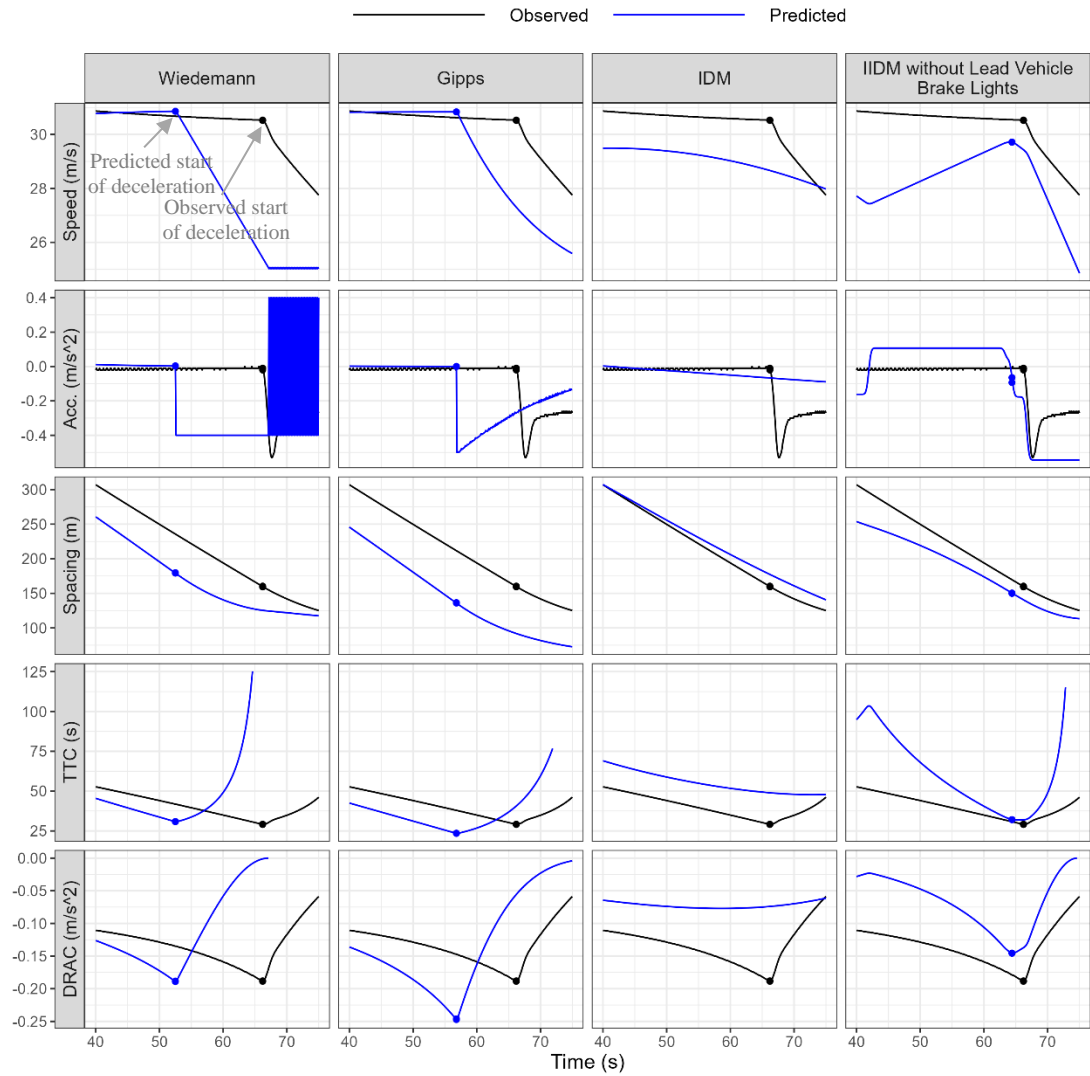
(a) Trajectories in Approaching Condition

**Fig. 6-17. Observed and Predicted Trajectories of a Crash Case from Moving-LV Scenario**
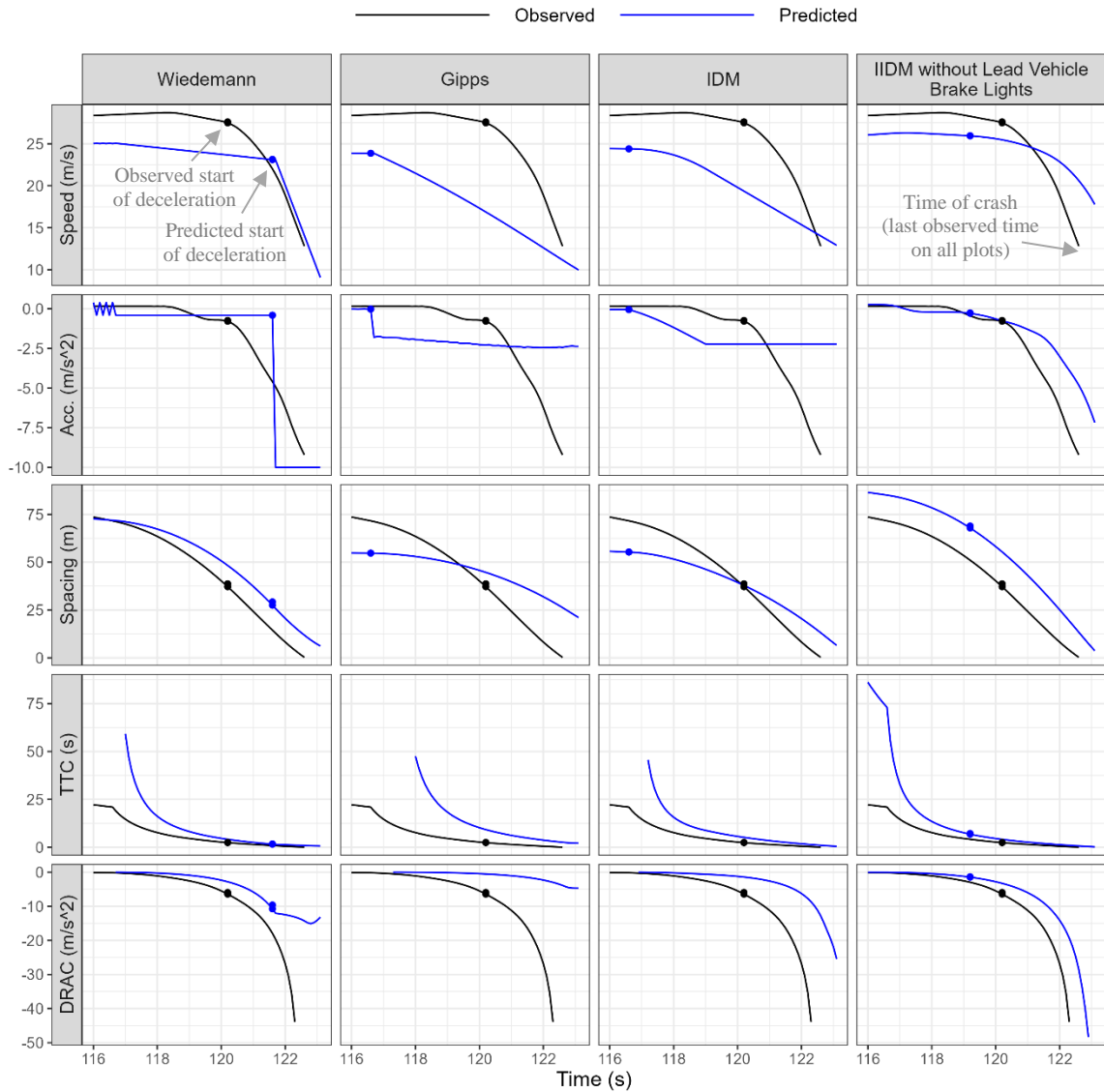
(b) Trajectories in Braking Condition

**Fig. 6-17. Observed and Predicted Trajectories of a Crash Case from Moving-LV Scenario (Continued)**

In the approaching condition, it is expected that the driver reduces speed from his/her desired speed to the lead vehicle speed. In the scenario in Fig. 6-17 (a), the lead vehicle speed was 25 m/s. The predicted speed of the Wiedemann Model and the Gipps Model

were most similar to the observed speed. However, the predicted deceleration occurred much earlier than the observed deceleration, and it also decreased more abruptly which produced unrealistically high predicted jerk (not shown). As a result, the minimum TTC and the maximum DRAC predicted by the Wiedemann Model and the Gipps Model occurred earlier than the observed values in time. This earlier occurrence of high crash risk also results in earlier drivers' deceleration which reduces the predicted crash risk compared to the actual crash risk (i.e., higher TTC and lower DRAC).

Furthermore, since the IDM does not have a reaction time, defining the start of reaction is not always possible. This is clear from the trajectories of the IDM in Fig. 6-17 (a). As the IDM produced very smooth trajectory profiles, the deceleration started much earlier than the actual start time of deceleration. Therefore, the predicted minimum TTC never decreased to the actual minimum TTC, and the predicted DRAC remained mostly constant and was less than the actual DRAC (i.e., lower deceleration). Thus, the IDM predicted lower crash risk than the actual crash risk.

Although the IIDM did not produce similar initial speed trajectory in free-driving condition, the start time and pattern of deceleration was the most similar to the observed data. Therefore, the time and magnitude of the predicted minimum TTC and maximum DRAC of the IIDM were closest to the observed data compared to the other models.

Fig. 6-17 (b) shows the trajectories in the braking condition when the actual crash occurred for the same driver discussed above. In the Moving-LV scenario, the driver was required to decelerate to stop behind a decelerating lead car. Compared to the observed data, the Wiedemann Model predicted a delayed start of deceleration. This resulted in a

large DRAC and higher crash risk initially. However, later, the Wiedemann model produced an abrupt and large deceleration with an unrealistically large jerk that reduced DRAC. Consequently, the minimum TTC was larger and the required DRAC was smaller. The predicted spacing by the Wiedemann model was 6.2 m when the actual spacing was 0 (i.e., when the crash occurred).

In contrast, the Gipps Model and the IDM predicted earlier start of deceleration than the actual start of the deceleration, which results in lower crash risk than the actual crash risk as shown in Fig. 6-17 (b). The predicted spacing by the Gipps Model and IDM at the time of crash were 21 m and 6.5 m, respectively.

As in the approaching condition, the IIDM predicted the start time and pattern of deceleration most similar to the observed deceleration in the braking condition (Fig. 6-17 (b)). Although the IIDM did not predict a crash (i.e., zero or negative spacing), it predicted a smaller spacing of 3.7 m at the time of actual crash.

Similar results were obtained in the crash in the Stopped-LV scenario as shown in Fig. 6-18. In this scenario, the Wiedemann model produced unrealistically large jerk to reach a large required deceleration after a delayed start of deceleration. The Gipps Model and the IDM produced similar magnitudes of deceleration compared to the observed deceleration. However, the Gipps model produced unrealistically abrupt change in deceleration and the IDM predicted significantly earlier start of deceleration than the observed deceleration.

The IIDM initially predicted similar deceleration compared to the observed deceleration, but later higher deceleration due to higher speed difference and desired spacing. However, the large predicted deceleration was insufficient to avoid a crash similar

to the observed deceleration. Therefore, the IIDM predicted a crash unlike the other models although the predicted crash occurred a few seconds earlier than the actual crash. Note that the other models predicted a spacing greater than 20 m at the time of actual crash. These examples demonstrate that the IIDM can predict the crash risk more realistically than the other models.
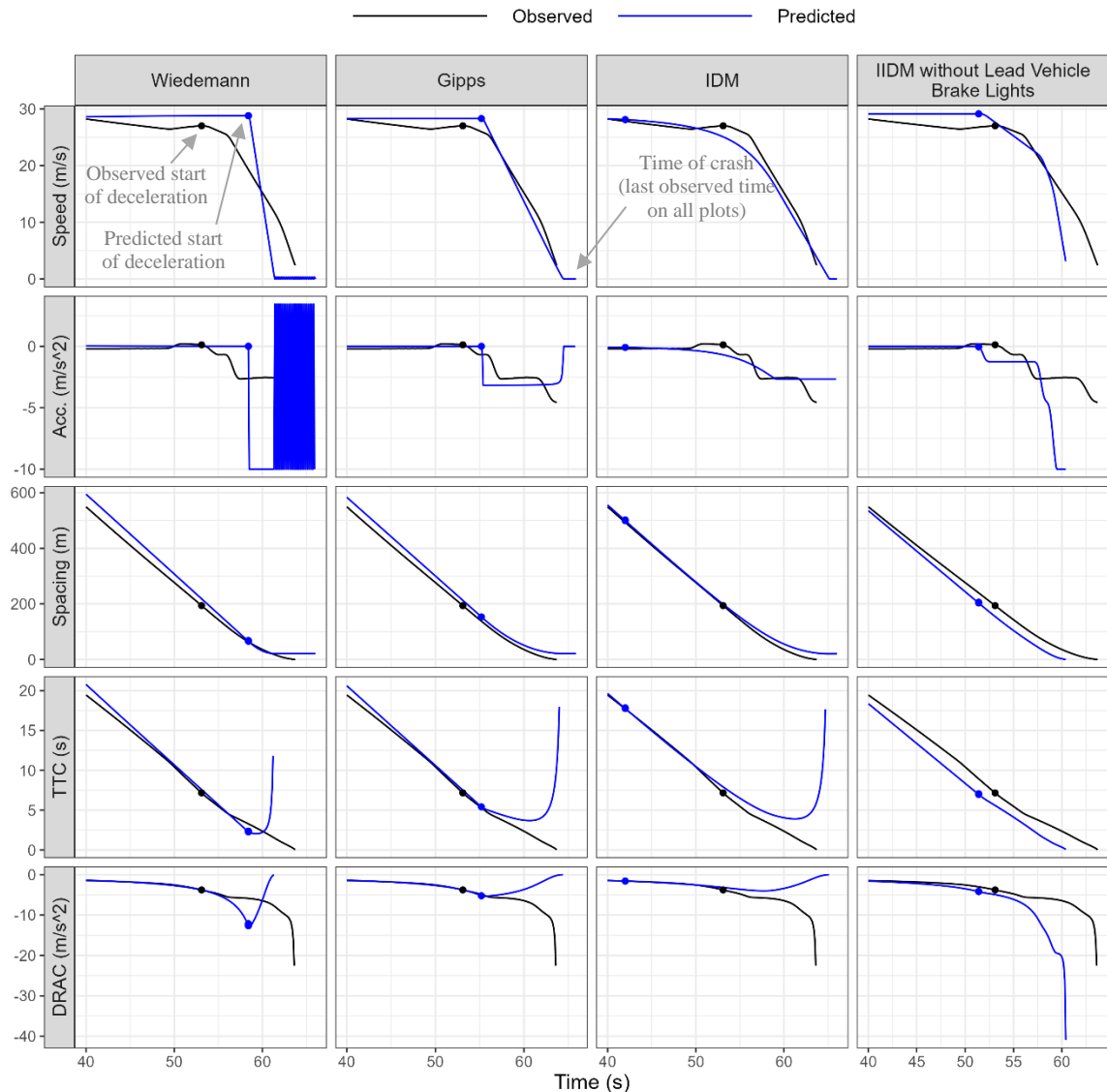


**Fig. 6-18. Observed and Predicted Trajectories of a Crash Case from Stopped-LV Scenario**

*Comparison of Predicted Minimum Time-to-Collision (TTC) among Models*

The minimum TTC was estimated for each run (the driving simulator data) or subject vehicle (the I-80 data) using both observed and predicted trajectory data. The negative values of minimum TTC were discarded as they indicated a crash. Fig. 6-19 compares the observed and predicted minimum TTC and the Root Mean Squared Error (RMSE).

In all datasets, the minimum TTC values estimated using the Wiedemann model were generally larger than the observed values. Therefore, the RMSE was the highest for the Wiedemann model in the Moving-LV scenario and second-highest in the Stopped-LV scenario. Higher predicted minimum TTC by the Wiedemann Model than the observed value is because the predicted deceleration increased faster than the observed deceleration as shown in Fig. 6-11. Thus, the Wiedemann Model generally underestimates actual crash risk (i.e., longer minimum TTC).
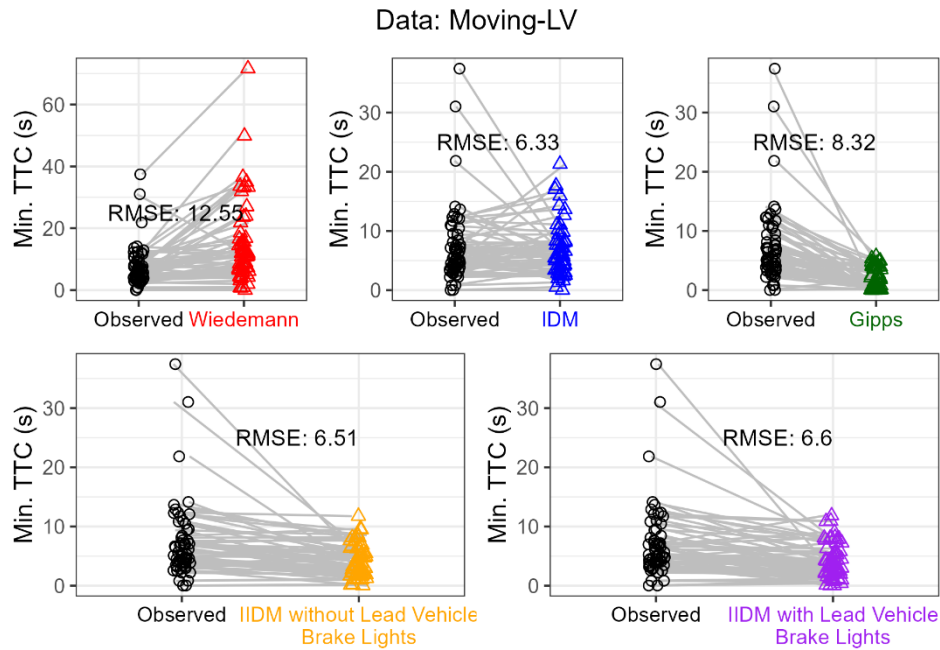


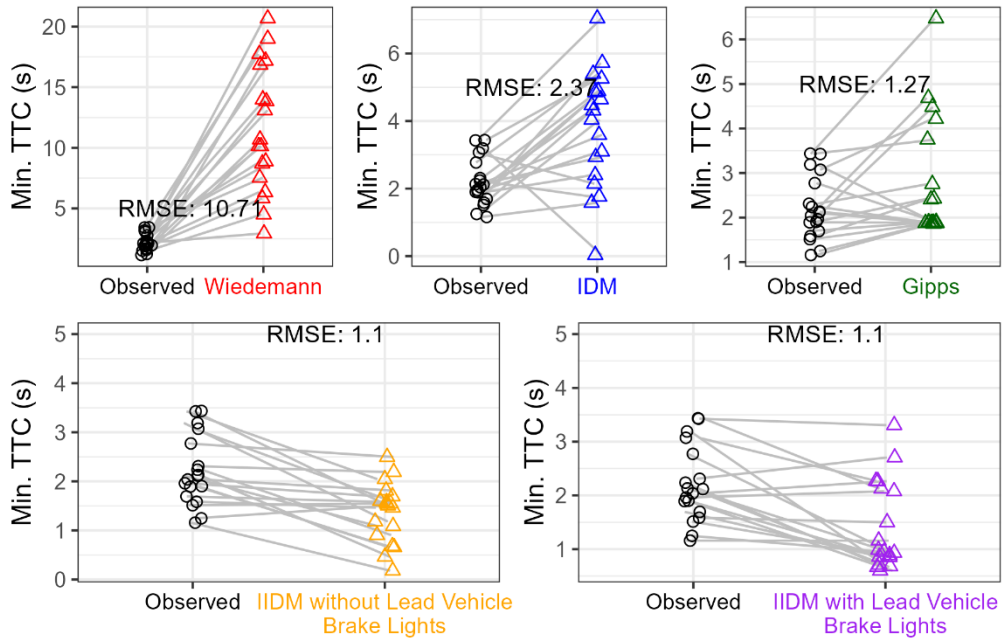(a) Minimum TTC per run in the Moving-LV Scenario

**Fig. 6-19. Observed and Predicted Minimum Time-to-Collision (TTC)**
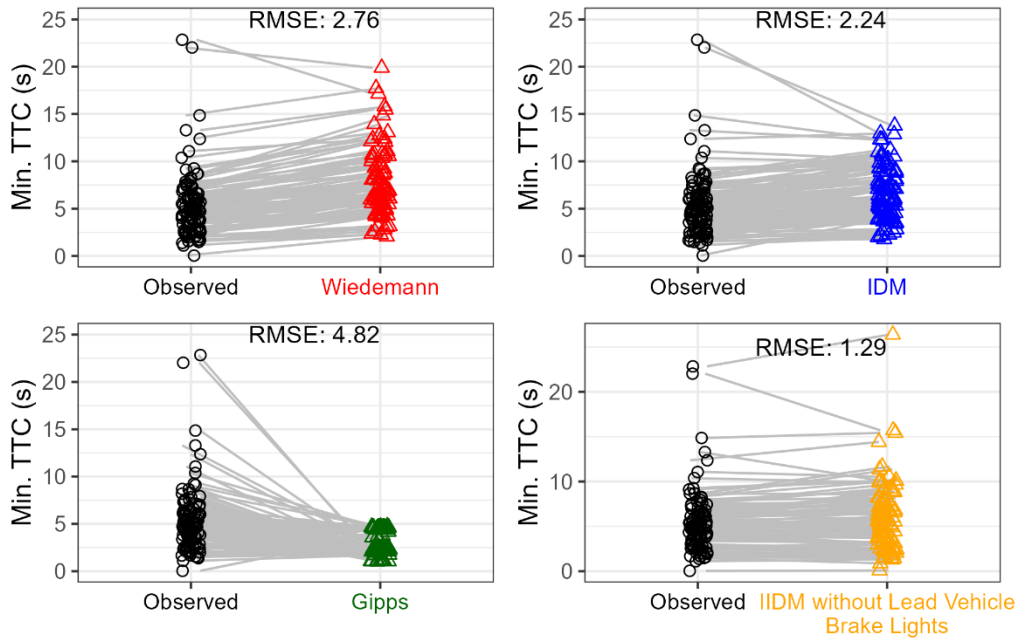
(b) Minimum TTC per run in the Stopped-LV Scenario



(c) Minimum TTC per Subject Vehicle in the I-80 data

**Fig. 6-19. Observed and Predicted Minimum Time-to-Collision (TTC) (Continued)**

The Gipps Model generally predicted lower minimum TTC than the observed value in the driving simulator data (second-highest RMSE) as shown in Fig. 6-19 (a) and (b), but only higher minimum TTC in the I-80 data (Fig. 6-19 (c)). The Gipps Model frequently predicted very small spacing or negative spacing due to crashes in the driving simulator data as shown in Fig. 6-12. This was because the Gipps Model assumes a constant reaction time which works well in close-following conditions but this assumption was invalid when the model was used in a mix of large and small spacing conditions.

The minimum TTC values estimated using the IDM were generally similar to the observed minimum TTC values in the driving simulator data. On other hand, IIDM consistently showed similar values of TTC to the observed values in all data sets. Although the IIDM predicted lower minimum TTC than the observed value, RMSE values of the IIDM were lower than the other models except for the Moving-LV scenario.

Fig. 6-20 shows the distributions of observed and predicted DRAC greater than 3.4 m/s$^2$ (i.e., the threshold of conflict) in the driving simulator data. The median DRAC is also labelled on the distributions and the number of data points are noted underneath the data label on x-axis. There were no instances where DRAC was greater than 3.4 m/s$^2$ in the I-80 data. A pairwise comparison of DRAC was not possible because some values of DRAC were very large as they were estimated from the predicted and observed trajectories which significantly fluctuated over time.

As shown in Fig. 6-20, the IIDM produced the distributions of DRAC most similar to the observed distributions of DRAC. These results demonstrate that the IIDM can better

predict the start of deceleration and the magnitude of deceleration in the approach and braking conditions, and thereby produce more realistic surrogate measures of safety.
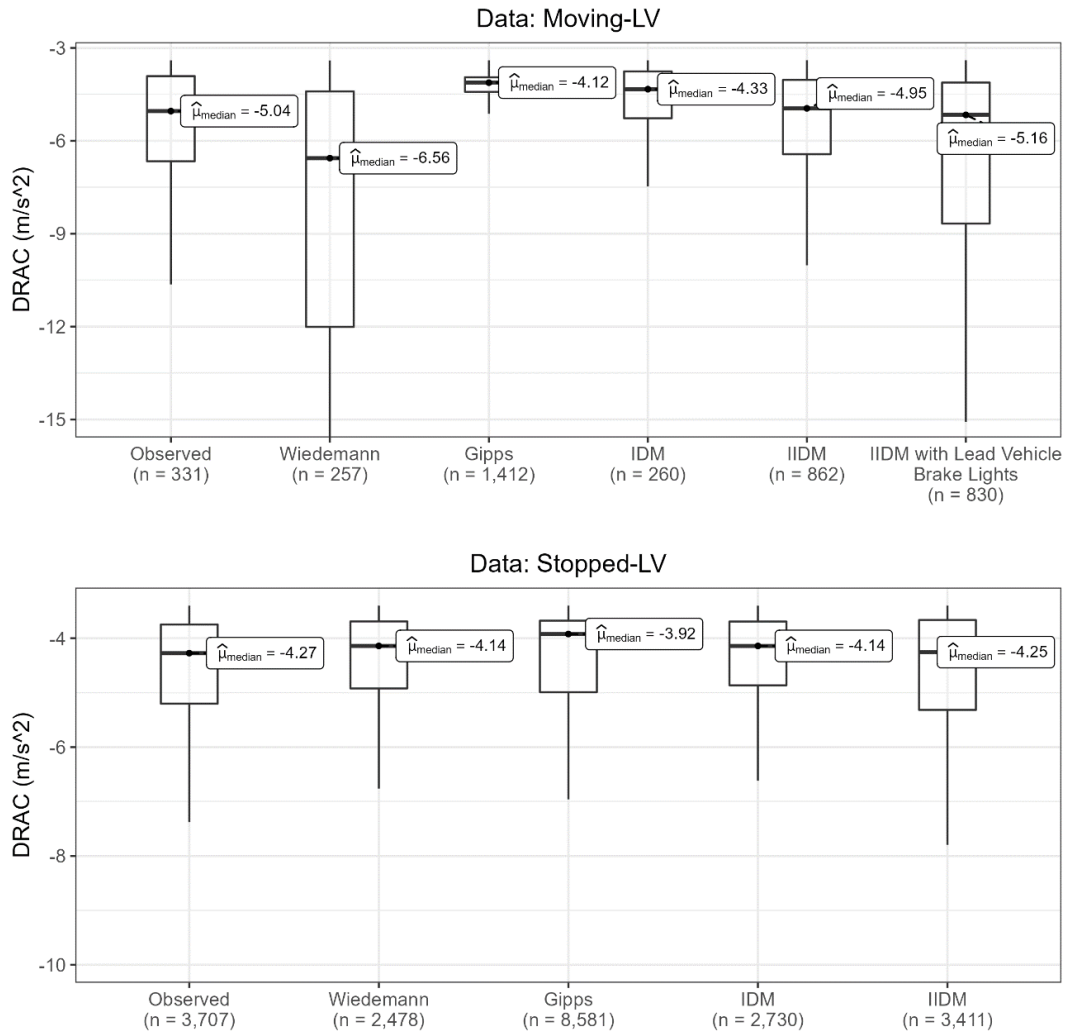


**Fig. 6-20. Distributions of Deceleration to Avoid Crash (DRAC) greater than 3.4 m/s$^2$**

## 6.4    Chapter Summary

The major findings of the hypothesis testing and modeling efforts conducted in this thesis are summarized below:

1. The theoretical concept of the evidence accumulation framework provides plausible explanation on the time of releasing accelerator and applying brakes in both approaching and braking conditions for different types of lead vehicle (car and truck). This is because drivers did not react at a specific threshold of evidence (tau-inverse/angular velocity) or after a fixed reaction time. Drivers generally reacted when the accumulation of evidence over time reached a threshold.

2. The Accumulator model predicted the start time of deceleration more accurately based on the accumulation of evidence. The model showed good prediction accuracy using not only angular velocity due to the width of lead vehicle or tau-inverse, but also other perceptual and symbolic cues such as angular velocity due to the height of the lead truck and the lead vehicle brake lights.

3. The Intermittent Intelligent Driver Model (IIDM) developed in this thesis incorporated the Accumulator model and a realistic shape and duration of acceleration adjustments, which were adapted from the Markkula's Framework of Sensorimotor Control in Sustained Motion Tasks. As a result, the IIDM predicted more realistic vehicle trajectories than the three conventional car-following models – the Wiedemann Model, the Gipps Model, and the IDM. Moreover, the IIDM produced the smallest error in spacing, time-to-collision and deceleration required to avoid crash in driving simulator scenarios as well as empirical vehicle trajectory data.

# Chapter 7: Conclusions and Recommendations

## 7.1    Conclusions

The findings and conclusions are summarized below in light of the research objectives discussed in Chapter 1.

*Prediction of start time of driver reaction*

Three hypotheses were tested to determine how the driver deceleration starts while following a slow lead vehicle or approaching a stopped vehicle. The key findings are as follows. First, the drivers perceived and reacted (e.g., released the accelerator pedal or applied the brake pedal) when the perceptual variable (tau-inverse) reaches different values. This is not consistent with the assumption of the Wiedemann's car-following model that drivers perceive and react when the perceptual variable reaches the same perception threshold. Second, the drivers did not react after a specific reaction time from the start of perception. These findings indicate that driver reaction cannot be realistically predicted using the absolute values of perception and reaction thresholds, and the fixed reaction time. Third, the drivers who followed the lead car and truck generally reacted when the accumulation of evidence (tau-inverse) over time – i.e., the areas under accumulation curves of perceptual variable - reached a threshold. Thus, the theoretical concept of the evidence accumulation framework provides plausible explanation on the start time of reaction in both approaching and braking conditions for different types of lead vehicle (car and truck).

*Identification of new perceptual and symbolic cues for predicting driver reaction*

Various perceptual and symbolic cues such as angular velocity (width and height), tau-inverse, and the lead vehicle brake lights were found to be closely related to the start time of driver reaction. In particular, the cues affecting the driver reaction were different for different types of lead vehicle (car and truck). The model that predicts the start time of reaction (Accumulator model) has a better fit when the angular velocity due to the height of the lead truck and lead vehicle brake lights were used instead of tau-inverse and angular velocity due to the width of the lead vehicle. This finding is in contrast with the assumption in the existing car-following model (Wiedemann model) that the driver starts reaction when the angular velocity due to the width of the lead vehicle reaches a fixed threshold. Thus, angular velocity due to the height of the lead truck and the lead vehicle brake lights are important factors in predicting the start time of deceleration in approaching and braking conditions.

*Development of a new car-following model*

To predict the start time of reaction and the magnitude of reaction more realistically, a new car-following called the Intermittent Intelligent Driver Model (IIDM) was developed based on the Markkula's Framework of Sensorimotor Control in Sustained Motion Tasks. The IIDM uses the evidence accumulation process to estimate the start time of driver reaction. The model also uses the shape and duration of acceleration adjustments based on the observed data. The performance of the IIDM was evaluated with the comparison with the three existing car-following models – the Wiedemann Model, the Gipps Model and the Intelligent Driver Model (IDM) – using the observed car-following data from a driving

simulator (uncongested conditions) as well as the vehicle trajectory data from Interstate-80 (I-80) highway (congested conditions).

The results showed that the IIDM with and without lead vehicle brake lights generated more realistic trajectories of speed, acceleration, jerk and spacing in both congested and uncongested conditions compared to the other three car-following models. Consequently, the IIDM also predicted surrogate measures of safety such as the minimum time-to-collision and deceleration to avoid crash more accurately. Thus, the IIDM can be used to simulate the driver's car-following behaviour and produce more reliable estimate of rear-end crash risk in car-following conditions.

In summary, the main contribution of this study is the development of a new car-following model that adapts intermittent nature of the driver's reaction to accurately reproduce the start and the magnitude of the driver reaction in different car-following conditions. The new car-following model can generate more realistic vehicle trajectories of speed, acceleration, jerk, and spacing, which are fundamental input data for the estimation of traffic delay, crash risk, and vehicle fuel consumption and emission. Thus, the proposed car-following model can be used in various traffic engineering applications such as the prediction of vehicle speeds, the assessment of traffic safety, and the evaluation of environmental impacts of traffic control strategy.

However, there are a few limitations in this study. First, the sample size of drivers in the driving simulator experiment was relatively small (50) and most drivers were young (18-25 years old). Thus, the findings in this study require further validation for more representative driver group using large scale data such as naturalistic driving data. Second, the performance of the IIDM can be degraded if the calibration of model parameters is

inadequate. The IIDM can occasionally produce unrealistically large jerk if the model is not properly calibrated. Third, the IIDM can occasionally produce large oscillation in speed profile, i.e., very rapid acceleration and deceleration, although the fitness function of spacing produces a very small error. Thus, it is important to ensure that the IIDM can realistically reflect the actual number and start times of acceleration/deceleration adjustments, and reproduce speed, acceleration and jerk profiles in short time intervals at trajectory level.

## 7.2    Recommendations for Future Work

In the future studies, it is recommended to consider other evidence for driver's reaction, not only the lead vehicle motion, such as road width (perceived based on the distance between lane markings), roadside objects and environmental conditions. These factors can potentially affect driver's car-following behaviour (e.g., more cautious driving in a narrower road, poor visibility in adverse weather). In particular, drivers can also collect this additional evidence via vehicle-to-vehicle communication with the lead connected and autonomous vehicles (CAV). Moreover, although CAV does not require manual driving, drivers are required to take over the control of vehicle when CAV can no longer perform automated driving (e.g., Level 3 automation). In this case, the evidence accumulated during the take-over process following the warning will affect driver's car-following behaviour after take-over. This way, the proposed IIDM can be applied to the prediction of car-following behaviour in CAV environment. Similarly, not only different size of the lead vehicle (car or truck), but also driving patterns can be considered as additional evidence. For instance, drivers are more likely to follow the lead vehicle more closely if the lead vehicle motion is more stable (e.g., constant speed) for a longer period. Within the

proposed car-following model framework, this evidence can be included in addition to perceptual variables for more accurate prediction of the start time and magnitude of reaction in different road geometric conditions and driving patterns of the lead vehicle.

It is also recommended to investigate the driver reaction time and the acceleration, not only deceleration, particularly when the lead vehicle accelerates. Unlike the deceleration which is required to avoid a crash in close following and braking conditions, the driver is not likely to initiate acceleration immediately after the lead vehicle starts accelerating. This behavioural difference between acceleration and deceleration conditions may require different model functional specification. For instance, positive (acceleration) and negative (deceleration) control errors can be separately considered for prediction of acceleration and deceleration adjustments.

Lastly, it is recommended to incorporate the other existing car-following models, instead of the Intelligent Driver Model, in the new car-following model framework and evaluate the model performance. For instance, those existing car-following models that use information in driver visual system such as the visual angle models can be integrated into the new car-following model framework. The visual angle models could be more useful than the conventional car-following models as they use perceptual variables such as visual angle and angular velocity that are perceived by a driver's visual system. However, these models were not used in this study as they contain a reaction time parameter. Thus, it is recommended to modify the visual angle models to predict the start time of driver reaction using the Accumulator model instead of a fixed reaction time.

# References

AASHTO (2001) "A policy on geometric design of highways and streets," *American Association of State Highway and Transportation Officials, Washington, DC*, 1(990), p. 158.

Aghabayk, K. *et al.* (2013) "A Novel Methodology for Evolutionary Calibration of Vissim by Multi-Threading," in *Australasian Transport Research Forum 2013 Proceedings*, pp. 1–15.

Aghabayk, K., Sarvi, M. and Young, W. (2012) "Understanding the Dynamics of Heavy Vehicle Interactions in Car-Following," *Journal of Transportation Engineering*, 138(12), pp. 1468–1475. doi: 10.1061/(ASCE)TE.1943-5436.0000463.

Aghabayk, K., Sarvi, M. and Young, W. (2015) "A State-of-the-Art Review of Car-Following Models with Particular Considerations of Heavy Vehicles," *Transport Reviews*, 35(May 2015), pp. 82–105. doi: 10.1080/01441647.2014.997323.

Bando, M. *et al.* (1998) "Analysis of optimal velocity model with explicit delay," *Physical Review E*, 58(5), pp. 5429–5435. doi: 10.1103/PhysRevE.58.5429.

Boer, E. R. (1999) "Car following from the driver's perspective," *Transportation Research Part F: Traffic Psychology and Behaviour*, 2(4), pp. 201–206. doi: 10.1016/S1369-8478(00)00007-3.

Brackstone, M. and McDonald, M. (1999) "Car-following: a historical review," *Transportation Research Part F: Traffic Psychology and Behaviour*, 2(1999), pp. 181–196.

Brown, J. F., Obenski, K. S. and Osborn, T. R. (2002) *Forensic engineering reconstruction of accidents*. Charles C Thomas Publisher.

Carnegie Mellon University (2002) *ACT-R*. Available at: http://act-r.psy.cmu.edu/ (Accessed: December 3, 2017).

Chandler, R. E., Herman, R. and Montroll, E. W. (1958) "Traffic Dynamics: Studies in

Car Following," *Operations Research*, 6(2), pp. 165–184. doi: 10.1287/opre.6.2.165.

Elhenawy, M., El-Shawarby, I. and Rakha, H. (2017) "Modeling the perception reaction time and deceleration level for different surface conditions using machine learning techniques," *Advances in Intelligent Systems and Computing*, 481(540), pp. 131–142. doi: 10.1007/978-3-319-41627-4_13.

FHWA (2015) *Next Generation Simulation (NGSIM)*. Available at: https://www.fhwa.dot.gov/publications/research/operations/07030/index.cfm (Accessed: April 1, 2015).

FHWA (2016) *Research Data Exchange*. Available at: https://www.its-rde.net/ (Accessed: June 15, 2016).

Fritzsche, H. and Ag, D. (1994) "A model for traffic simulation," *Traffic Engineering & Control*, 35(5), pp. 317–321.

Gazis, D. C., Herman, R. and Rothery, R. W. (1961) "Nonlinear Follow-the-Leader of Traffic Flow," *Operations Research*, 9(4), pp. 545–567. doi: 10.1287/opre.9.4.545.

Gipps, P.G. (1981) "A behavioural car-following model for computer simulation," *Transportation Research Part B: Methodological*, pp. 105–111. doi: 10.1016/0191-2615(81)90037-0.

Giszter, S. F. (2015) "Motor primitives-new data and future questions," *Current Opinion in Neurobiology*, 33, pp. 156–165. doi: 10.1016/j.conb.2015.04.004.

Green, M. (2000) "How long does it take to stop - methodological analysis of driver perception brake times," *Transportation human factors*, 2(3), pp. 195–216.

Green, M. (2017a) "Collision Analysis 1: Longitudinal Geometries," in *Roadway Human Factors: From Science to Application*. Tucson, AZ: Lawyers & Judges Publishing Company, Inc., pp. 245–306.

Green, M. (2017b) "Collison Analysis 4: Perception-Response Time," in *Roadway Human Factors: From Science to Application*. Tucson, AZ: Lawyers & Judges

Publishing Company, Inc., pp. 409–443.

Green, M. (2017c) "Psychophysics and Operant Learning," in *Roadway Human Factors: From Science to Application*, pp. 23–45.

Green, M. (2017d) "Space and Ecological Optics," in *Roadway Human Factors: From Science to Application*.

Hancock, P. (1999) "Is car following the real question – are equations the answer?," *Transportation Research Part F: Traffic Psychology and Behaviour*, 2(4), pp. 197–199. doi: 10.1016/S1369-8478(00)00006-1.

Higgs, B., Abbas, M. and Medina, A. (2011) "Analysis of the Wiedemann Car Following Model over Different Speeds using Naturalistic Data," *3rd International Conference on Road Safety and Simulation*, pp. 1–22.

Hoefs, D. H. (1972) "Entwicklung einer Messmethode uber den Bewegungsablauf des Kolonnenverrkehrs," *Universitat (TH) Karlsruhe, Germany*.

Hoefs, Dierk Hans (1972) "Untersuchung des Fahrverhaltens in Fahrzeugkolonnen," *Strassenbau U Strassenverkehrstech*, (140).

Hoffman, E. (1994) "Estimation of time to vehicle arrival -- effects of age on use of available visual information," *Perception*, 23(8), pp. 947–955.

Hoffmann, E. R. and Mortimer, R. G. (1996) "Scaling of relative velocity between vehicles," *Accident Analysis and Prevention*, 28(4), pp. 415–421. Available at: Pubmed 8870768.

Kesting, A. and Treiber, M. (2008) "Calibrating car-following models by using trajectory data methodological study," *Transportation Research Record*, (2088), pp. 148–156. doi: 10.3141/2088-16.

Khodayari, A. *et al.* (2012) "A modified car-following model based on a neural network model of the human driver effects," *IEEE Transactions on Systems, Man, and Cybernetics Part A:Systems and Humans*, 42(6), pp. 1440–1449. doi:

10.1109/TSMCA.2012.2192262.

Killick, R. and Eckley, I. A. (2014) "changepoint: An R Package for Changepoint Analysis," *Journal of Statistical Software*, 58(3), pp. 1–19. Available at: http://www.jstatsoft.org/v58/i03/.

Kim, T. and Lovell, D. J. (2005) "Observation of Real Driving Behavior in Car-Following: Preliminary Results," in *Vehicular Technology Conference, 2005. VTC 2005-Spring. 2005 IEEE 61st*, pp. 2939–2943. doi: 10.1109/VETECS.2005.1543885.

Lamble, D., Laakso, M. and Summala, H. (1999) "Detection thresholds in car following situations and peripheral vision: Implications for positioning of visually demanding in-car displays," *Ergonomics*, 42(6), pp. 807–815. doi: 10.1080/001401399185306.

Lee, D. N. (1976) "A theory of visual control of braking based on information about time-to-collision," *Perception*, 38(6), p. 858.

Li, J. (2017) *Free Web app Comparing Wiedemann 74 and 99 model & Replicating Dissipation of stop-and-go waves via AV control*. Available at: https://www.linkedin.com/pulse/free-web-app-comparing-wiedemann-74-99-model-waves-av-li-p-e-ptoe/ (Accessed: January 1, 2018).

Lu, H., Song, G. and Yu, L. (2018) "The 'acceleration cliff': An investigation of the possible error source of the VSP distributions generated by Wiedemann car-following model," *Transportation Research Part D: Transport and Environment*, 65(August), pp. 161–177. doi: 10.1016/j.trd.2018.08.004.

Maddox, M. E. and Kiefer, A. (2012) "Looming threshold limits and their use in forensic practice," in *Proceedings of the Human Factors and Ergonomics Society*. SAGE Publications Sage CA: Los Angeles, CA, pp. 700–704. doi: 10.1177/1071181312561146.

Makowski, D., Ben-Shachar, M. and Lüdecke, D. (2019) "bayestestR: Describing Effects and their Uncertainty, Existence and Significance within the Bayesian Framework," *Journal of Open Source Software*, 4(40), p. 1541. doi: 10.21105/joss.01541.

Markkula, G. (2014) "Modeling driver control behavior in both routine and near-accident

driving," in *Proceedings of the Human Factors and Ergonomics Society*. SAGE
Publications Sage CA: Los Angeles, CA, pp. 879–883. doi: 10.1177/1541931214581185.

Markkula, G. et al. (2016) "A farewell to brake reaction times? Kinematics-dependent
brake response in naturalistic rear-end emergencies," *Accident Analysis and Prevention*,
95, pp. 209–226. doi: 10.1016/j.aap.2016.07.007.

Markkula, G. et al. (2018) "Sustained sensorimotor control as intermittent decisions
about prediction errors: computational framework and application to ground vehicle
steering," *Biological Cybernetics*, 112(3), pp. 181–207. doi: 10.1007/s00422-017-0743-9.

Markkula, G. et al. (2020) "Evidence accumulation , not a perceptual threshold ,
constrains neural and behavioural responses in human collision threat detection."
PsyArXiv.

Markkula, G. (2020) "Model and figure code for 'Modeling driver control behavior in
both routine and near-accident driving.,'" *OSF*. doi: 10.17605/OSF.IO/KHDT7.

Markkula, G. et al. (2021) "Accumulation of continuously time-varying sensory evidence
constrains neural and behavioral responses in human collision threat detection," *PLOS
Computational Biology*, pp. 1–21. doi: 10.1371/journal.pcbi.1009096.

Michaels, R. M. (1963) "Perceptual Factors in car following," *Proceedings of the 2nd
International Symposium on the Theory of Road Traffic Flow (London, England), OECD*,
pp. 44–59.

Montanino, M. and Punzo, V. (2015) "Trajectory data reconstruction and simulation-
based validation against macroscopic traffic patterns," *Transportation Research Part B:
Methodological*, 80, pp. 82–106. doi: 10.1016/j.trb.2015.06.010.

Ni, D. (2015) *Traffic Flow Theory: Characteristics, Experimental Methods, and
Numerical Techniques*. Butterworth-Heinemann.

Ossen, S. and Hoogendoorn, S. P. (2011) "Heterogeneity in car-following behavior:
Theory and empirics," *Transportation Research Part C: Emerging Technologies*, 19(2),
pp. 182–195. doi: 10.1016/j.trc.2010.05.006.

Pariota, L. and Bifulco, G. N. (2015) "Experimental evidence supporting simpler Action Point paradigms for car-following," *Transportation Research Part F: Traffic Psychology and Behaviour*, 35, pp. 1–15. doi: 10.1016/j.trf.2015.08.002.

Peeta, S., Zhang, P. and Zhou, W. (2005) "Behavior-based analysis of freeway car-truck interactions and related mitigation strategies," *Transportation Research Part B: Methodological*, 39, pp. 417–451. doi: 10.1016/j.trb.2004.06.002.

Powers, W. T. (2008) "Living control systems III: The fact of control."

Saifuzzaman, M. and Zheng, Z. (2014) "Incorporating human-factors in car-following models: a review of recent developments and research needs," *Transportation Research Part C: Emerging Technologies*, 48, pp. 379–403. doi: 10.1016/j.trc.2014.09.008.

Salvucci, D. D. (2006) "Modeling driver behavior in a cognitive architecture.," *Human factors*, 48(2), pp. 362–380. doi: 10.1518/001872006777724417.

Salvucci, D. D., Boer, E. R. and Liu, A. (2001) "Toward an Integrated Model of Driver Behavior in Cognitive Architecture," *Transportation Research Record: Journal of the Transportation Research Board*, 1779(01), pp. 9–16. doi: 10.3141/1779-02.

Salvucci, D. D. and Gray, R. (2004) "A two-point visual control model of steering," *Perception*, 33(10), pp. 1233–1248. doi: 10.1068/p5343.

Sarvi, M. and Ejtemai, O. (2011) "Exploring heavy vehicles car-following behaviour," in *Australasian Transport Research Forum (ATRF), 34th*. Adelaide, South Australia, Australia, pp. 1–11.

Scrucca, L. (2013) "GA: A Package for Genetic Algorithms in R," *Journal of Statistical Software*, 53(4), pp. 1–37.

Shinar, D. (2017) "Driver Information Processing: Attention, Perception, Reaction Time, and Comprehension," *Traffic safety and human behavior*. Second, pp. 189–256.

Summala, H., Lamble, D. and Laakso, M. (1998) "Driving experience and perception of the lead car's braking when looking at in-car targets," *Accident Analysis and Prevention*,

30(4), pp. 401–407. doi: 10.1016/S0001-4575(98)00005-0.

Svärd, M. *et al.* (2017) "A quantitative driver model of pre-crash brake onset and control," *Proceedings of the Human Factors and Ergonomics Society*, 2017-Octob, pp. 339–343. doi: 10.1177/1541931213601565.

Tian, J. *et al.* (2016) "Improved 2D intelligent driver model in the framework of three-phase traffic theory simulating synchronized flow and concave growth pattern of traffic oscillations," *Transportation Research Part F: Psychology and Behaviour*, 41, pp. 55–65. doi: 10.1016/j.trf.2016.06.005.

Todosiev, E. P. (1963) *The action point model of the driver-vehicle system*. Doctoral dissertation, The Ohio State University.

Treiber, M. and Kesting, A. (2013) "Traffic flow dynamics," *Traffic Flow Dynamics: Data, Models and Simulation, Springer-Verlag Berlin Heidelberg*.

Wang, X. *et al.* (2016) "Drivers' rear end collision avoidance behaviors under different levels of situational urgency," *Transportation Research Part C: Emerging Technologies*, 71, pp. 419–433. doi: 10.1016/j.trc.2016.08.014.

Weber, E. H. (1905) *Tastsinn und gemeingefühl*. W. Engelmann.

Wiedemann, R. (1974) *Simulation des Strassenverkehrsflusses*.

Wiedemann, R. and Reiter, U. (1992) "Microscopic traffic simulation: the simulation system MISSION, background and actual state," *Project ICARUS (V1052) Final Report. Brussels, CEC*, 2, pp. 1–53.

Wu, K. F. and Lin, Y. J. (2019) "Exploring the effects of critical driving situations on driver perception time (PT) using SHRP2 naturalistic driving study data," *Accident Analysis and Prevention*, 128, pp. 94–102. doi: 10.1016/j.aap.2019.04.003.

Xue, Q. *et al*. (2018) "Using perceptual cues for brake response to a lead vehicle: Comparing threshold and accumulator models of visual looming," *Accident Analysis and Prevention*, 118(May), pp. 114–124. doi: 10.1016/j.aap.2018.06.006.

Yilmaz, E. H. and Warren, W. H. (1995) "Visual control of braking: A test of the! τ̇ hypothesis," *Journal of Experimental Psychology: Human Perception and Performance*, 21(5), pp. 996–1014.

# Appendix A. Predicted Trajectories of Different Car-following Models

The trajectories of the four car-following models were compared for a sample of 15 drivers or subject vehicles. The driver number and lead vehicle type are shown at the top of all figures for the driving simulator data. Similarly, the vehicle ID (vid) and the preceding vehicle ID (precid) are shown on top of all the figures for the I-80 data.
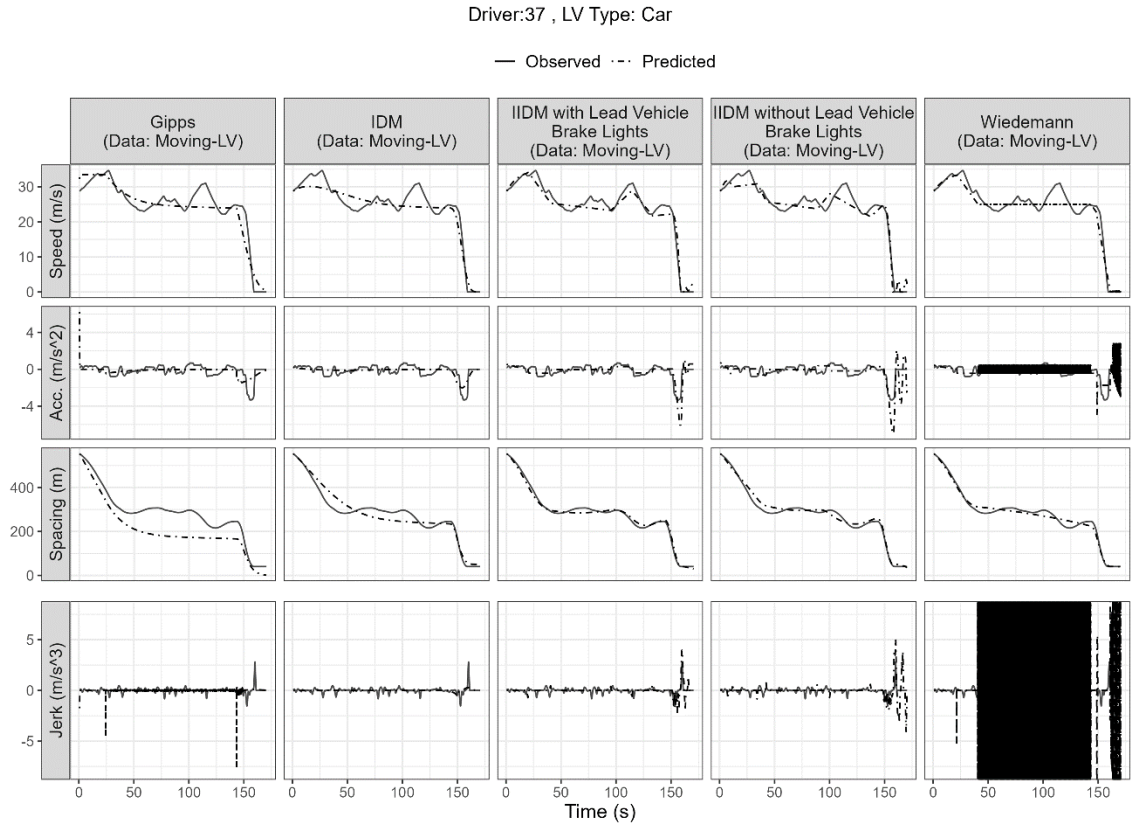


Driver:37 , LV Type: Car

Driver:14 , LV Type: Car
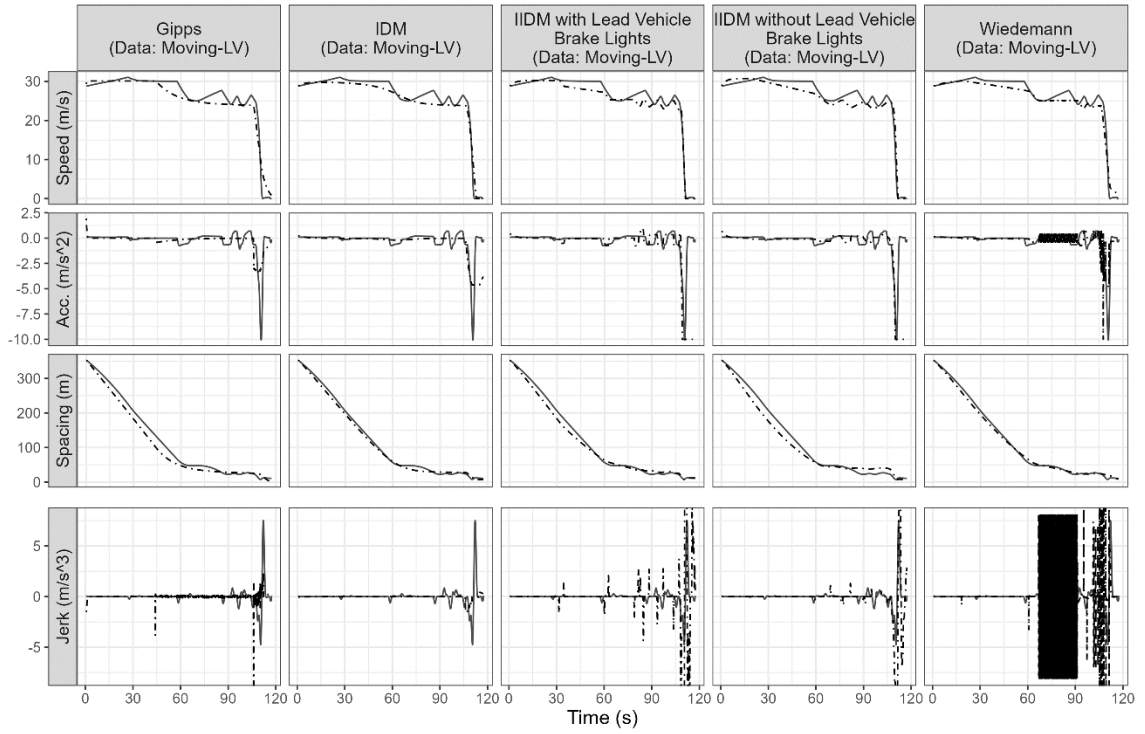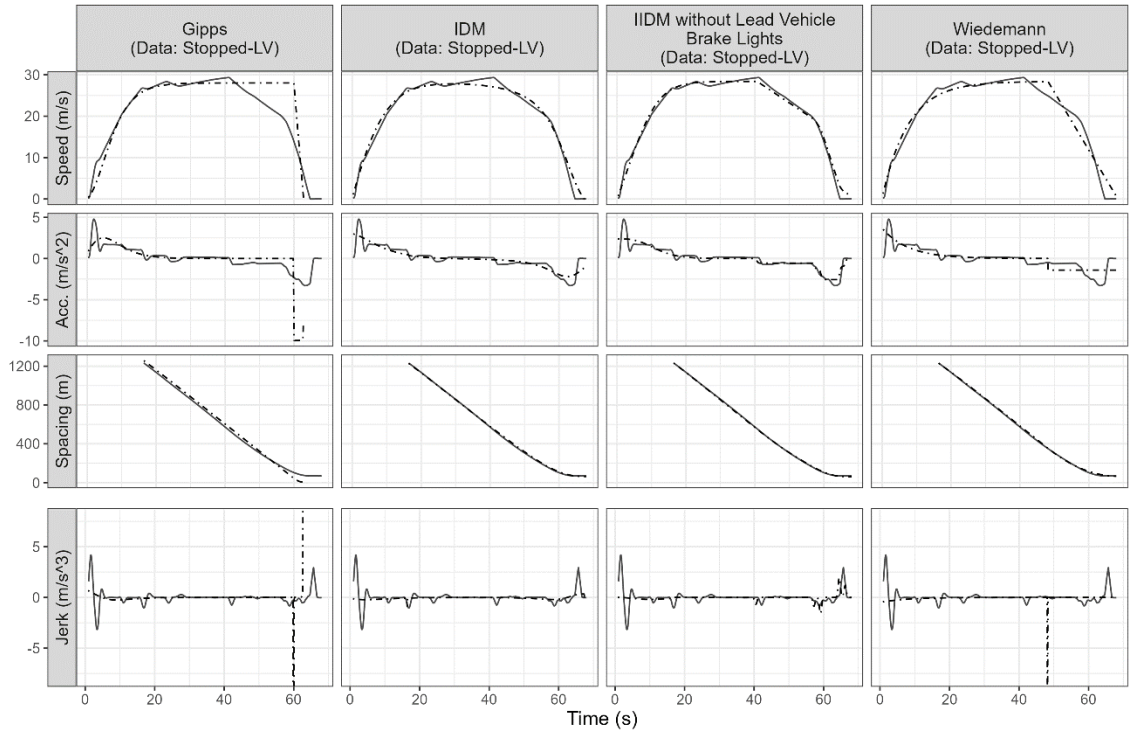
Driver:09 , LV Type: Car

Driver:49 , LV Type: Car
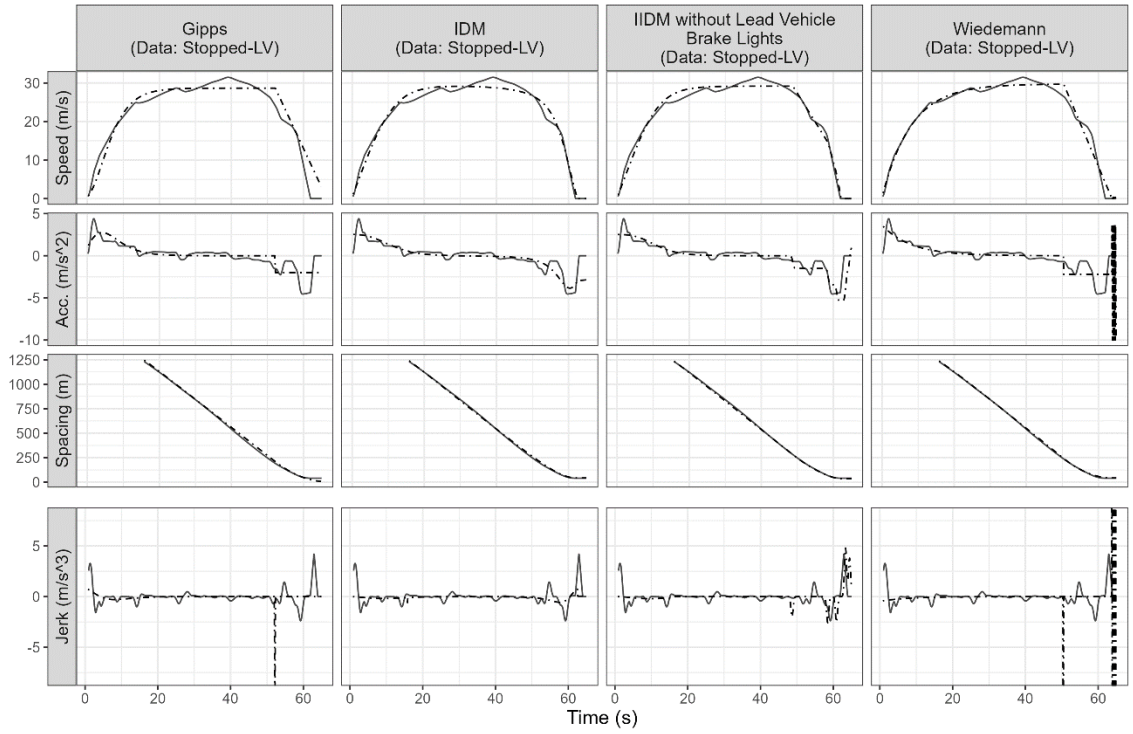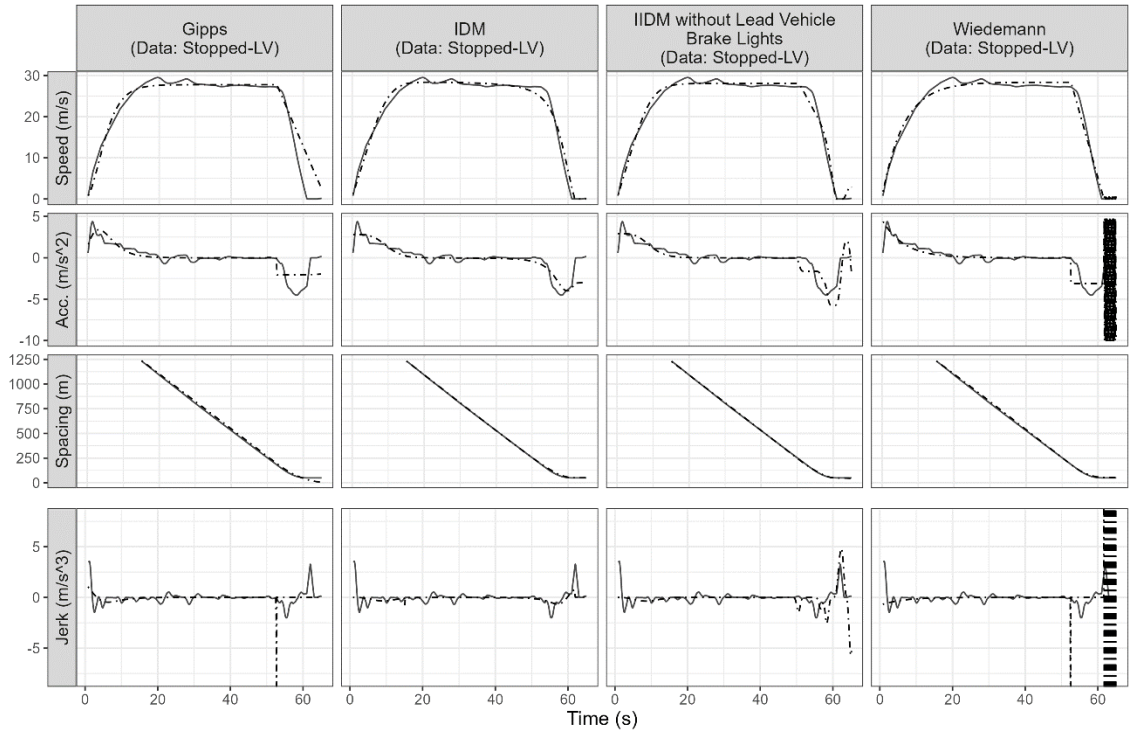


Driver:21 , LV Type: Car
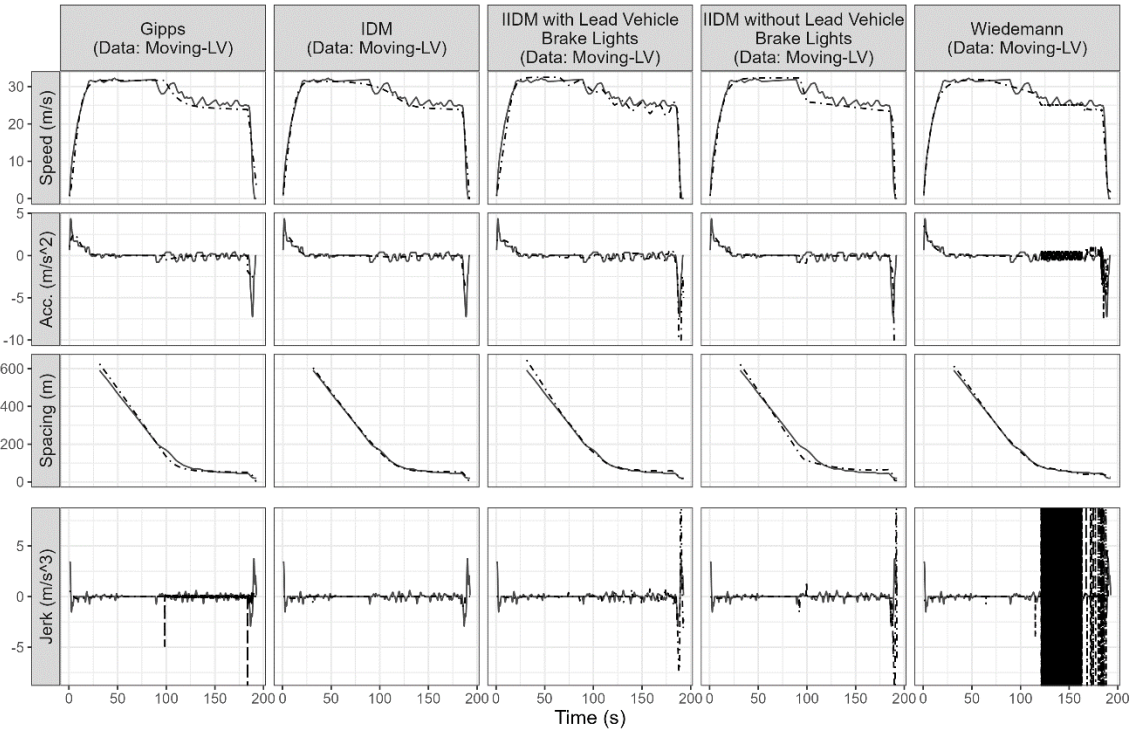
Driver:04 , LV Type: Car
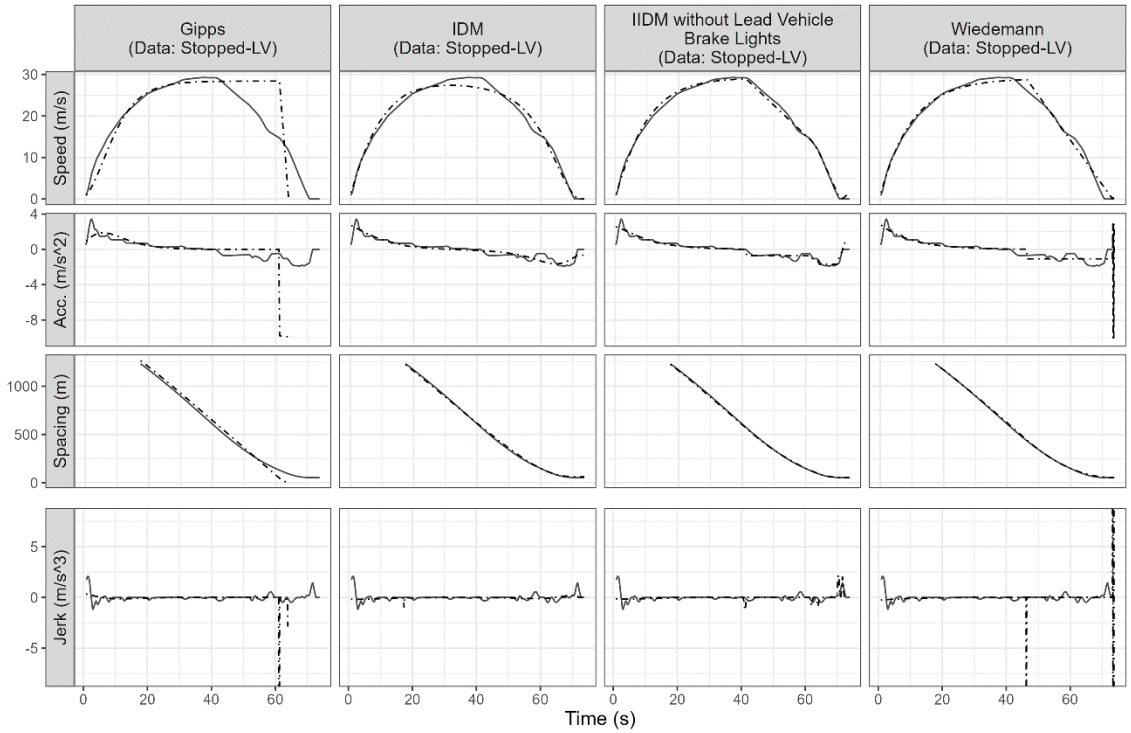

Driver:32 , LV Type: Car

Driver:09 , LV Type: Car
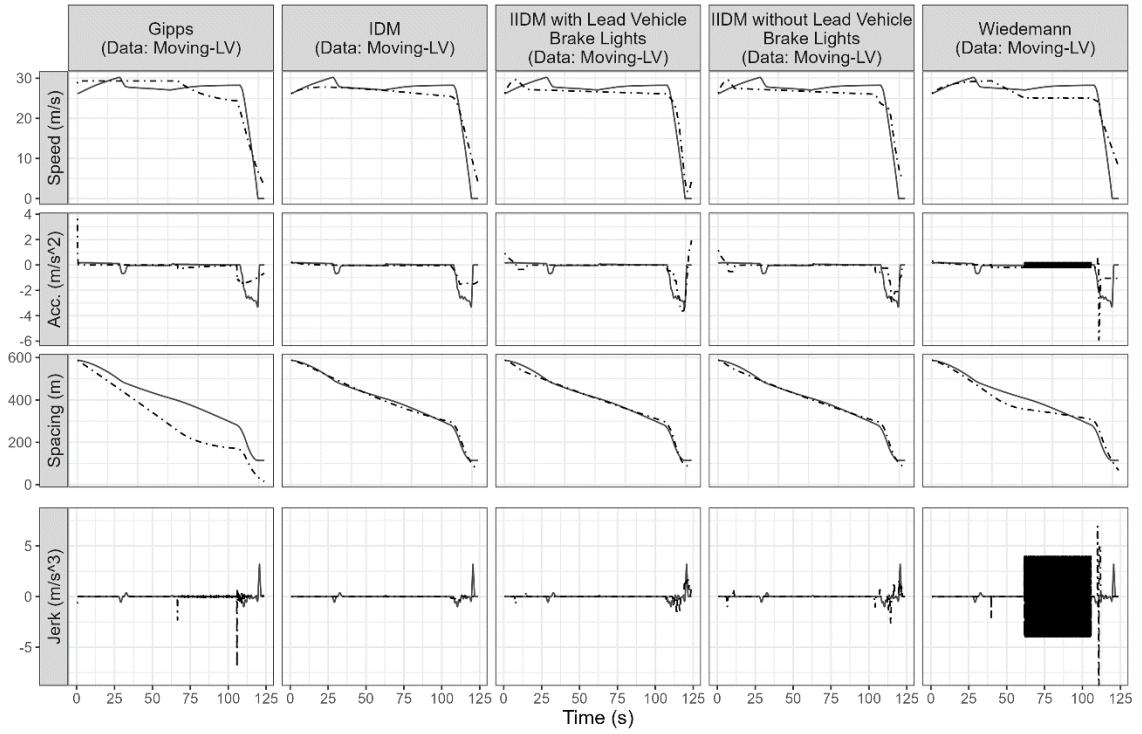


Driver:35 , LV Type: Car

182
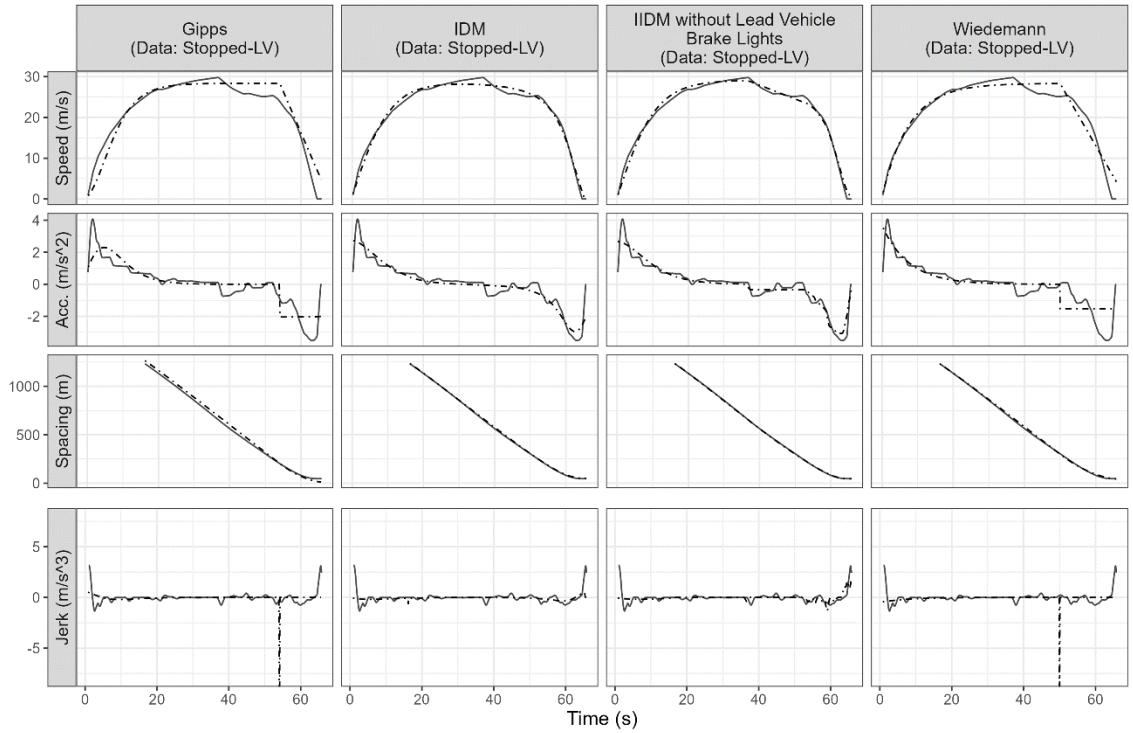
Driver:47 , LV Type: Truck
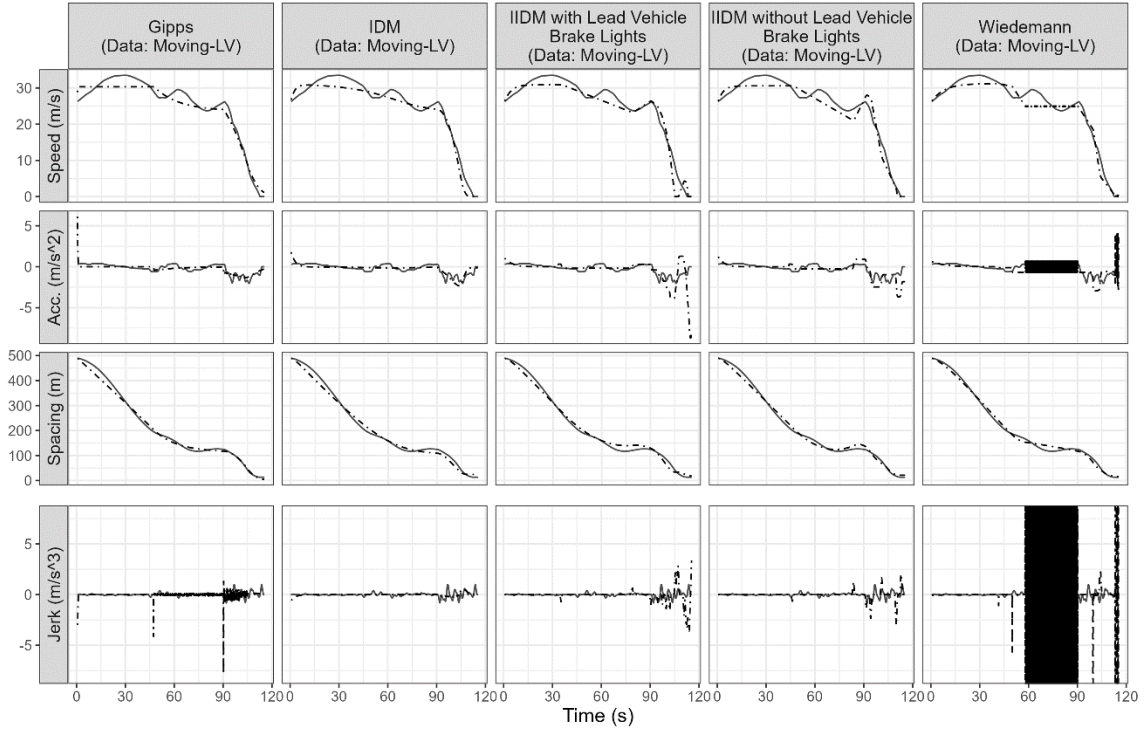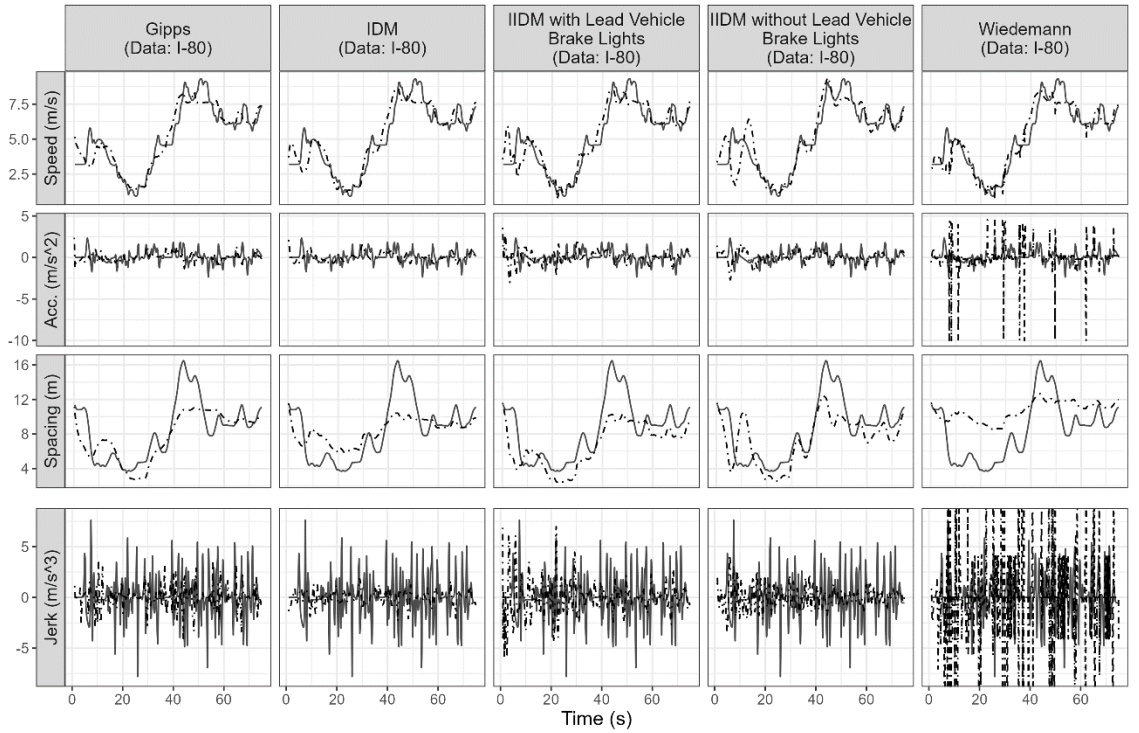


vid: 13, precid: 15
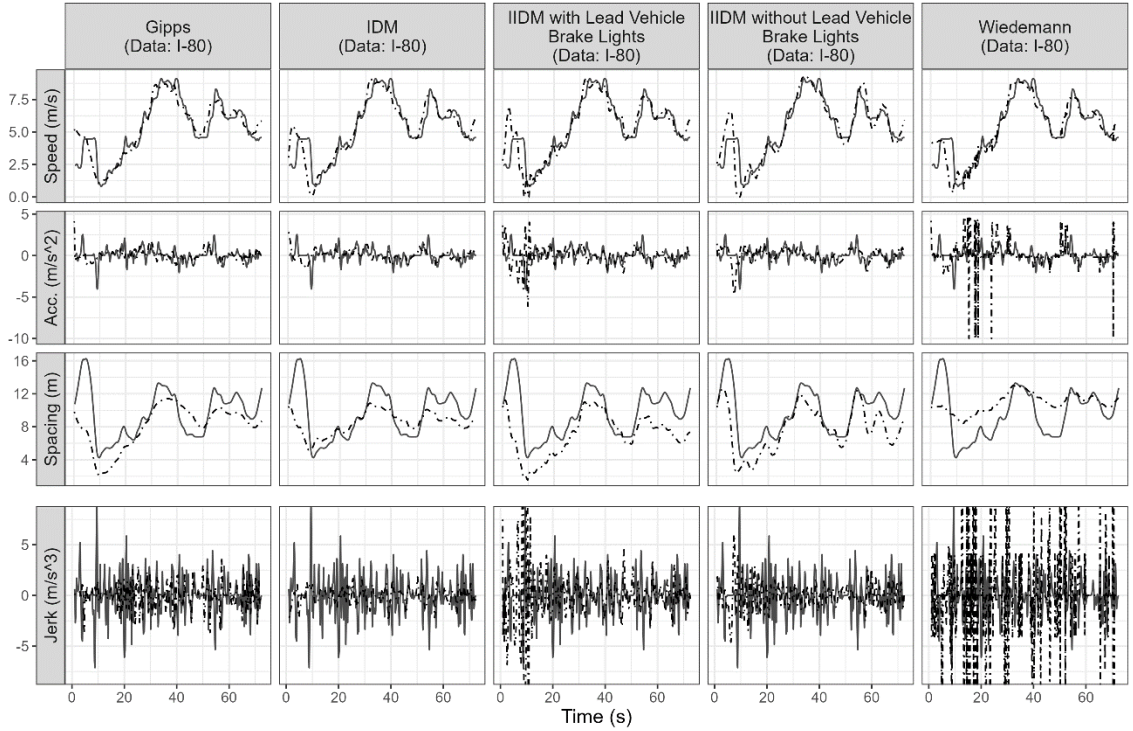
vid: 2174, precid: 2166

— Observed  ·–· Predicted
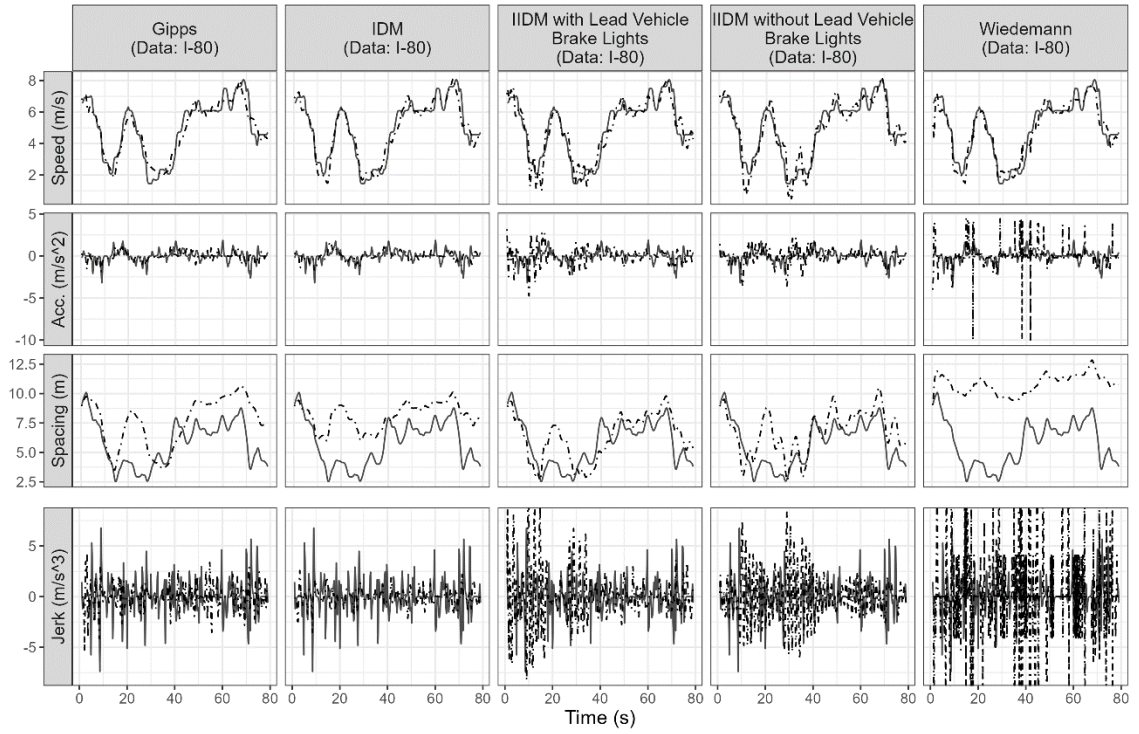


vid: 2261, precid: 2256

— Observed  ·–· Predicted

vid: 3053, precid: 3051
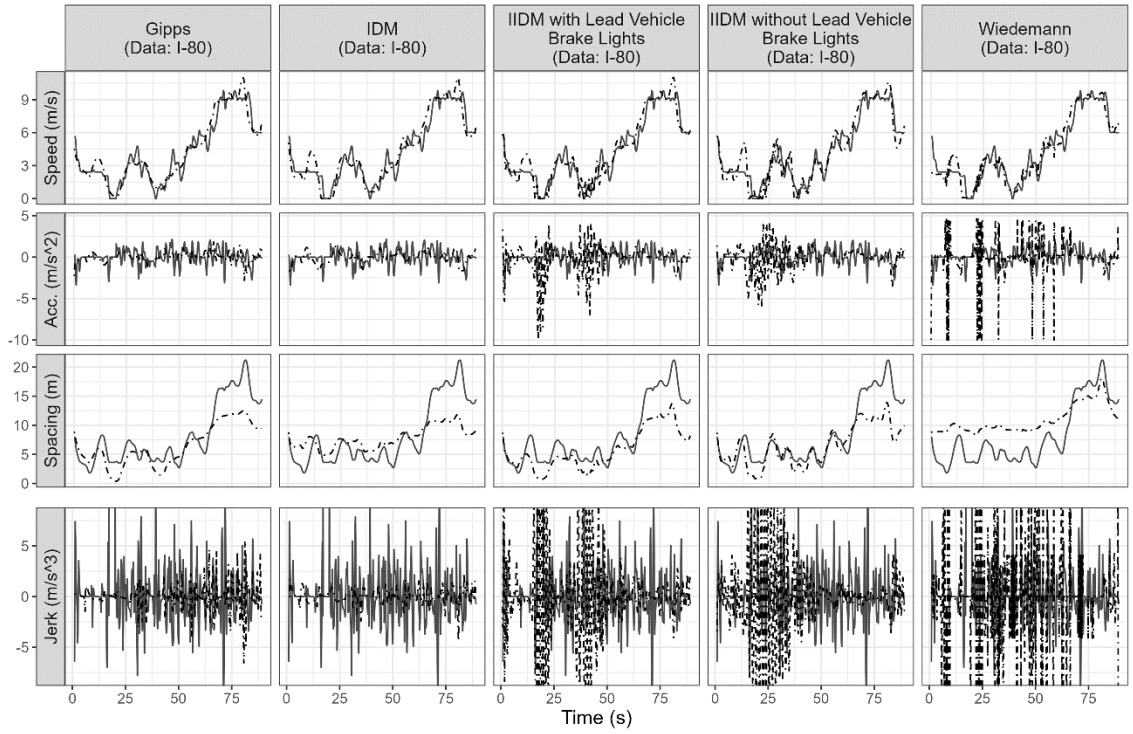
# Vita Auctoris

|                   |                                                               |
|-------------------|---------------------------------------------------------------|
| NAME:             | Umair Durrani                                                 |
| PLACE OF BIRTH:   | Lahore, Pakistan                                              |
| YEAR OF BIRTH:    | 1987                                                          |
| EDUCATION:        | Punjab College of Science and Technology, Lahore, Pakistan, 2005 |
|                   | University of Engineering and Technology, Lahore, B.Sc., Lahore, Pakistan, 2009 |
|                   | University of Windsor, Ph.D., Windsor, ON, 2022              |